UNIVERSITY of CALIFORNIA
Santa Barbara

Development of Deep Ultraviolet (UV-C) Thin-Film Light-Emitting Diodes Grown on SiC

A dissertation submitted in partial satisfaction of the
requirements for the degree of

Doctor of Philosophy

in

Materials

by

Burhan Khalid SaifAddin

Committee in charge:

Professor James S. Speck, co-chair
Professor Steven P. DenBaars, co-chair
Professor Shuji Nakamura
Professor Dmitri Strukov

December 2018

The dissertation of Burhan Khalid SaifAddin is approved:

_____

Dmitri Strukov

_____

Shuji Nakamura

_____

Steven P. DenBaars, co-chair

_____

James S. Speck, co-chair

June 2018

Development of Deep Ultraviolet (UV-C) Thin-Film Light-Emitting Diodes Grown on SiC

Burhan Khalid SaifAddin

To my parents

Acknowledgment

Many people contributed to my research by providing ideas, technical assistance, time, peripheral discussions, funds, and friendship. I express my sincere thanks to all of them.

First and foremost, I would like to thank Professors Jim Speck, Steve DenBaars, and Shuji Nakamura. They assembled an amazing group of PhD students, researchers, engineers, and staff at UCSB, and I am grateful for their guidance and support during my research. I was very fortunate and privileged to work in a research and innovations group that demanded initiative and independent thinking. I thank Jim for his challenging technical discussions, and inspiring attitude and for the many enjoyable discussions that ranged from the various electrical and mechanical impacts of threading dislocations to why point sources are a light designer's dream to croissants and Arabic coffee. Jim carefully read and edited my papers and dissertation, even if he had to stay-up very late into the night. Steve and Shuji built world-class MOCVD labs, and I am thankful for their trust, contagious excitement, and innovative technical advice and feedback on my papers and presentations. They always asked me great questions and offered encouragement, and they were always cheerful and gratifying to talk to. I hope to have learned from their deep insight, encyclopedic knowledge, and intuition about device engineering, materials growth, and processing. Lastly, I am grateful for their interest in helping develop nitride semiconductors, devices, and energy efficiency research in Saudi Arabia. I wish to thank Professor Dmitri Strukov for his assistance and encouragement and for asking me great and numerous questions about my research during a special meeting for my PhD defense.

Next, I would like to thank the amazing UV team. Humberto Fornada worked very hard with me on this project in 2015, and he provided me with all the samples for the work

conducted in Chapters 2 and 3. I am grateful to Mike Iza for his deep knowledge of MOCVD instrumentation and for his inspiring attitude about life. His efforts were essential in the successful growth of AlGaN LEDs, and without his MOCVD know-how, we would not have made progress on this project, as discussed in Chapters 4 and 5. I am grateful to Abdullah Almogbel and Chris Zollner for their inspiring dedication and diligence and for working very closely with me on growth, specifically in the second half of 2017, which was essential to my work described in Chapter 5. Chris also provided timely and very useful feedback on all my papers and most of my PhD dissertation. I am grateful to Jianfeng Wang for her excitement about growing n-AlGaN for UV LED tunnel junctions, even if the LEDs turned out to be diodes without any UV light. I enjoyed the UV LED meetings with Jim, Humberto, Mike, Abdullah, Chris, and Jianfeng, and Richard C. Cramer, especially when we had enlightening and instructive disagreements.

I am fortunate to have worked and learned from some of the best nitride researchers in the world. I am indebted to many people in the greater nitride community at UCSB. I am thankful to Stacia for her encouragement and advice and for her cheerful attitude about MOCVD growth problems, her prior experience with UV LEDs research and SiC growth, as well as for sharing some of her vision about the future of nitride research. Thanks to Dan Cohen for his insightful comments and critical questions and for always being available to answer any questions I had. I thank Abdullah Alhassan for his discussions about visible LED growth and processing. I thank Changmin Lee for exciting discussions about GaN growth, LEDs, laser diodes, Li-Fi, Silicon Valley culture, and Korean culture. I would like to thank Asad Mugahl for providing assistance with Hall and CTLM measurements. John Leonard was always very helpful, and he modernized the LIV lab view programs, which made my work much easier. I

am thankful to Brian Thibeault and Ben Yonkee for teaching me many things about processing. I am also thankful to Ben for teaching me about the PEC liftoff process of thin-film LEDs, which was indirectly beneficial to my work on thin-film UV LEDs. Thanks to Tal Margalith for organizing LED meetings and for inviting me to give a nitride seminar and several other talks, as well as for teaching me a few kicks at the UCSB Taekwondo club. Thanks to Erin Young for helping with KACT/KAUST quarterly reports and for teaching me about MBE. Thanks to Dan Haeger for introducing me to X-ray characterization and for teaching me about processing. I would like to thank Feng Wu for the TEM work on AlN and AlGaN layers. I am grateful to Mike Cantouri and Sang Ho for teaching me about LED packaging and for troubleshooting the lapping/grinding tools. I would like to thank Ludovico.Megalini, Ben Yonkee and John Leonard for helping me with the MOCVD in other non-UV projects. Thanks to Leah Kuritzky for helping me get started with LightTools. Chris Pynn and Mike Iza designed and built an online MOCVD database to retain growth knowledge and make it more accessible; this had a large impact on my research progress. I am thankful for Professor Mishra's continuous encouragement and for teaching two classes to share his understanding of device physics. I am also thankful for fruitful technical discussions with Professor Claude Weisbuch on light extraction from LEDs and to Professor Chris Van de Walle on hydrogen, DX centers and point defects in AlGaN. I enjoyed teaching an introduction to materials engineering course with Professor Chris Bates. I also happily assisted with Professor Mishra's device physics course by grading the class homework, which exposed me to the various excellent ways new PhD students at UCSB approached and solved the class challenging problems.I want to thank the IEEE photonics chapter, which was a venue to plan and arrange fun professional and social activities. I especially thank Demis John, Eric Stanton, Akhilesh Khope, Changmin Lee, Daniel

Becerra, Kareem Hamdy, Minh Tran, Philip Chan, Robert Zhang, Takako Hirokawa, Tanya Das, Victoria Rosborough, Brandon Isaac, and many others.

Thanks to many friends at UCSB and elsewhere: Saleem Aldajani, Hisham Alhasan, Muhammad Aldawood, Faisal Nawab, Muath Alkhalaf, Ahmed Almheiri, Bassam Albahra, Changmin Lee, Asad Mugahl, Yuewei Zhang, Abdullah Almogbel, Abdullah Alhassan, Chris Zollner, Humberto Fornada, Mike Iza, Jiangfeng Wang, Stacey Kowsz, Michel Khoury, Daniel Myers, Dan Haeger, Guillaume Lheureux, Bastien Bonef, Karem Hamdy, Andrew Espenlaub, Sang Ho, Senguing Lee, Charles Forman, John Leonard, Ludovico Megalini, Erin Kyle, Joonho Back, Chris Pynn, Mohammed Aboalreesh, Jalal Al-Yagoub, Ayman Al-Shammasi, and many others.

Thanks to the wonderful and supportive staff at the UCSB cleanroom, who helped me in so many ways. I would like to especially thank Brian Thibeault, Tom Reynolds, Demis John, Aidan Hopkins, Don Freeborn, Tony Bosch, Ning Cao, Adam Abrahamsen, Bill Mitchell, Mike Silva, and Luis Zuzunaga. I also wish to thank the CNSI technical staff. I learned a lot from Tom Mates and enjoyed all of my discussions with him. He helped me with SIMS and XPS measurements. I thank Youli Li for maintaining the XRD lab and Mark Cornish for his immediate assistance with AFM and cathodoluminescence SEM. In addition, I wish to thank the dedicated and kind administrative staff at UCSB, especially Yukina Warner, Fukiko Miyazaki, Tawny Hernandez, Joyclin Guzman, Tara Owens, Oura Neak, and Val DeVeyra.

From outside UCSB, I wish to thank Professor Grossman, David Weitz, Guo Ming, Ho-Cheol Kim, Zain Yamani, Fahhad Alharbi, Miri Kazes, Robert Miller, John D. Bass, Campbell Scott, Qing Song, and Xin Ai for encouraging me to pursue a PhD. I am honored and privileged that KACST has been a strong supporter of my research, and I thanks

Abdulrahman Almuhana, Ahmed Yamani, Abdurahman Albadri, Hamad Albraithen, Munir Eldesouki, Anas Alfaris, and Turki Al Saud for their support.

Last but certainly not least, I am most grateful for my parents (Khalid and Abeer), brothers (Eyad and Ziyad), sisters (Lujain and Layan), aunts (especially, Huda), uncles, Renad, Khalid, and the new member of the family: Elaine Khadija. They have provided unconditional love and support throughout the years, which was essential to my success.

Curriculum Vita

Burhan K. SaifAddin, Ph. D.

June 2018

Personal Information

Email: bksaif@gmail.com
LinkedIn: https://goo.gl/H1s1Cq
Google Scholar: http://goo.gl/6KLEks

Education

University of California, Santa Barbara **2018**
PhD in Materials Science and Engineering
Development of Deep Ultraviolet Thin-Film Light-Emitting Diodes (UV-C LEDs) Grown on SiC
Advisors: James S. Speck, Steven P. DenBaars, Shuji Nakamura,
Staff Scientists: Michael Iza, Stacia Keller, Tal Margalith, and Robert M. Farrell.

Massachusetts Institute of Technology (MIT) – Cambridge, MA **2011**
Master of Engineering in Materials Science and Engineering. MEng Thesis "The Challenges of Organic Polymer Solar Cells." Advisor: Jeffry C. Grossman.

King Fahd University of Petroleum and Minerals (KFUPM) – Dhahran, Saudi Arabia **2008**
Double B.S. in Physics and Electrical Engineering with High Honors. Senior Project: Building and Designing a Dielectric Phase Shifter.

Publications

1. **B. K. Saif Addin**, Abdullah Almogbel, C J. Zollner, Abdulrahman Albadri, Ahmed Alyamani, Michael Iza, Feng Wu, Shuji Nakamura, S. P. DenBaars, J. S. Speck. "High EQE 264 nm thin-film Ultraviolet Light-Emitting Diodes (UV-C)," (Manuscript in preparation).
2. **B. K. SaifAddin**, Abdullah Almogbel, C J. Zollner, Abdulrahman Albadri, Ahmed Alyamani, Michael Iza, Feng Wu, Shuji Nakamura, S. P. DenBaars, J. S. Speck. "3X Light extraction enhancement of UV-C thin-film light-emitting diodes (278 nm) via KOH roughening of AlN," (Manuscript in preparation).
3. **B. K. SaifAddin**, Michael Iza, Abdullah Almogbel, C J. Zollner, Humberto Foronda, Abdulrahman Albadri, Ahmed Alyamani, Feng Wu, Shuji Nakamura, S. P. DenBaars, J. S. Speck. "First demonstration of high light-extraction thin-film-flip-chip(TFFC) ultraviolet light emitting diodes grown on SiC,"*(* Manuscript in preparation*)*.
4. **B. K. SaifAddin**, C J. Zollner, Abdullah Almogbel, Humberto Foronda, Abdulrahman Albadri, Ahmed Alyamani, Michael Iza, Feng Wu, Shuji Nakamura, S. P. DenBaars, J. S. Speck. "Fabrication technology for high light extraction ultraviolet thin-film flip-chip (UV TFFC) LEDs grown on SiC," *SST. (Manuscript sumbitted)*.
5. **B. K. SaifAddin**, C J. Zollner, Abdullah Almogbel, Humberto Foronda, Abdulrahman Albadri, Ahmed Alyamani, Michael Iza, Feng Wu, Shuji Nakamura, S. P. DenBaars, J. S. Speck. "Developments in AlGaN and UV-C LEDs grown on SiC (Late News)," *Proc. SPIE 9748, Gallium Nitride Materials and Devices XI*, 97481B. (2018).
6. H. M. Foronda, F. Wu, C. J. Zollner, Alif MEA, **B. K. SaifAddin**, A. Almogbel, M. Iza, S. Nakamura, S. P. DenBaars, J. Speck. "Low threading dislocation density aluminum nitride on silicon carbide through the use of reduced temperature interlayers," *J. Cryst. Growth* 483 134. (2018).
7. D. Hwang, B. P. Yonkee, **B. K. SaifAddin**, R. M. Farrell, S. Nakamura, J. S. Speck, S. DenBaars, "Photoelectrochemical liftoff of LEDs grown on freestanding c-plane GaN substrates," *Opt. Express*, vol. 24, no. 20, pp. 22875–22880. (2016).

8. B. P. Yonkee, **B.K. SaifAddin**, J. T. Leonard, S. P. DenBaars, S. Nakamura, "Flip-chip blue LEDs grown on bulk GaN substrates utilizing photoelectrochemical etching for substrate removal," A*ppl. Phys. Express*, vol. 9, no. 5, p. 56502. (2016).
9. I. Alhassan, R. M. Farrell, **B.K. SaifAddin**, A. Mughal, F. Wu, S. P. DenBaars, S. Nakamura, J. S. Speck, "High luminous efficacy green light-emitting diodes with AlGaN cap layer," *Opt. Express*, vol. 24, no. 16, pp. 17868–17873. (2016).
10. E. C. Young, B. P. Yonkee, F. Wu, **B. K. SaifAddin**, D. A. Cohen, S. P. DenBaars, S. Nakamura, J. S. Speck, "Ultraviolet light emitting diodes by ammonia molecular beam epitaxy on metamorphic AlGaN/GaN buffer layers*," J. Cryst. Growth*, vol. 425, pp. 389–392. (2015).
11. **K. SaifAddin**, "The challenges of organic polymer solar cells," Master of Engineering Thesis. Massachusetts Institute of Technology. (2011).

Conference Publications

1. A. Almogbel, **B. K. SaifAddin**, C. J. Zollner, M. Iza, H. Albraithen, A. Alyamani, A. Albadri, S. P. DenBaars, S. Nakamura, J. S. Speck. "MOCVD Growth of AlGaN on SiC Substrates for High Efficiency Deep UV LED," *Compound Semiconductor Week (CSW). Boston, MA. (2018).*

2. A. Almogbel, **B. K. SaifAddin**, C. J. Zollner, M. Iza, H. Albraithen, A. Alyamani, A. Albadri, S. P. DenBaars, S. Nakamura, J. S. Speck. "Optimization of AlGaN MOCVD growth for deep UV LED,"*19th International Conference on Metalorganic Vapor Phase Epitaxy. Nara, Japan. (2018).*

3. **B. K. SaifAddin**, C. J. Zollner, A. Almogbel, H. M. Foronda, A. Albadri, Ahmed Al Yamani, M. Iza, F. Wu, Shuji Nakamura, S. P. DenBaars, J. S. Speck. "Developments in AlGaN and UV-C LEDs grown on SiC (Late News)," *SPIE Photonics West. San Fracisco. CA. (2018).*

4. **B. K. SaifAddin**, H. M. Foronda, H. M., A. Almogbe, C. J. Zollner Chris , Samsudin M.E.A. , M. Iza, S. Nakamura, S. P. DenBaars, J. S. Speck. "First demonstration of lateral thin-film flip-chip ultraviolet light emitting diodes grown on SiC (Late News)," *12th International Conference on Nitride Semiconductors (ICNS 12). Strasbourg, France. (2017).*

5. **B. K. SaifAddin**, H. M. Foronda, M. Iza, S. Nakamura, S. P. DenBaars, J. S. Speck. "Epi-Transfer Technology for High EQE UV LEDs Grown on SiC (Late News)," *MRS Int. Work. Nitride Semicond. (IWN 2016). Orlando, FL. (2016).*

6. **B. K. SaifAddin**, H. M. Foronda, B. Yonkee, M. Cantore, S. H. Oh, R. Farrell, T. Margalith, E. C. Young, S. Nakamura, S. P. DenBaars, J. S. Speck. "Nanostructure Patterning of AlN Surface and Removal of SiC Substrates for High Extraction Efficiency Thin Film UV LEDs (Late News)," *42nd Int. Symp. Compd. Semicond. Santa Barbara, CA. (2015).*

Patents

1. A. Almogbel, **B. K. SaifAddin**, C. J. Zollner, M. Iza, H. Albraithen, A. Alyamani, A. Albadri, S. P. DenBaars, S. Nakamura, J. S. Speck. "Method for Fabricating Conductive Nitride Layers," Docket 30794.0689-US-P1. Prepared by Gates and Cooper LLP. Filed on Aug. 22, 2018.
2. C. J. Zollner, **B. K. SaifAddin**, A. Almogbel H, M. Iza, S. Nakamura, S. P. DenBaars, J. S. Speck. "Method for the fabrication of electrically conductive semiconductor layers," Docket 30794.0686-US-P1. Prepared by Gates and Cooper LLP. Filed on Jul. 18, 2018.
3. A. Almogbel, **B. K. SaifAddin**, C. J. Zollner, H. M. Foronda, M. Iza, S. Nakamura, S. P. DenBaars, J. S. Speck. "Method for Fabricating III-Nitride Layers," Docket 30794.660-US-P1. Prepared by Gates and Cooper LLP. Filed on Sep. 22, 2017.
4. C. J. Zollner, **B. K. SaifAddin**, A. Almogbel H, M. Iza, J. S. Speck, S. Nakamura, S. P. DenBaars. "Method for Thermal Treatment Of Polar Semiconductor Layers Without Inversion Domain Formation," Disclosed on Nov 1, 2017.
5. D. Hwang, N. G. Young, B. Yonkee, **B. K. SaifAddin**, S. P. DenBaars, J. S. Speck, S. Nakamura. "III-V micro-led arrays and methods for preparing the same," Patent US20170236807A1. Filed on Apr. 28 , 2017.

6. B. P. Yonkee, E. C. Young, C. Forman, J. T. Leonard, Seunggeun Lee, D. Cohen, R. M. Farrell, M. Iza, **B. K. SaifAddin**, A. Almogebl, H. Foronda, J. S. Speck, S. P. Denbaars, S. Nakamura . "Contact architectures for tunnel junction devices," US2017/047342/WO2018035322A1. Filed on November 1, 2016
7. D. Hwang, N. G. Young, B. Yonkee, **B. K. SaifAddin**, S. P. DenBaars, J. S. Speck, S. Nakamura. "Flexible arrays of micro light emitting diodes using a photoelectrochemical (PEC) liftoff technique," Patent US2015/057850/WO2016069766A1. Filed on October 28, 2014.

Honors and Awards

SSLEC Outstanding Researcher Award 2017

SSLEC Outstanding Researcher Award 2016

King Abdullah Fellowship 2012

KAUST Discovery Scholarship 2007

International Physics Olympiad, Bali, Indonesia. 2002

Software and Modeling Skills

Python, Matlab, Mathematica, SiLENSe, TF Calc, ImageJ, LabVIEW, Microsoft Office.

Materials Fabrication Techniques

Metal-organic chemical vapor deposition (MOCVD), plasma-enhanced chemical vapor deposition (PECVD), RF/FC sputtering, thermal evaporation, e-beam evaporation, inductive coupled plasma etching (ICP etching), reactive-ion etching (RIE etching), dicing saw, wafer lapping, chemical-mechanical polishing (CMP), flip-chip bonding.

Materials Characterization Techniques

SEM, AFM, Photoluminescence, Cathodoluminescence, UV-Vis spectroscopy, Ellipsometry, XRD, 4-pt probe, LIV characterization, Hall testing, Laser scanning confocal microscopy. Vacuum systems.

Research Experience

Harvard University – Cambridge, MA **2012**
Special student, Imaged confocal microscopy samples to study the stochastic mechanical properties of the cytoplasm Advisors: Ming Guo and David Weitz.

Consultant, MIT Consulting Club **Jan-Feb 2012**
Prepared and presented a study on the commercialization and market segmentation of quantum cascade lasers (1-10 μm) to the CEO of EOS Photonics, Mark Witinski.

King Abdul Aziz City for Science and Technology (KACST)– Riyadh, Saudi Arabia **2008-Current**
Researcher, National Institute of Nanotechnology.
- Synthesized silicon nanoparticles by electrochemical deposition.
- Presented a lecture on photoacoustic systems, a lecture on Titania nanorods synthesis and a tutorial on the basics of solar cells.
- Troubleshooting the electronics control board of an electrodeposition system.

Graduate summer visitor, Stanford University. Course Work: Solid State Physics for Mechanical Engineers, Programming Methodology, Probability and Statistics.

Visiting researcher, Advanced Organic Materials Group, IBM Almaden Research Center.
- Synthesized self-assembled block copolymer structures to direct the format ion of periodic nanoscale features.
- Fabricated patterned Titania nanorods arrays by sol-filling and by electrochemical deposition.

Measured the IV characteristics of colloidal quantum dots (CdTe, PbS) solar cells.
Presented Titania nanorods synthesis in quarterly meeting of KACST-IBM project that included Vice President of Science and Technology at IBM Watson Research Center.

Saudi Aramco – Ras Tanura, Saudi Arabia **Summer 2007**

Summer Intern at the Marine Department.
Troubleshooted electrical systems and control systems in buildings and in vessels.
Troubleshooted vessels' motors.

Undergraduate Researcher, Energy Research Center, KFUPM – Dhahran, Saudi Arabia **Spring 2007**

Performed and analyzed atmospheric ozone measurements using Photoacoustic Spectroscopy.
Presented the results to the Physics department faculty, KFUPM.

Teaching Experience

- **Teaching assistant (TA), University of California, Santa Barbara** **2017**
  - Introduction to Materials Science and Engineering with Prof. Chris Bates.
    - Taught a section, wrote homework and exam problems and graded them.
  - Device Physics with Prof. Umesh Mishra.
    - Graded homework and answered questions.
- **Tutor, Department of Materials Science and Engineering, MIT.** **2011**
  - Solid State Chemistry (3.091)
- **Splash Teacher, MIT Educational Studies Program** **2010**
  - The Energy Challenge and Solar Cells
- **Let's Get Ready (LGR) teacher, Boston, MA.** **2010**
  - Taught SAT math for low-income high school students.

LEADERSHIP / EXTRACURRICULAR

- 2011 MIT Consulting Club. Consulting for EOS (Infra Red Laser Startup).
- 2011 Member, MIT Energy Club. Gathered data for MIT Energy Club Factsheets.
- 2011 Member, MIT Science Policy Initiative. Organized a talk: Scarce Energy Materials by Prof. Robert Jaffe.
- 2011 Co-organized The 8th MIT Arab Student Organization Annual Science and Technology Awards
- 2011 Mentor at the International Sustainable World Project Olympiad (I-SWEEEP)
- 2010 Volunteer, Support universities in Iraq by Inventorying academic books for shipment; Planning; fund raising.
- 2010 College admissions mentor in Saudi Arabia, MIT Arab student Association.
  - Presented a talk to 10 school managers on the challenges facing students applying to US universities.
- 2009 Directed public relations, Saudi Physical Society Student Magazine: Interviewed two scientists and administered the online group.
- 2009 President of Physics Club, KFUPM: Organized lab tours and organized scientific video lectures.
- 2009 Online Teaching Assistant: helped high school science teachers learn about Thermal Physics at KFUPM.

Abstract

Development of Deep Ultraviolet (UV-C) Thin-Film Light-Emitting Diodes Grown on SiC

By

Burhan K. SaifAddin

UV-C LEDs in the range of 265–280 nm are needed to develop new disinfection and biotechnology applications. The market share for UV-C LED, versus UV-C lamps (Hg discharge and Xe), increased from 8% in 2008 ($240M) to 25% in 2018 ($810M). However, while low-pressure mercury lamps are ~30% energy efficient, the best commercial UV-C LEDs in the 265–280 nm range are ~2% energy efficient; InGaN blue LEDs are 80% energy efficient. Research on AlGaN LEDs has made significant progress into AlGaN material quality (including threading dislocation density and n-AlGaN electrical conductivity) but has lagged regarding light extraction efficiency. Light extraction from UV LEDs is limited by p-GaN absorption because of the lack of p-contact to p-AlGaN with AlN fraction (AlN content >50%). Furthermore, AlGaN emitters at the 265–280 nm range emit 40–50% of their emissions as transverse magnetic (TM) waves, which are harder to extract than transverse electric (TE) waves.

SiC is an absorbing substrate that has been largely overlooked in developing UV-C LEDs, even though it has a small lattice mismatch with AlN (~1%) and a similar Wurtzite crystal structure and is more chemically stable. We demonstrate the first lateral thin-film flip-chip (TFFC) ultraviolet (UV) light-emitting diodes grown on SiC. UV LEDs were made at 310 nm, 298 nm, 278 nm, and 265 nm.

In this dissertation, we discuss the design, epi development, and fabrication of TFFC AlGaN LEDs with reflective p-contacts. The AlGaN:Mg growth temperature and the Mg doping profile in AlGaN:Mg were found to significantly impact the electroluminescence (EL) efficiency of the AlGaN MQWs. KOH roughening enhanced the light-extraction efficiency (LEE) by 100% and by ~180–200% for UV LEDs with 10 nm p-GaN and 5 nm p-GaN, respectively, without affecting the devices' IV characteristics.

The thin-film architecture led to a high LEE of about ~28–30% without LED encapsulation when used with LEDs with 5 nm p-GaN. The best light extraction efficiency in the literature is ~24% (without LED encapsulation) for a 275 nm flip-chip LED grown on PSS sapphire substrate. KOH roughening of AlN is discussed and is compared to KOH roughening of N-Face GaN. To advance LEE further, we attempted to develop LEDs with transparent current n-AlGaN spreading layers as well as highly doped n^+-AlGaN tunnel junctions on top of UV-C LEDs. Reflective and ohmic n-contacts with low resistivities were developed for the n-$Al_{.58}Ga_{.42}N$ regrown by MBE. Furthermore, a highly reflective MgF_2/Al omnidirectional mirror was developed, which can be used with n-contact microgrid to further enhance the LEE in UV-C LEDs with a transparent tunnel junction.

Committee Co-Chairs:

Prof. James Speck

Prof. Steven DenBaars

Table of Contents

Chapter 1: Introduction

"Let light be made (Fiat lux)"

1.1. AlGaN LED applications at 280-265 nm

Part of sunlight disinfects and sanitizes earth, food, bacteria, and viruses. Disinfecting ultraviolet light (UV-d) (250-280 nm) is an even more extreme part of sunlight and is blocked by the Earth's ozone layer, which allowed life to evolve over the last two billion years. The development of economical, safe, easy-to-use, and energy-efficient technologies for water disinfection and sanitation is an important research goal to improve human health and development. Several types of disinfection technologies have been developed over the last few centuries: thermal (heat above 65 °C), chemical (ozone, chlorine) , and mechanical (membrane filtration). We have known about the lethal impact of UV light on bacteria and viruses since the 1870's [1]. In 1903, Niels Finsen used UV light to treat Lupus (antibiotics luckily replaced UV). It was later found that UV-d light (250-280 nm) causes direct damage to DNA and RNA and disinfect microorganisms with a peak efficacy at 265 nm. Leo Arons invented the mercury gas discharge lamp in 1892, but it was not until the early 1980s, nearly a century later, that mercury discharge lamps were used in water disinfection and sanitization systems.

UV LEDs' compact footprint and integrability will probably cause a large positive change in the frontiers of disinfection and sterilization systems similar to how the move from cathode ray tubes to OLEDs and LEDs in display technologies changed how we interact and use displays. At present, commercial AlGaN LEDs energy efficiency is less than 4.1%; however, in the future, the their expected energy efficiency will be above 90% (akin to InGaN blue

LEDs; refer to Table 1.2) [2,3]. Furthermore, compared to gas discharge lamps such as mercury and xenon, UV LEDs and UV LEDs displays have (refer to Table 1.1 and Figure 1.1):

- a compact footprint
- higher brightness
- adaptable wavelength
- higher disinfection efficacy per joule
- lower operating voltage
- longer lifetime
- simpler driving circuitry
- smart digital on/off capability
- unlimited cycling
- more temperature independent
- mercury-free

Figure 1.1a shows that the power density of typical commercial UV LEDs (at 30 mW) is much higher than a typical low-pressure mercury lamp (LP-Hg, 254 nm) and a typical medium-pressure mercury lamp (MP-Hg, a broad spectrum that includes non-disinfecting wavelengths). Additionally, UV LEDs are more temperature independent (refer to Figure 1.1b) and can be heat sinked more effectively for a stable and robust operation. Figure 1.2 shows the limitations of UV disinfection reactor employing fragile Hg lamp that contain tens of milligrams of mercury. Replacing Hg lamps with UV LEDs displays will improve the reactor efficiency, costs, design, and will have simpler and more robust driving circuits (no ballast). Furthermore, UV LED reactors will not contain mercury, which is a neurological toxin and is costly to recycle.

Table 1.1. Comparison of UV-C and Hg discharge technology

UV light technology	Wavelength (nm)	Voltage (mW)	Power Efficiency	Architecture	Comments
Low-pressure UV mercury lamp (LP-Hg)	254 atomic line with long warm-up time	110-240V and complex circuitry	30%	Cylindrical tubes with low brightness	Hg (20-200 mg) is toxic. Will be banned in the future.
UV LEDs	Adaptable with digital/smart on/off capabilities	6-12V	3-4.1% (LG Innotek)	Verstaile, array of point sources with high brightness	Simpler driving circuits, versatile from, robust, and easier to integrate and control

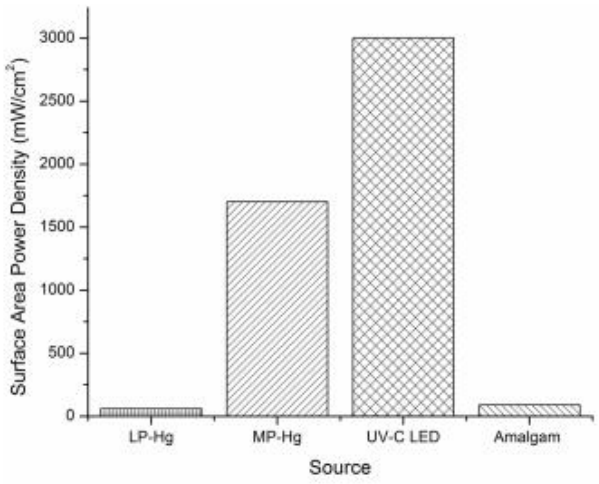

(a) Comparison of power density between a UV LED (30 mW) and a typical medium and a low-pressure mercury lamp.

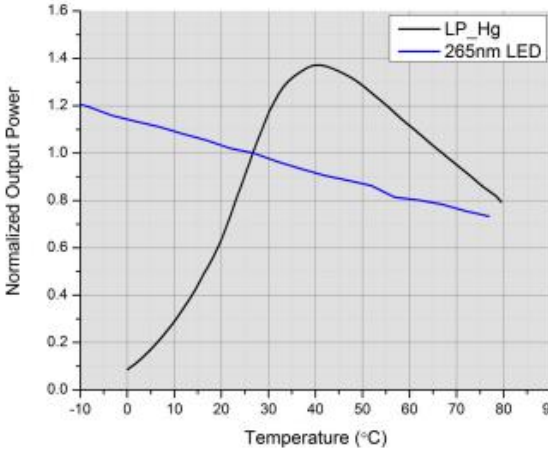

(b) Output power as a function of temperature. For a low-pressure mercury lamp and a 265 nm LED.

Figure 1.1. Advantages of UV LEDs over gas discharge lamps. The surface for the lamp is defined as the area of the glass envelope. The surface area of the LED is defined by the semiconductor chip. Adapted from Jennifer Pagan and Oliver Lawal. “Coming of Age - UV-C LED Technology Update”. AquiSense Technologies.

UV disinfection could increase access to healthy water in many parts of the world, especially because access to healthy water becomes more challenging as population grows and climate warms. According to the World Health Organization, 10,000 people die every day due to unsafe drinking water (e.g., diarrhea causes 1.4 M preventable child deaths per year). Furthermore, anthropogenic mercury accumulates and persists in the ecosystem and food chain, and it has significant effects on human health and the ecosystem. The United Nations' Manitoba treaty aims to phase out the commercial and industrial use of mercury, including in lighting products, such as CFL and UVC mercury-based lamps (20-200 mg of Mercury are needed in a typical LP-Hg lamps).

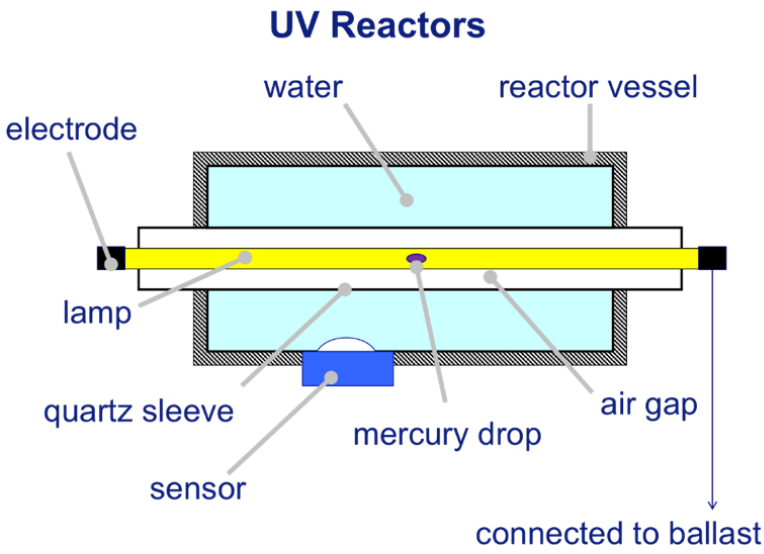

Figure 1.2. Typical Hg lamp-based UV reactor. (Figure is from Michael Templeton, Imperial College London)

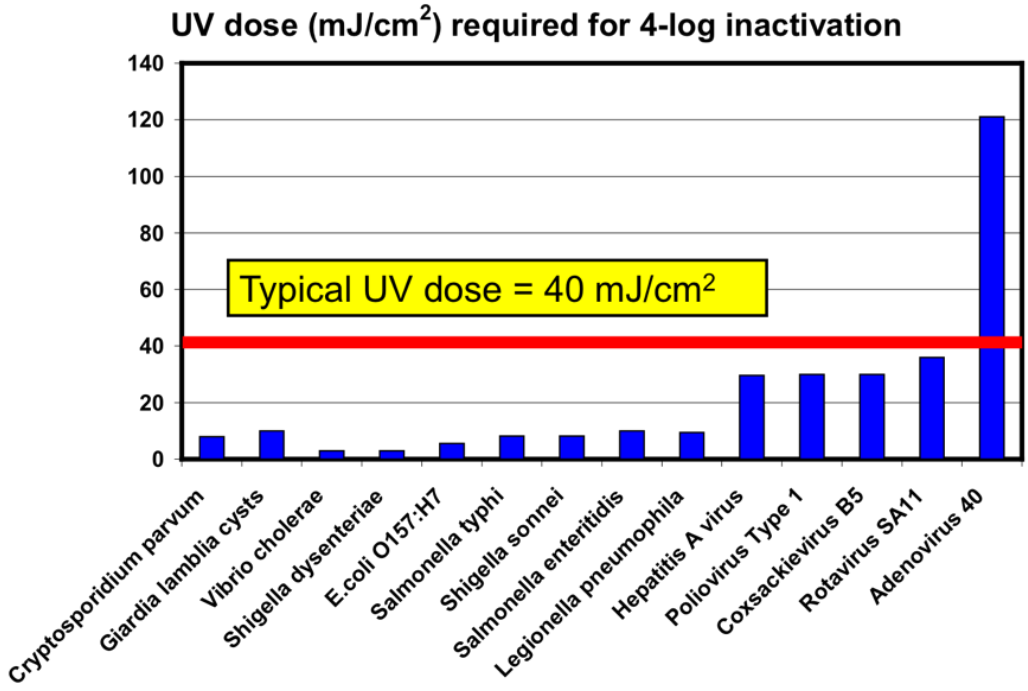

Figure 1.3. The ultraviolet dose required to inactivate common and medically important bacteria and viruses. (Figure is from Michael Templeton, Imperial College London).

Figure 1.3 shows the UV kill dose for typical bacteria. Most medically important bacteria and virus populations are inactivated (a 4-log reduction) with a 40-120 mJ/cm^2 dose. Most microorganisms require a dose of 40 mJ/cm^2, with the exception of a few organisms, such as adenovirus, which requires three times that dose (120 mJ/cm^2). [4–6]

1.2. UV-C disinfection and sterilization

DNA and RNA have peak absorption at 265 nm in water at a pH of 7, as shown in Figure 1.4a. The inactivation of a microbe is broader than the UV absorption of DNA. The germicidal efficacy of UVC depends on the LED spectrum and the microorganism, cellular environment, and so on, as shown in Figure 1.4b, not just the peak wavelength or DNA absorption in a petri dish. Microbes' spectral sensitivity depends on their type and the extracellular/intercellular environment. The absorption of a type of common water bacteria (B.

Subtilis spores, which are an example of a target organism in water disinfection systems) in an aqueous solution is shown in Figure 1.4a. Figure 1.4b shows a commercial UV LED's killing efficiency as a function of the LED spectral distribution (which determines the LED's peak WL and FWHM). While the 265-280 band is of great interest for air and water disinfection applications, the 275-280 nm LEDs are more effective in disinfection on a power-delivered basis with current AlGaN material technology. At 275 nm, the LEDs are more than 100% more powerful than at 265 nm due to better light extraction and contact reflectivity, less p-GaN absorption, better radiative efficiency and injection efficiency. Therefore, based on current AlGaN material technology performance, it is best to focus on UV emitters in the 270-280 nm range to deliver maximal LED performance and germicidal power efficiency.

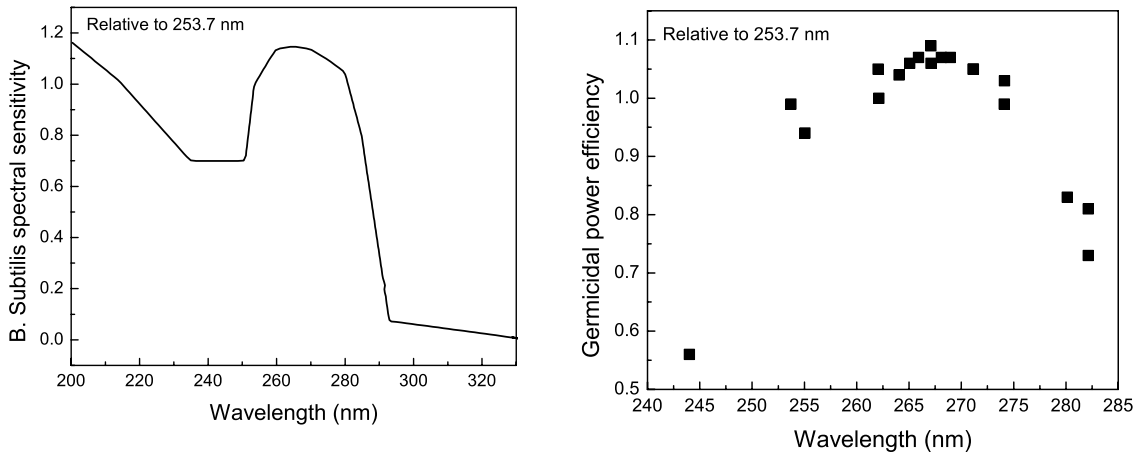

(a) (b)

Figure 1.4. In a manner akin to a human eye's cone cells' sensitivity to the visible spectrum, bacterial vitality is sensitive in the 250-280 nm range. (b) This plot shows the germicidal power efficiency of a common type of bacteria found in unhealthy water (B. Subtilis) using ÖNORM, the Austrian National Standards for a UV biodosimeter. The germicidal power is estimated by the convolution of the microbe's spectral sensitivity with a full-spectrum UV LED. The target wavelength for UV LED disinfection is 265-280 nm. (Data is from Crystal IS.)

1.3. UV-lumens or disinfectors?

As a measure of the total lethal UV light emitted by a source, we could use a metric similar to lumens, which quantify a human eye cone cells' sensitivity to a spectrum of light, unlike the term, radiant flux, which captures all electromagnetic waves that could be unimportant in certain contexts. The human eye is spectrally sensitive to light in the 390-700 nm range, and microorganisms are sterilized by light in the 250-280 nm range of UV light. A human eye's vision cells determine its luminosity functions (LF) as a function of light wavelength λ. The human eye has two main LFs: the photopic LF for everyday light levels which is used in the international commission on illumination (CIE) 1931 and 1978 standards, and scotopic LF for low light levels which is used in CIE 1951. Similarly, defining disinfection functions $DF_{pathogen}(\lambda)$ for a group of pathogens using data, as shown in Figure 1.4b might be useful to professionals in the field.

The luminous flux Φ_{L} (lumen) represents the total radiant power perceived by a human eye. The luminous flux accounts for the eye's spectral sensitivity by weighting the power at each wavelength with a normalized luminosity function $\mathrm{A_{eye}}\ LF_{eye}(\lambda)$. For a light source with spectral radiant flux $\Phi_{\lambda}(\lambda)$ (W/nm), the luminous flux Φ_{L} (Lumen) is given by the inner product of $LF_{eye}(\lambda)$ and $\Phi_{\lambda}(\lambda)$:

$$\Phi_{\mathrm{L}} = \mathrm{A_{eye}} \int_0^{\infty} LF_{eye}(\lambda)\ \Phi_{\lambda}(\lambda) d\lambda$$

Where $\mathrm{A_{eye}}$ is a lumen–watts conversion factor that normalizes $LF_{eye}(\lambda)$ to unity at its 555 nm peak (555 nm as measured in air). $A_{\mathrm{eye}} = 683.002\,\frac{Lumen}{W}$ because 1 lumen of a light-source is defined as a the total radiant power of 1/683 W at 540 THz (i.e., 555.016 nm). Similarly, for

a light source with spectral radiant flux $\Phi_\lambda(\lambda)$ (W/nm), the disinfection flux Φ_D (Lethal Lumen, or Disinfection) is given by the inner product of $DF_{pathogen}(\lambda)$ and $\Phi_\lambda(\lambda)$:

$$\Phi_L = A_{pathogen} \int_0^\infty DF_{pathogen}(\lambda)\, \Phi_\lambda(\lambda) d\lambda$$

Where $A_{pathogen}$ is a lethal-lumen–watts conversion factor that normalizes the disinfection function for a pathogen $DF_{pathogen}(\lambda)$ to unity at its 265 nm peak (265 nm as measured in air).

1.4. UV-C market

The main markets for UV LEDs-d (250-280 nm) are in water and surface disinfection systems, DNA and protein assays, medical diagnostics systems, and possibly optogenetics. The market research firm Yole Développement reported that the market share for UV-C LEDs from the UV-illumination market increased from 8% LEDs in 2008 ($240M) to 25% LEDs in 2018 ($810M). It expects the UVC disinfection market to have an annual growth of ~40% during the next five years in various biotechnology applications, including disinfection and instrumentation. Companies such as UV-Di, Tru-D, and Zynex are commercializing UV systems with decades-old technologies, such as gas-discharge technology, including mercury and xenon discharge lamps. A few companies, such as Aquisense, started to integrate solid-state UV LEDs into new novel water and food disinfection systems. In the next section, I will briefly discuss a potential markets for 265-280 nm LEDs.

1.4.1. Hospitals

Hospitals have recently begun to seriously consider UV disinfection as an additional disinfection/sterilization step [7–10]. Hg lamps were invented a ~ 100 years ago and have been used in water and air disinfection systems since the 1980s but have not been used in hospitals

until recently; this is perhaps because of the complexity of powering and monitoring gas discharge lamps, which complicates regulations. Mercury and xenon UV systems are now used in thousands of hospitals in the US and are expected to be a common technology in all hospitals in the future (operating rooms, high-risk units, patient units, HVAC systems, etc.). Researchers from Mayo Clinic reported a 30% reduction in C. Diff, which is a challenging drug-resistant bacteria that causes diarrhea and is also resistant to many chemical surface treatments. Other clinical studies have reported a 25% reduction of drug infection cases after the application of an additional step of UV disinfection [10]. The typical 6-log kill dose for most bacteria and viruses is below 40 mJ/cm^2, with some organisms requiring higher doses (refer to Figure 1.3). For example, the Adenovirus 40 requires a dose of 120 mJ/cm^2. [4,5]

1.5. Introduction to AlGaN LEDs

A light-emitting diode is a device that comprises an active material sandwiched between a p-type and an n-type region. AlGaN is grown at higher temperature than GaN (1050-1200 °C), relatively lower III/V rations (100:1100) and lower pressure (< 100 torr) to reduce parasitic TMA reaction with NH_3 which results in TMA-NH3 adduct formation [11]. When a positive bias is applied across the diode, electrons and holes can recombine radiatively to emit light at a spectrum determined by the active region, multi-quantum wells (MQWs). Due to the difference in the refractive index and the necessity of momentum conversation, most of the photons generated by the active layer will be trapped inside the crystal, by total internal reflection (TIF). Additional chip processing is needed to increase the LEE by increasing light scattering, reducing the effective refractive index, and by chip-shaping. UV LED InAlGaN-based active layers are typically grown on sapphire, and AlN substrates.

Due to the lack of UV-C (200-280 nm) transparent conductors, UV-C LEDs are flip-chipped onto a new thermally conductive substrate and emit through the substrate's surface and side walls. Since UV-C LEDs are limited by light extraction efficiency (LEE), our approach was to find a good substrate on which to grow the AlGaN LEDs and then flip-chip (FC) the LED but remove the substrate. This approach led to high LEE UV-C LEDs.

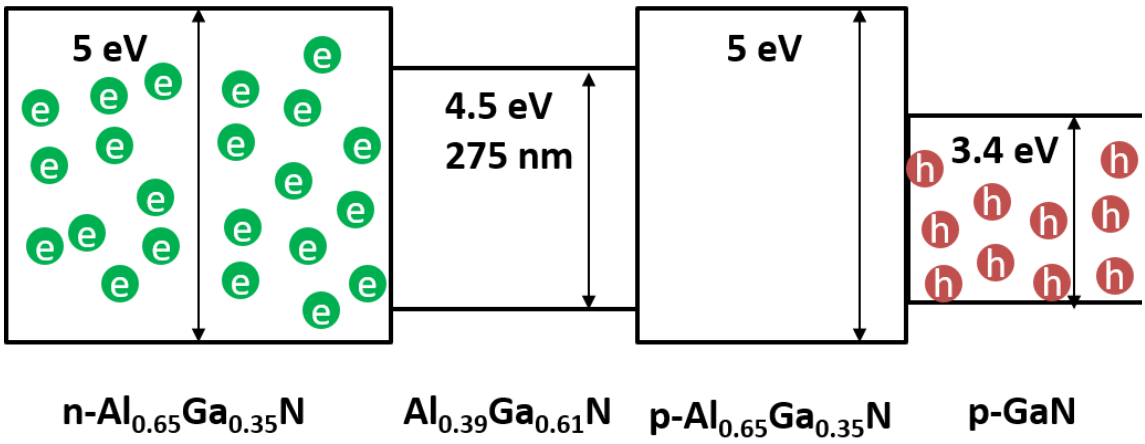

Figure 1.5 The bandgaps of AlGaN layers needed for 275 nm LEDs.

Figure 1.5. shows a bandgap of the layers needed for a UV LED. The active region consists of several barrier/well regions to increase the likelihood of electron-hole recombination, yet most of the emission seems to come from the first well.

The electron-hole wavefunction confinement in the MQWs is reduced by the electric field inside the wells as described by quantum-confined stark effect (QCSE). In AlGaN LEDs, to help confine carriers, thick barriers are used which results in little coupling between the wells, and the well closest to the p-AlGaN dominate radiative emission. Increasing the aluminum atoms fraction in the MQWs' barriers and in the LED cladding, helps confine carriers, reduces light absorption and applies a compressive stress on the wells, which increase TE emission. To

reduce light absorption in the barriers and cladding layers to below 10^3 cm^{-1} [12,13], their energy bandgap need to be 0.5 eV higher, to reduce light absorption.

The band gap of an $Al_xGa_{1-x}N$ semiconductor can be interpolated from the energy gap of AlN and GaN by Vegard's law with the addition of a bowing parameter B_g:

$$E_{Al_xGa_{1-x}N} = x\,E_{AlN} + (1-x)E_{GaN} + B_g x(1-x)$$

Researcher reported numerous bowing parameters for AlGaN prepared at different growth conditions. The value of bowing parameter reported in the literature varies depending on the growth conditions, processing method, and the considered AlGaN alloy range [14]; researcher reported values from - 0.8 eV to 2.6 eV [14,15], however many more recent experiment reported $B_g = 0$ [16,17].

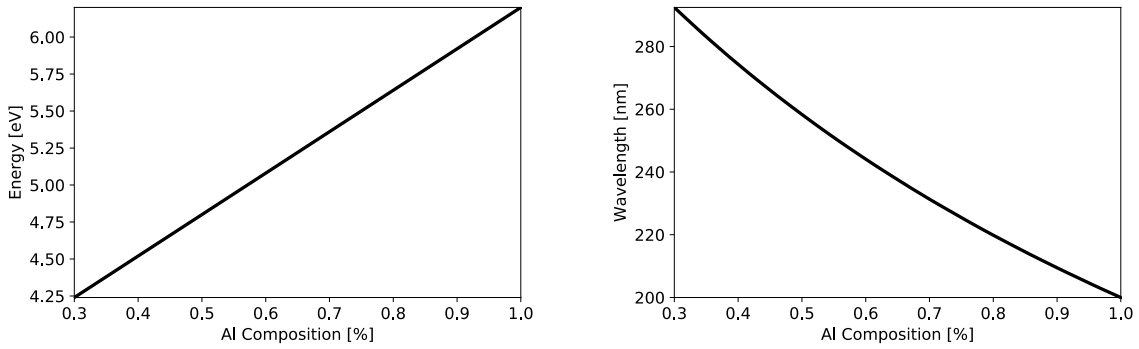

(a) AlGaN energy gap as function of Al composition

(b) AlGaN wavelength as function of Al composition

Figure 1.6. Band gap of a AlGaN interpolated from the AlN and GaN energy gaps calculated using Vegard's law and assuming a bowing parameter, $B_g = 0$ [16,17].

Table 1.2. UVC LED device characteristics compared to blue LEDs

Parameter	Blue InGaN LEDs	Best 280-260 nm LED in the literature	TFFC UV LED (278 nm) in this work
Internal quantum efficiency (IQE)	>95%	60%	6%
Electrical injection efficiency (EIE)	>95%	80%	
Light extraction efficiency (LEE)	>90%	16% without encapsulation 20% with encapsulation (limited lifetime)	30% without encapsulation (estimate)
Electrical efficiency (EE)	>95%	30-90% depending on trade-offs with EQE	33% because of high n-contact resistance
External quantum efficiency (EQE)	>80%	20% (19% at 50 mA)	1.8 % at 95 mA
Wall plug efficiency (WPE) or power conversion efficiency (PCE)	>80%	10%	0.6 % at 95 mA

AlGaN LED researchers have made significant progress in the last 30 years or so [18–34]; currently, however, applications and market for UV LEDs are relatively limited because of low power conversion efficiency (PCE) (also known as wall-plug-efficiency [WPE] is low) The best commercial LEDs reports 2-4% PCE; however, in the future, UV LEDs are expected to be as efficient as blue LEDs (refer to Table 1.2). The main reason for their low PCE is their low LEE (refer to Table 1.2). Improving the LEE was one of the main focuses of this dissertation by developing thin-film flip-chip (TFFC) UV LEDs that are grown on SiC (refer to Figure 1.8).

AlGaN LEDs technology is limited by LEE [35–45] for five main reasons. 1) The large ionization energy for the p-type dopant (Mg) in AlGaN results in a resistive AlGaN:Mg layer. Therefore, a highly absorbent layer of p^+-GaN is used as a supplier of holes and to make an ohmic p-contact; the undoped GaN absorption coefficient was measured to be about of $1.5x10^5$ cm^{-1} at 275 nm [46]. 2) The lack of a UV-transparent current-spreading layer over p-AlGaN, such as indium tin oxide (ITO), which is used in blue LEDs, necessitates the use of a FC LED

architecture with a reflective p-contact. 3) The reflectivity of the best p-contacts is limited to ~70-85%, below 280 nm [47]. 4) The light from the AlGaN MQW emitters at these wavelengths is 40-50% transverse magnetic (TM) polarized depending on the emission wavelength and the strain of the MQWs [40,41,48,49]. TM emission propagates laterally, parallel to the LED emission surface, and is harder to extract than transverse electric emission (which propagates vertically toward the surface); for example, Ryu et al.'s studies of LEE in LEDs using finite-difference time-domain (FDTD) indicated that the LEE of TM emission is >10X less efficient than the LEE of transverse electric (TE) emission in typical volumetric FC LEDs [39] (in volumetric FC LEDs, light has to travel through the transparent growth substrate) [38,39]; however, they estimated that the LEE of TM emission in a textured thin-film LEDs is >6X higher than in volumetric AlGaN FC-LEDs [39]. 5) There is a lack of encapsulants with a high refractive index that are UV transparent and stable [50–54].

1.5.1. What is the best substrate to process high LEE TFFC LEDs?

One of the reasons the LEE is limited is that the LEE of TM is more challenging, especially from bulk FC LEDs. Our approach was to consider UV thin-film LEDs, which are better suited, to increase the LEE of both emissions: TE and TM. Currently, the best substrates used for AlGaN LEDs research are sapphire substrates and AlN substrates (refer to Figure 1.7 and Table 1.3). SiC substrates have very low lattice mismatch but it's use have been largely overlooked except for early attempts by UCSB [21,24,55–58] and other limited attempts [59,60]. The main reason SiC was overlooked is because it is absorbing yet this is not an issue if the substrates are processed into thin-film LEDs (as shown in Figure 1.8) which is challenging for AlGaN LEDs grown on Sapphire, AlN substrates and GaN substrates (see Table 1.3). Another

limiting reason was that thick AlN growth (1 >μm) on SiC suffer tensile stress that results in cracks; however, this issues has been resolved by high temperature nitridation of SiC under NH_3/H_2 [61]. The origin of the AlN tensile stress on SiC (despite a larger lattice constant for AlN) is bit unclear but is possibly attributed to islands coalescence [62,63], threading dislocations inclination [64], or thermal coefficient of expansion (TCE) mismatch [58].

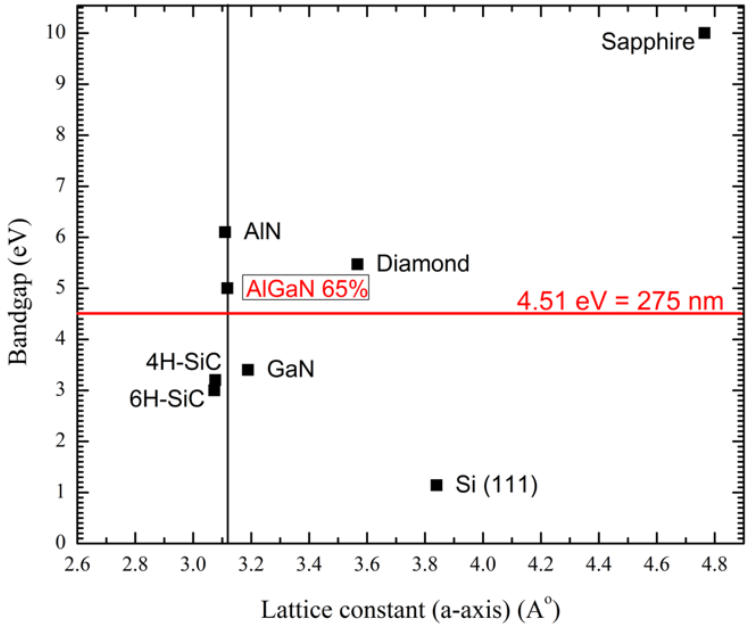

Figure 1.7. Substrate selection for 275-nm UV LEDs. The global AlGaN UV LED research community has invested heavily in sapphire and AlN substrates. SiC substrates were largely ignored because they are absorbing, yet high-extraction-efficiency thin-film LEDs can be made from AlGaN LEDs grown on SiC.

Table 1.3. Comparison between different substrates technologies for AlGaN LEDs.

Substrates for AlGaN devices	**Transparent**	**Thin-film process ?**	**TDD**	**AlN Epi stress**	**Disadvantages**
AlN grown by Physical vapor transport (PVT)	Defect absorption (~10^3 cm^{-1}) at 264 nm (4.7 eV) [65]	PEC etching in semi-polar planes	1×10^5 cm^{-2}	Compressive for AlGaN epi	Absorptive, expensive
AlN grown by Hydride vapor phase epitaxy (HVPE)	Yes	PEC etching in semi-polar planes	1.5×10^8 cm^{-2} [66]	Compressive for AlGaN epi	expensive
Sapphire	Yes	Laser lift off	$<8\times10^8$ cm^{-2}	Compressive	Has a large lattice mismatch (13.3%) .
Bulk GaN	No	PEC lift-off [67–69]		Tensile	AlN requires >1200 °C growth temperature. GaN decomposes
Si	No	SF_6 etching	Claimed to be $< 10^9$ cm^{-2} (cross-sectional TEM)[44]	Tensile	AlN requires >1200 °C growth temperature. Si decomposes
SiC	No	SF_6 etching	$<8\times10^8$ cm^{-2} [25] $4x10^8$ cm^{-2} (300 nm thick AlN by MBE) [64]	Tensile (cracks from thick AlN epi are eliminated by high temperature nitridation of SiC [61])	

1.6. Synopsis of the Dissertation

In this dissertation, we discussed how we developed high LEE thin-film LEDs grown on SiC. The thin-film FC schematics are shown in Figure 1.8. This design enhances the LEE by reducing the effective refractive index of the roughened AlN and scattering light. Moreover, it uses a highly reflective p-contact mirror with as little p-GaN as possible. Additionally, it

eliminates n-contact shadowing and wire bonding shadowing. It also has lower thermal resistance and can be integrated into high-density chips without wire bonding.

We demonstrated the best UV LEDs grown on SiC substrates. Moreover, the LED performance results were better or competitive with the best UV LEDs reported in the literature (grown on sapphire or AlN substrates) in some key measures. For example, the LEE of TFFC LEDs (the 278 nm LEDs) is estimated to be the highest reported LEE for UV LEDs. Moreover, Figure 1.10 shows that the 265 nm LEDs have the third highest reported EQE, and the 278 nm LED had EQE ~ 2%, despite the low IQE active region.

The summary of our progress is shown in Table 1.4 and Figures 1.9 and 1.10. We demonstrate a simple and flexible route for improving AlGaN LEDs' power conversion efficiency (PCE) and high external quantum efficiency (EQE). Although we conducted the demonstration on LEDs with area limited to ~ 0.1 mm^2, we showed that the LED area is scalable to larger LEDs areas (> 1 mm^2).

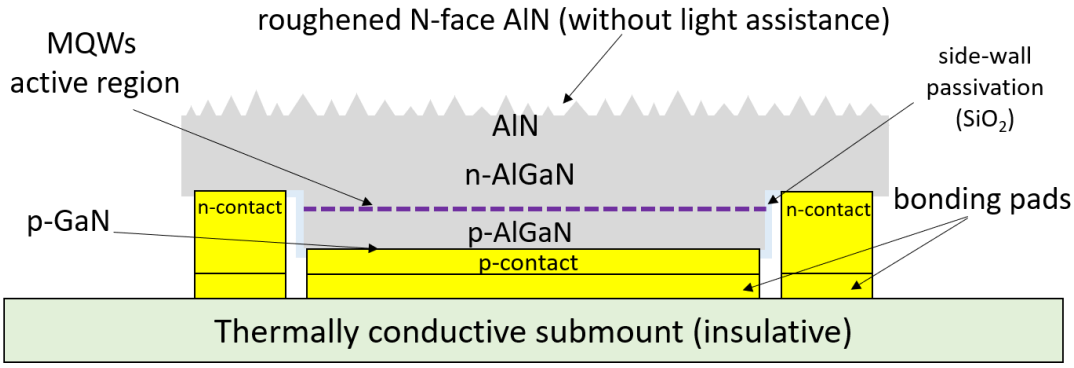

Figure 1.8. Sketch for thin-film flip-chip (TFFC) LED with high LEE.

In Chapter 2, we discuss how the epi is transferred onto a new substrate (sapphire, Si, SiC, and a flexible substrate) and how the SiC growth substrate is removed. We discuss the

development of a highly selective etch to remove SiC and the use of an AlN etch-stop layer (that was grown by Humberto Foronda on Veeco MOCVD reactor).

In Chapter 3, we discuss KOH roughening of exposed and pristine nitrogen-faced AlN without light assistance. We show that the photoluminescence (PL) of MQW wells in an n-i-n structure can be enhanced by roughening if we use a highly reflective p-contact by 3.9X. We also discuss the mechanism and etch rate differences between the KOH roughening of N-face GaN and N-face AlN, with and without light assistance. We discuss how KOH temperature impacts the roughening of the cones sizes.

In Chapter 4, we discuss the development of a process to make thin-film flip-chip (TFFC) microLEDs (297 nm) with high LEE and low voltages. Hexagonal cone generation by KOH was used to roughen the exposed thin film LED surface, and the power and LEE increased by 2X. We indicate that this is the first time KOH roughening of an AlN surface was used to enhance the light extraction in a UV LED. We discuss how the KOH induced the cones density affects LEE.

In Chapter 5, we discuss the development of a process to make TFFC LEDs (278 nm and 265 nm) with 70-80X higher power density and 50% higher LEE than the LEDs developed in Chapter 4, which had a highly dislocated AlN template. The LED voltages were high because our n-AlGaN sheet resistance was 60 mΩ-cm. We (with Abdullah Almogbel, Chris Zollner, and Mike Iza) reduced the n-AlGaN sheet resistivity to 10 mΩ-cm but this was not incorporated into an LED. We showed (with Jianfeng Wang, who grows AlGaN with MBE on AlN/SiC templates grown by MOCVD) that with the use of V-based contacts, we can have n-contact specific resistivity in the 10^{-6} Ω-cm range.

Table 1.4. Summary of main dissertation milestones

Milestone	Main Achievement
Zero generation devices 2015	Developed a process for AlN/AlGaN epi transfer to fabricate high LEE AlGaN TFFC LEDs. It was demonstrated to enhance light extraction in MQWs PL by 4X with roughening and using a p-contact mirror (.2 nm Pt/Al/Ni/Au) with 90% reflectivity. (part of the increased PL enhancement was due to increased pumping of MQW by laser)[70]. [70][71][67][67][67]
1st generation LEDs	**310-298 nm LEDs** [71,72]
2016	• Developed a Ti-based ohmic n-contact process for n-$Al_{0.52}Ga_{0.48}N$ grown by MOCVD. • LEE was enhanced by 2X after KOH roughening [72] • Developed a highly reflective UV mirror (>95.5% for vertical incidence, and 100% for total internal reflection rays) made from MgF_2/Al which can be employed in TJ-UV LEDs. • TFFC UV LEDs with high voltage efficiency.
2nd generation LEDs	**280-265 nm LEDs** [25,61,72–74]
2017	• High-temperature anneal to remove cracks from AlN with low TDDs ($<10^9$ cm^{-2}) [61] • Developed V-based n-contact process for n-$Al_{0.6}Ga_{0.4}N$ (n-contact process results in non-ohmic contact on n-$Al_{0.6}Ga_{0.4}N$ grown by MOCVD; however, results in ohmic contact on n-$Al_{0.58}Ga_{0.42}N$ grown by MBE) • LEE was enhanced by 3X after KOH roughening [73,74]
Future work: **3rd generation LEDs**	• Reduce forward voltage The 2017 LEDs suffer from high voltage because of n-contact resistance. In early 2018, we tried to reduce the voltage but the improved new n-AlGaN grown by Abdullah Almogbel and Chris Zollner were not incorporated into the LEDs because of reactor issues. • Improve LEE to > 80% Employ transparent junction, current spreading, and highly reflective mesh contacts to increase LEE. The TJ LEDs we attempted with Jianfeng in 2018 but EL wasn't measured. • Improve bonding Replace Au-Au with better bonding to improve thermal sinking and reliability. For example, use eutectic (e.g. InAu or sputtered Sn/Au) mixtures for low-temperature bonding to improve yield and contacts conformity.

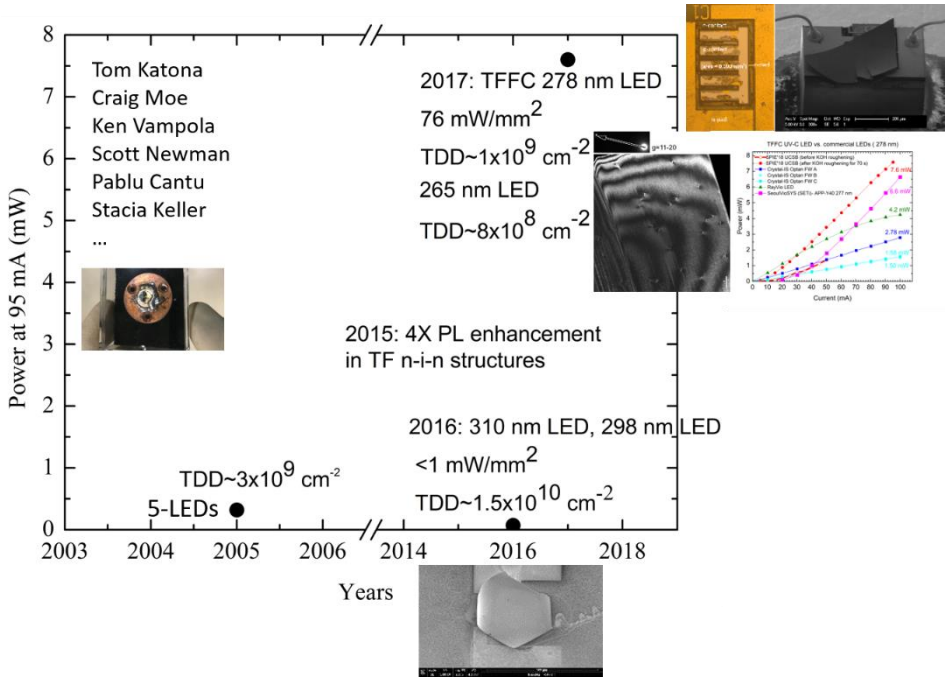

Figure 1.9. Summary of SiC-based UV LED development at UC Santa Barbara.

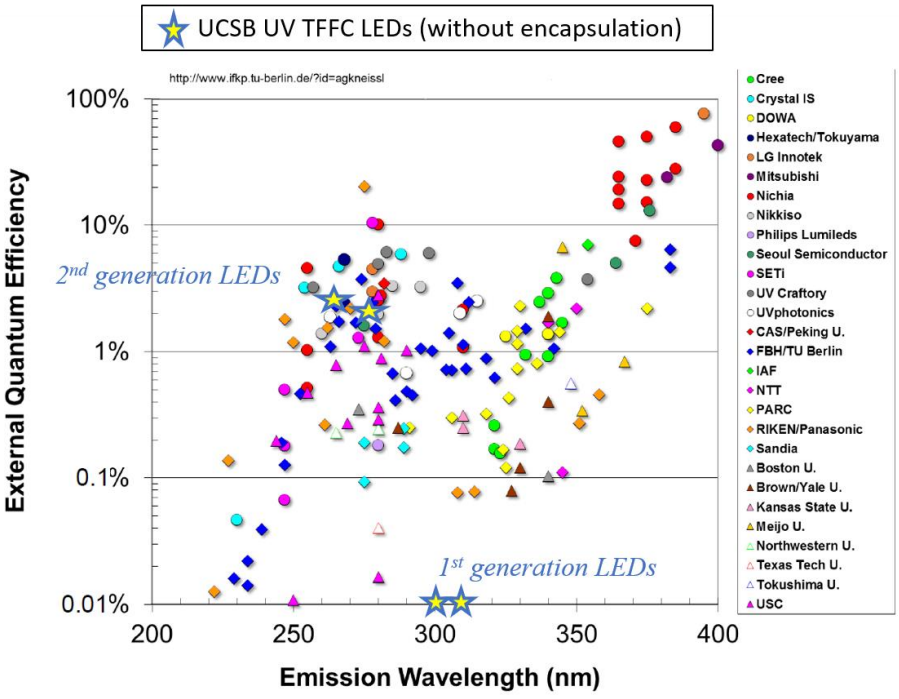

Figure 1.10. Summary of reports for External quantum efficiencies (EQE) for III-nitride based LEDs. There is large drop in EQE for LEDs below 360 nm because of limited because of limited light extraction efficiency (LEE). UCSB results are based on TFFC LEDs grown on SiC whereas all of the other reports are for FC bulk UV LEDs grown on Sapphire or AlN substrates. (Figure is from Michael Kneissl, TU Berlin; June, 2018).

Chapter 2: Thin-Film Flip-Chip LEDs Substrate Removal Process

"You can know the name of a bird in all the languages of the world, but when you're finished, you'll know absolutely nothing whatever about the bird... So let's look at the bird and see what it's doing -- that's what counts."

Richard Feynman (1918 - 1988)

In this chapter, we demonstrate epitaxial transfer and heterogeneous integration technology of AlGaN and AlN substrate into a new carrier. We transferred AlN and AlGaN into Sapphire, Si, SiN/SiC and insulative SiC substrate via metal bonding. Furthermore, AlN was observed to bond into O_2 cleaned Sapphire surface via covalent bonding. AlGaN and AlN epi-transfer and heterogeneous integration technology can be employed to improve the LEE in AlGaN light-emitting diodes (LEDs), the performance of photodiodes (PDs) [75], high electron mobility transistors (HEMTs) [76,77], bulk acoustic resonators (BARs) [78–80] and high aspect ratio SiC microstructures and devices [81–84].

The basic process flow for the TFFC LEDs process is shown in Figure 2.1. In this chapter, we discuss wafer-to-wafer bonding, and thinning and developed a high-reliability SiC substrate removal process with no micro masking defects, precise epitaxial control, and without degrading the plasma etching system health (refer to Tables 2.1, 2.2, 2.3 and 2.4 for a summary of substrate removal process parameters parameters). This was not possible without building on the work that was done 10-15 years ago at UCSB [55–58].

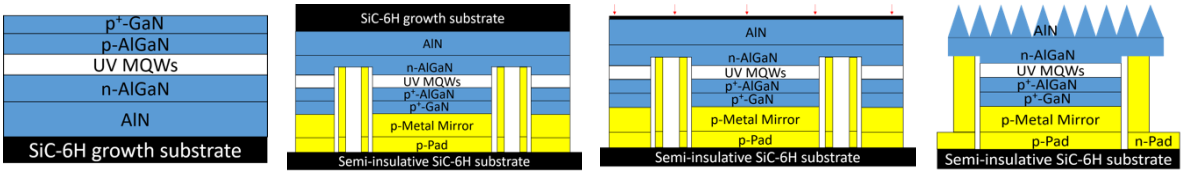

(a) UV LED grown on SiC

(b) wafer-to-wafer FC bonding

(c) thinning and etching of SiC with selective SF_6 plasma

(d) TFFC LED singulation and KOH roughening

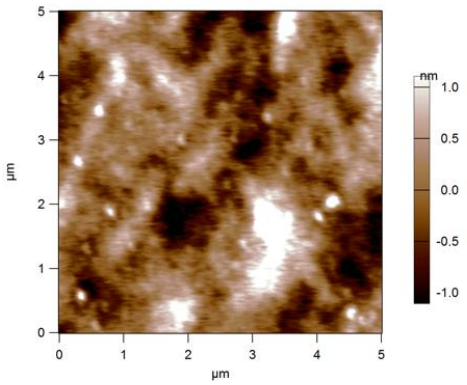

(e) AFM image of the surface of exposed AlN surface as (roughness ~0.6 nm) after complete etching of SiC in step (c).

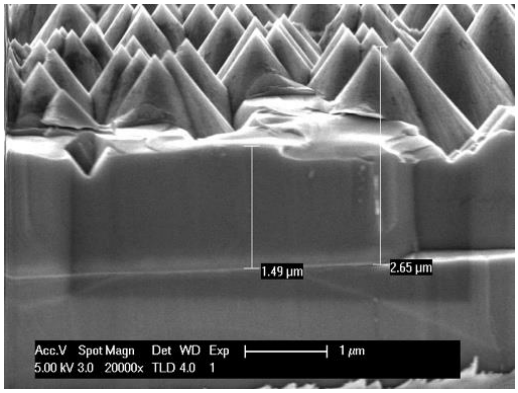

(f) Cross-sectional SEM image of nano-sharp hexagonal pyramids that are produced after KOH roughening of N-face AlN in step (d).

Figure 4. Process flow (a-d) demonstrate UV-C thin-film flip-chip (TFFC) grown on SiC and (e) shows AFM of exposed AlN surface after completing SiC growth substrate removal in step (c). The hexagonal pyramids shown in (f) expand the effective angle of the light-extraction-cones. Figure adapted, with permission, from Ref. [25].

2.1 Wafer-to-wafer bonding

After processing the LEDs with n- and p-contacts, the LEDs were bonded to a new thermally conductive carrier as shown in Figure 2.1b. The bonding has four requirements: 1) strong mechanical adhesion at the device operation temperature and during the fabrication process; 2) low temperature bonding so the p-contact reflectivity does not degrade; 3) low

electrical contact resistance; and 4) low thermal impedance, and sufficient rate of heat transfer (heat sinking). Although, Sn/Au is commonly used in industry satisfy these conditions, Au-Au is simpler, as Au is simpler to deposit than Sn/Au eutectic at UCSB cleanroom, however, Sn/Au and InAu bonding could provide better adhesion and better heat sinking.

Thermocompression bonding relies on force and temperature. The LED results in this dissertation were bonded by Au-Au thermo-compression bonding, however, I will discuss briefly our experiments with three types of bonding: Au-Au bonding; InAu eutectic bonding; and liquid epoxy bonding that only conducts vertically. Figure 2.3 shows wafer-to-wafer bonding development with three type of bonding: Liquid epoxy polymer (LEP) that consists of a matrix of Ni/Au particles embedded in an epoxy (Dexerials, Inc.); In-Au eutectics, and Au-Au thermocompression bonding. The LEP bonding (refer to Figure 2.3a) was a thermally conductive epoxy that conduct only vertically (Dexerials, Inc) because it was made from a low density matrix of Ni/Au particles in an epoxy) but could not be implemented because the liquid bond was too thick and not uniform after curing. (see Fig. 2.2b). The Au-Au bonding (see Table 2.1 and refer to Figure 2.3g)) provided acceptable performance in terms of preserving the p-mirror reflectivity which contributed to high LEE results from the LEDs. We attempted to use Au-In (refer to Figures 2.3b and 2.3c) to improve the bond strength. In/gold (90%/10%) melts at 180 °C before bonding, mix to (50%/50%) In/Au to melt at 400 °C after bonding). However, the Au-In bonding conditions attempted (5 min) were too long and the bonding caused shorting (refer to Figure 2.2a). Al-Al bonding is also an attractive choice to protect the p-contact reflectivity but were not attempted because they require double the maximum pressure provided by the Fintech bonder [85].

Table 2.1. Summary for Au-Au thermo-compression bonding characteristics with Finetech FC bonder.

Bonding type	Temperature and Force	Sample size
Au-Au thermo-compression bonding	To minimize p-mirror damage: 1-275 ºC, 5 min (30 N/cm^2) 2- 200 ºC, 2 hr (300 N/cm^2 with graphite fixture)	0.3x0.3 cm^2 to 1.5x1.5 cm^2

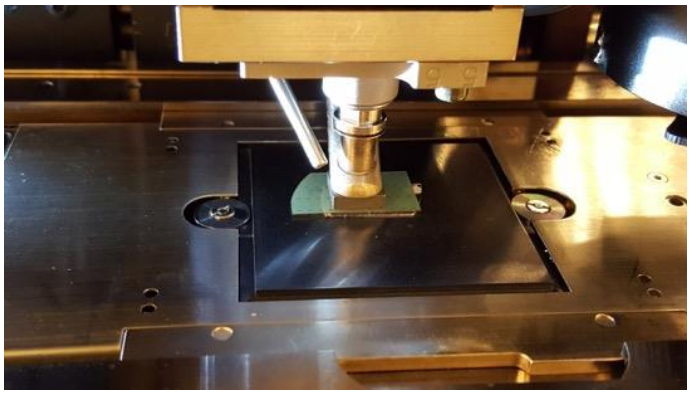

(a) Finetech flip-chip bonder

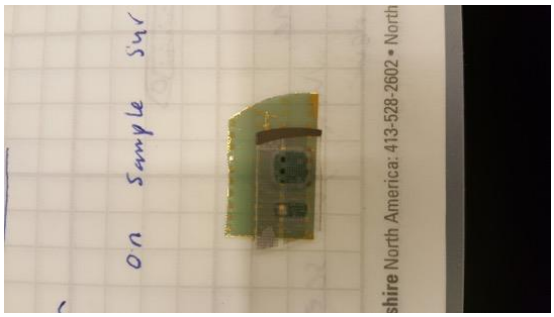

(b) SiC substrate with processed AlGaN/AlN/SiC structure bonded to a transparent sapphire submount (top).

Figure 2.2. Aligned wafer to waver bonding with Finetech flip-chip bonder.

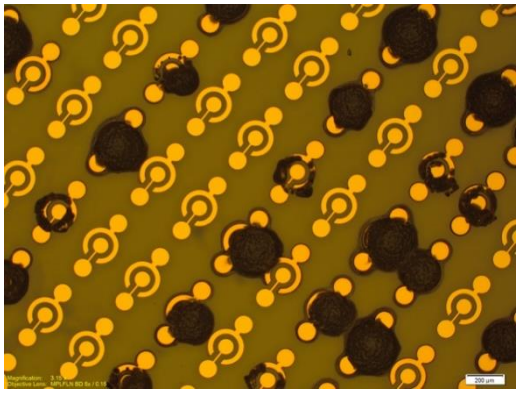

(a) Unsuccessful bonding with liquid epoxy than only conducts vertically (Dexerials, Inc.). The LEP Ni/Au particles epoxy (Dexerials, Inc.) was thick and non-uniform after bonding.

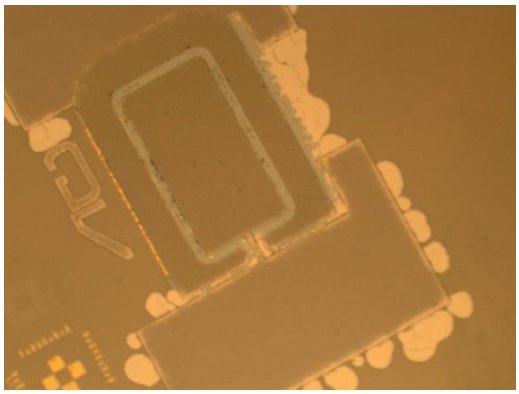

(b) Unsuccessful bonding with InAu at 200 °C for 5 min.

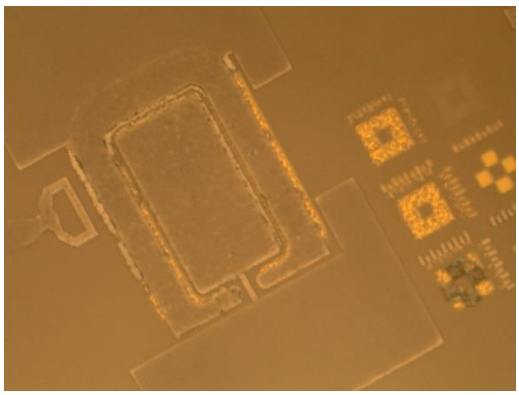

(c) Unsuccessful bonding with InAu at 200 °C for 5 min which caused shorting. Bonding might be successful if was done for 30 sec with thinner films of In and Au. Bond eutectic uniformity could be improved if deposited with sputtering rather than e-beam.

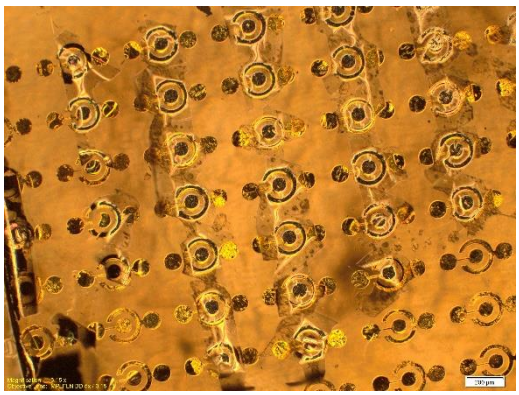

(d) Early development microscopic pictures for Au-Au bonding with circular LED structures. The Au-Au bond does not get etched in SF_6 at low bias, but can get covered with black residue if the etch took too long.

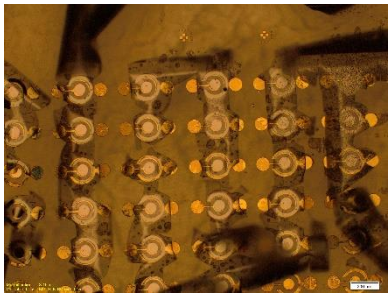

(e) Early development microscopic pictures for Au-Au bonding with circular LED structures. The SiC pillars can be removed completely with an optimized SF_6 etch and optimized process control (carrier wafer choice, etch chamber and carrier wafer seasoning pre-etch).

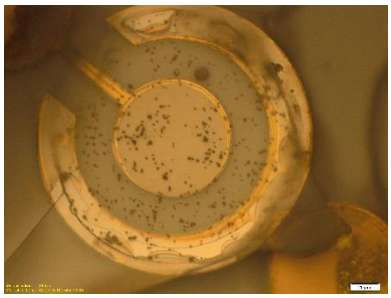

(f) Early development microscopic pictures for Au-Au bonding with circular LED structures. The SiC pillars can be removed completely with an optimized SF_6 etch and optimized process control (carrier wafer choice, etch chamber and carrier wafer seasoning pre-etch).

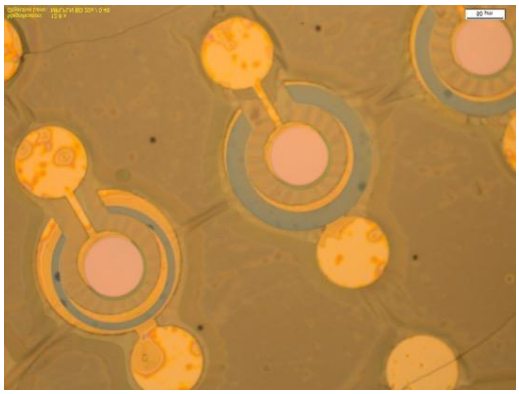

(g) Example on *successful* Au-Au bonding without SiC pillars or micromasking defects. Additionally, it was observed that the exposed N-face AlN could bond to the sapphire (submount in this example) without metal, through covalent bonding. Furthermore, mechanical wrinkling modes was observed in the AlN/AlGaN over the gap between the n-pad and p-pad.

Figure 2.3. Optical microscopes images for the surface of thin film LEDs show bonding results for these types of bond after completing the SiC substrate removal.

2.2 *SiC substrate thinning characteristics*

The importance of thinning the substrates lays in two goals: 1) lapping is faster than etching and thus can reduce ICP etch time; and 2) assist in the complete elimination of pillars with the as removing SiC pillars is easier in 100 µm thick substrate than in 250 µm thick substrate. In this work, it was observed that the pillars can be removed completely when lapping and then etching. Complete elimination of pillars was possible when thinning the sample to 150 µm or less. We found that if all the 250 µm of SiC substrates were ICP etched (without lapping), there were some pillars left (~ 1-2 pillars per LED) even after using the optimized etch process to remove them.

A vertical grinding machine (NV 6200A, Nano Factor. Refer to Figure 2.3) and South Bay Technologies Multipurpose Lapping System (Model 920. Image is not shown) for lapping were used for lapping. Both systems led to satisfactory results; however, the thinning with the vertical grinding machine took about an hour, while the thinning with the South Bay Technologies tool was much more flexible, as the lapping rates could be adjusted to be much higher using the appropriate lapping pads. Using CMP to smoothen the surface before etching was not needed.

A summary of thinning parameters in the South Bay Technologies tool is shown in Table 2.2. Typically, the SiC growth substrates were thinned from 250 µm to 75 µm by lapping with a Dia-Grid Diamond Disc (Allied High Tech Products, Inc.). The water-cooled lapping tool had a lapping rate of 50 µm/hr when using 15 µm grit diamond discs and a lapping rate of 29 µm/hr when using 9 µm grit diamond discs. The manufacturer estimates that the lapping damage generated by lapping with a 9 µm grit was approximately 3 x 9 µm = 27 µm, which

avoids damage to the active region. The mechanical lapping with South Bay Technologies systems yields a total thickness variation (TTV) of about 15-20 µm across a quartered 2-inch wafer.

(a) vertical grinding machine (NV 6200A, Nano Factor

(b) The sample is mounted flat on ceramic mount for the vertical grinding machine.

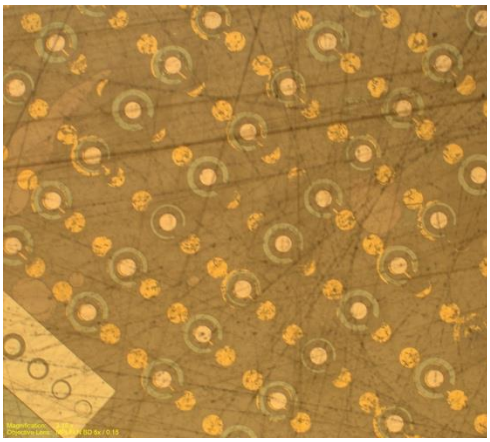

(c) Micrograph of a thinned SiC surface.

Figure 2.4. (a) one of the mechanical thinning systems used to the SiC substrates (Nanofactor Grinding setup). (b) submount for grinding setup. (c) micrograph for the surface of grinding setup on a processed test structure AlGaN/AlN/SiC that mimics an LED.

Table 2.2. Summary of lapping parameters used to mechanically thin SiC substrate with 9 µm diamond grid disc.

Lapping settings	Lapping etch rate
CCW 5 wafer rotation/ min 6 pad rotation /min	25-30 µm/min

2.3 SF_6 etching characteristics of SiC and AlN

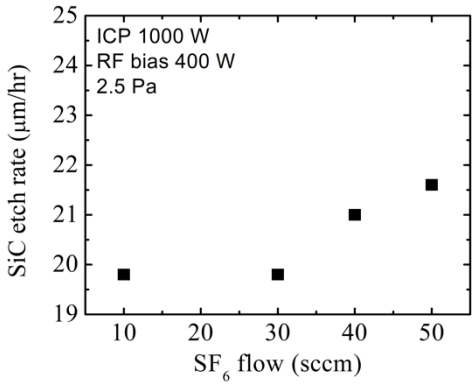

(a) Bulk SiC etch rate (μm/hr) vs SF_6 flow rate (sccm). Higher flow rate increases the etch rate and improves the lateral etch uniformity.

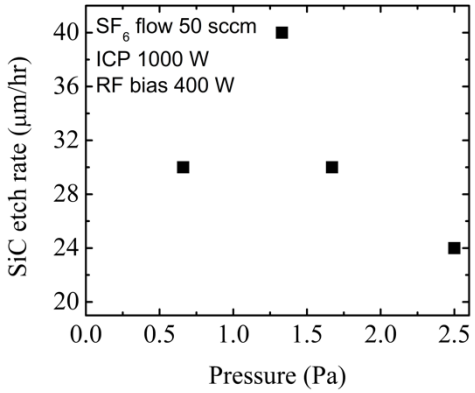

(b) Bulk SiC etch rate (μm/hr) vs pressure (Pa). The etch rate peaks at 1.33 Pa when the product of the ions' energies and the ion densities is maximum.

Figure 2.5. The SF_6 flow and process pressure, were examined to determine the trends between the etch parameters to optimize for a high SiC etch rate. The process parameters were fixed at 1000 W ICP, 400 RF bias, and SF_6 50 sccm flow. The etch rates were measured for bulk SiC over a period of ~40 min – on a fused silica carrier wafer.

Inductive coupled plasma (ICP) etching is plasma-etching technology that independently controls the power of the plasma's chemical etch, and the energy of the sputtering particles (physical etch), which is determined by the RF plasma, and to a less extent, by the chamber pressure. Wang et al. reported the use of NF_3 chemistries to etch SiC in the early 1990s. SiC has a low chemical etch rate in fluorine-based plasma, and high energy ion bombardment assistance is needed. In 1999, Khan et al. reported SF_6 as a promising etch for SiC, with etch rates of ~ 1 μm for a patterned SiC sample using ICP power of 900W and Bias of 450 W at 40 sccm of SF_6 at 0.8 Pascal [86]. Cho et al. showed that at 500 W ICP, SF_6 /O_2 power at 250 V dc bias, the selectivity for SiC over Al is high (~50) [87]. Fujitsu researchers

reported 2 μm/s etch rates using very high ICP power at 2000 W ICP coil power and 200 W substrate bias power using a Ni mask with an etch selectivity of ~100 for Ni at a pressure of 5 Pa. [88]. SiC substrate etching was patented by Cree for visible LED grown on SiC. Fluorine-containing plasma is effective in etching Si and SiC. Among the fluorides (NF_3, XeF_2, and SF_6), SF_6 gas has the highest fluorine fraction and the highest etch rates of Si and SiC. The plasma etch works at high power as a physical etch, and as a chemical etch at low power. At low bias power, the plasma etches mostly chemically, and the fluorine atoms react with AlN, creating a layer of AlF_3 that does not chemically etch in fluorine-based plasma (SF_6). SF_6 can yield selectivity between Si and AlO_3 in the range of 1000:1, and 5000: 1 for cryogenic silicon etching [89].

2.3.1.1 No polymer accumulation in etch chamber

Etching SiC with SF_6 plasma does not cause polymer accumulation in the etch chamber and the etch chamber is cleaned with a standard O_2 plasma clean after completely removing the SiC substrate. The etch of SiC by SF_6 plasma produces the volatile products SiF_4, SiF_2, CF_2, and CF_4 [90]; long etching (several hours, if needed) is consistent and reliable because of the absence of etch-induced polymer generation. Thus, long SF_6 etching does not need to be interrupted to clean the etch chamber because the etch chemistry does not cause polymer accumulation.

2.3.2 Carrier wafer choice

We compared the performance of several wafer carriers to etch SiC, as the standard Si wafers can't be used because the Si etch rate is much higher than that of SiC.

Deep etching of SiC requires a highly selective carrier wafer that does not deplete the plasma and does not sputter onto the sample or the etching chamber. Metal carrier wafers such

as Ni and Al have high etch selectivity (refer to Table 2.3); however, etching at high ion energy for long periods of time results in metal deposition on the sample, which in turn causes micromasking defects such as SiC pillars (refer to Figure 2.7 and 2.9). Furthermore, Ni and Al sputter metal atoms into the etch chamber walls, which affect subsequent etch environments, reduce the tool's lifetime, and require *manual* cleaning after every etching, which is not practical in a general use facility. There have been reports about Cu as a highly selective metal that does not sputter; however, Cu SF_6 plasma etching leaves a contaminating nonvolatile residue in the etch chamber and it was found that it also sputters into the etch chamber. Sapphire (Al_2O_3) and fused silica (SiO_2) have reasonable etch selectivities as shown in Table 2.3. Since the cost of fused silica wafers were 10% of the cost of sapphire wafers, fused silica was chosen as a carrier wafer. A layer of Ni or Al must be deposited on the back of an insulative carrier wafer such as fused silica because the ICP system uses an electrostatic chuck to hold the carrier wafer). The etch rates, selectivity, and drawbacks of each carrier wafer are summarized in the Table 2.3.

Table 2.3. Summary of the etch rate, and selectivity of SiC and various 6-inch carrier wafers used in the ICP system (at 1000 W ICP, 400 W RF bias, 1.33 Pa).

6" Carrier wafer	Etch rate (μm/hr)	SiC:Carrier wafer etch selectivity at 400 W RF bias	Cost	Comments
SiC	40	1:1	$1000	NA
Sapphire	5	8:1	$400	Satisfactory selectivity but expensive.
Fused Silica	20	1.9:1	$30	Satisfactory selectivity and inexpensive.
Al wafer	1.5-2	25:1	$200	Sputter into sample and etch chamber walls
Ni wafer	1	40:1	$200	Sputter into sample and etch chamber walls.
Cu film on Si wafer	NA	NA	NA	Sputter contaminating and nonvolatile etch byproducts into sample and etch chamber walls
Ni film on Si wafer	1	40:1	NA	Sputter into sample and etch chamber walls. Also, Ni films thicker than 2 μm buckle and delaminate due to high compressive stress.

2.3.2.1 Etch rate characterization

To characterize the etch rate of SiC, 2" 6H-SiC substrates were procured from SiCrystal. The goal was to measure bulk SiC etch rates over long periods of time; therefore: 1) the etch rate was measured for bulk, unpatterned SiC, and 2) the etch rates were measured over 40 minutes. The etch rates varied spatially across the sample by about 15% and were measured by DektaK and SEM. The SEM measurements of cleaved SiC samples was tricky because etch defects at the edge of the samples (SiC-walling), hid the actual thickness, so cleaving the substrates was necessary to measure the etch thickness correctly. The uncertainty in the etch measurements and the variance were 20%. Furthermore, the etch rate depends on the exposed

surface area of the sample, but this dependence was minimized by maximizing the SF_6 flow rates.

2.3.2.2 Impact of SF_6 and RF bias power

Increasing the SF_6 flow also helps increase the etch rate and the lateral etch uniformity (refer to Figure 2.5a). The etch rates increase proportionally with source power (plasma density) and bias power (ion energy). The ICP power was maintained at 1000 W to etch rates and to maintain the highest chemical etch rate to maximize selectivity.

The RF power was varied from 47 W to 450 W (maximum) to study its impact on etch rate and etch damage (refer to Figure 2.6a). At large RF bias, the physical etch rate of SiC dominates, while at low RF bias the physical etch rate is negligible and the SiC etch rate is completely dominated by chemical etching, which is temperature-dependent. Figure 2.6a shows the etch rate at 40 0W and 450 W to be around 40 µm/hr (refer to Figure 2.6a). At higher RF substrate bias power, the marginal change in etch rate was low. The etch rate at 450 W was slightly higher, but deeper craters (sputtering defect) were visible (etch damage) at 450 W than at 400 W. The etch craters were around 8-11 µm deep at 450W, and 3-7 µm deep at 400 W.

2.3.2.3 Impact of pressure

The pressure increases the ion density in the plasma and affects the etch rate of the SiC and AlN and the etch selectivity. The optimal pressure needed to achieve high etch rates or high selectivity depends on the ICP power and on the substrate RF bias power. For example, too high pressure crowds the ions and reduces the mean free path of particles in the chamber. Thus, there exists a point of lower pressure that yields the highest etch rates which was around 1.3 Pa as shown in Figure 2.5b

2.3.2.4 Surface roughness

Aside from observing bigger craters at an RF bias of 450 W than at 400 W, we did not investigate the impact of SF_6 on surface roughness, because our goal was to remove the SiC and expose a pristine AlN surface. The exposed AlN surface was very smooth at the low selective etch process parameters (RMS roughness was < 1 nm).

2.3.2.5 Impact of adding O_2 to SF_6 plasma

The reports on adding oxygen to increase SiC etch rate is contradictory in the literature. Some reports of etching deep groove into *patterned* SiC reported that adding 10% oxygen to the mix improves the etch rate by improving the removal of carbon., and some reports indicate no effect. We attempted adding 10% and 20% of oxygen to the mix, but the etch rates dropped for *bulk* etching of SiC. Furthermore, we did not use O_2 in our etching especially because, adding excess oxygen might cause pillars to appear, perhaps by SiO_x micro-masking.

2.3.2.6 SiC pillars formation and suppression

The formation of pillars during deep SiC plasma etching is a well-known challenge in the SiC etch literature. Furthermore, this was one of the challenges faced in previous UV LED on SiC work at UCSB[56,57]. Contrary to previous reports, it was found that the SiC pillars' formation (refer to Figures 2.8 and 2.9) depends mostly on: 1) the carrier wafer used, 2) cleaning and seasoning of the carrier wafer and etch chamber walls before etching in SF_6, and 3) thinning the sample to at least under 150 µm helped eliminate the pillars at the surface of the exposed AlN (refer to Figures 2.10 and 2.11). For samples that were etched completely, by passing the thinning of the 250 µm substrate, 10-60µm SiC pillars persisted at low density on some devices.

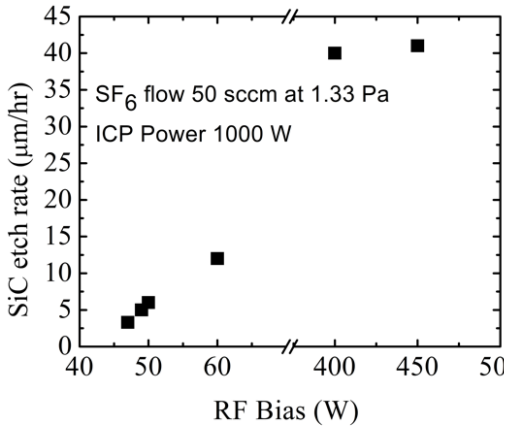

(a) Bulk SiC etch rate (μm/hr) vs RF bias (W).

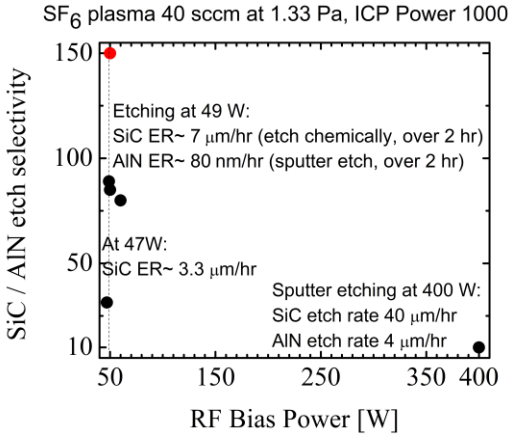

(b) SiC:AlN etch selectivity as function of RF bias power (W).

Figure 2.6. In Figure 2.6a, at high RF bias, the SiC etch rate was dominated by sputter etching, however, at low RF bias sputter etch rate is minimal, and SiC is primarily chemically etched. Figure 2.6b shows that SiC:AlN etch selectivity has a strong dependence on RF bias below 60 W. The SiC:AlN etch selectivity at 49 W RT bias was 90:1 during a 2 hr etch, however, the selectivity decreased below 47 W. A higher SiC:AlN etch selectivity 150:1 (shown in red) was measured at a lower process pressure (0.8 Pa).

Table 2.4. Summary of etch parameters for the two-steps ICP SF_6 etch to selectively remove SiC (using fused silica as a carrier).

Process parameter	**Fast SiC etch**	**Selective SiC etch (slow)**
Pressure	1.33 Pa	1.33 Pa
ICP power	1000 W	1000 W
SF_6 Flow	50 sccm	50 sccm
ICP bias	400 W	49 W
Etch rate	40 μm/hr (40 min) 46 μm/hr (90 min) 47 μm/hr (2 hr)	~7 μm/hr (2 hr)
SiC:AlN Selectivity	10:1	~90:1 (~150:1 at 0.8 Pa)
Impact on SiC surface	Rough hydrophilic SiC surface	After SiC is completely etched, the surface changes from hydrophilic to hydrophobic; smooth N-face AlN surface (RMS roughness < 1 nm) is exposed.

2.3.3 SiC:AlN etch selectivity

SiC/AlN high etch selectivity is crucial for removing the SiC substrate without over etching to the devices by stopping at the AlN buffer layer with precise epitaxial control. The etch selectivity was dependent on the substrate temperature (He-cooled and maintained at 11 °C), process pressure, and the RF bias power below 60 W, especially in the 47-49 W region.

At high RF bias of 400 W, the etch rate of SiC (over 40 min) is about 40 μm/hr, and SiC:AlN etch selectivity is (10:1). The effective etch rates over SiC over more than 1.5 hours of etch could be as high as 46 um/hr. Therefore, an appropriate safety margin should be assumed. For example, for an 85-90 μm SiC thick substrate, 1.5 hours of etching at high bias and 1.5-2 hours of etching at low bias is enough to remove the substrate. To remove a 250 μm without thinning, 5 hours of high etch rate at 400 W, and 1.5 hours of etch at 49 W was sufficient to fully remove the substrate (thus, it is advisable to thin the substrate first to less than 70 μm).

At low RF bias, we measured the SiC:AlN etch selectivity to be 90:1 SF_6 at 1.3 Pa. At a lower process pressure of 0.8 Pa, the etch selectivity was measured to be 150:1. The etch selectivity could be increased further by optimizing the process pressure and by increasing the ICP power. In contrast, Senesky et al. [81] reported an SF_6 etch selectivity (at low RF bias) of 16:1 (SiC:AlN) using AlN deposited with reactive sputtering, and reported Ni selectivity of about 50-40 (at high RF bias). Thus, the high bulk SiC etch selectivity obtained with MOCVD-grown AlN (at low RF bias, 1000 W ICP) suggest that MOCVD-grown AlN could replace Ni as a hard mask in fabricating deep high aspect ratio (AR) SiC microstructures,

microelectromechanical systems (MEMS) and devices [82,83]. In addition to its novel use as a substrate for high light extraction thin-film AlGaN UV LEDs, removing the SiC substrate or deep etching of SiC has several potential applications in other fields. For example, it can be employed to enhance the performance of photodiodes (PDs) [75] and bulk acoustic resonators (BARs) [78–80]. SiC substrate is used widely in power electronics such as high-electron mobility transistors (HEMTs) [76]. Another application of SF_6 deep etching of SiC is the fabrication of micro-fin structure into bulk SiC is in order to improve its heat exchange performance even further for demanding applications that are limited by thermal performance, and high aspect ratio SiC microstructures and devices [81–84].

2.3.3.1 SiC:AlN etching selectivity decreases below 47 W

Figure 2.6b shows a strong dependence of SiC/AlN selectivity on RF bias at low RF bias. The SiC/AlN selectivity is limited by minimum RF bias necessary to etch SiC. The etch selectivity reaches a maximum at 49 W and drops below 47 W.

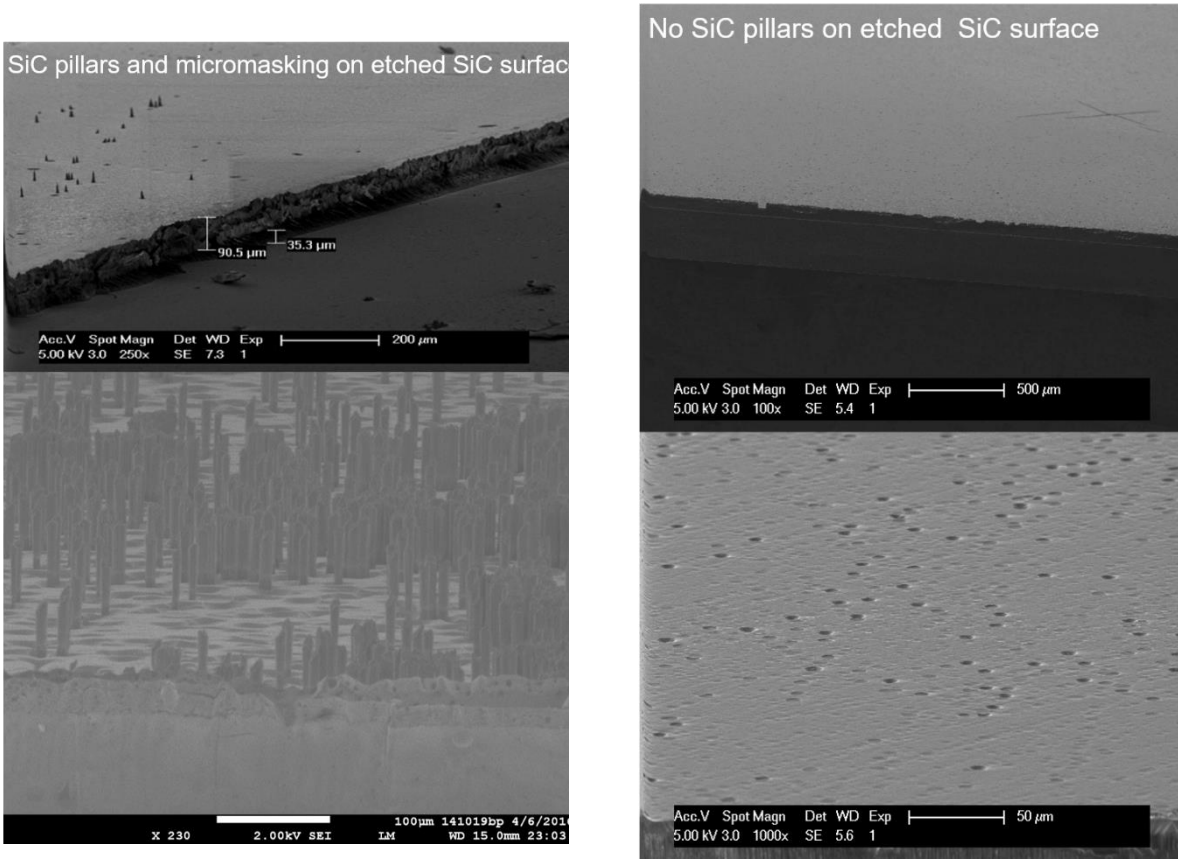

(a) (b)

Figure 2.7. SiC pillars can be completely removed from the surface if appropriate process controls are applied. The image on the left (a) shows SiC pillars (mircomasking defects) that can form during etching and that will not be completely etched even when the highly selective etch is subsequently applied. The SiC pillars formation was suppressed by an optimized process controls as shown on the right (b): 1) Metal carrier wafers were avoided (fused silica carrier was employed). 2) The carrier wafer and etch chamber were seasoned with SF_6 plasma prior to etching.

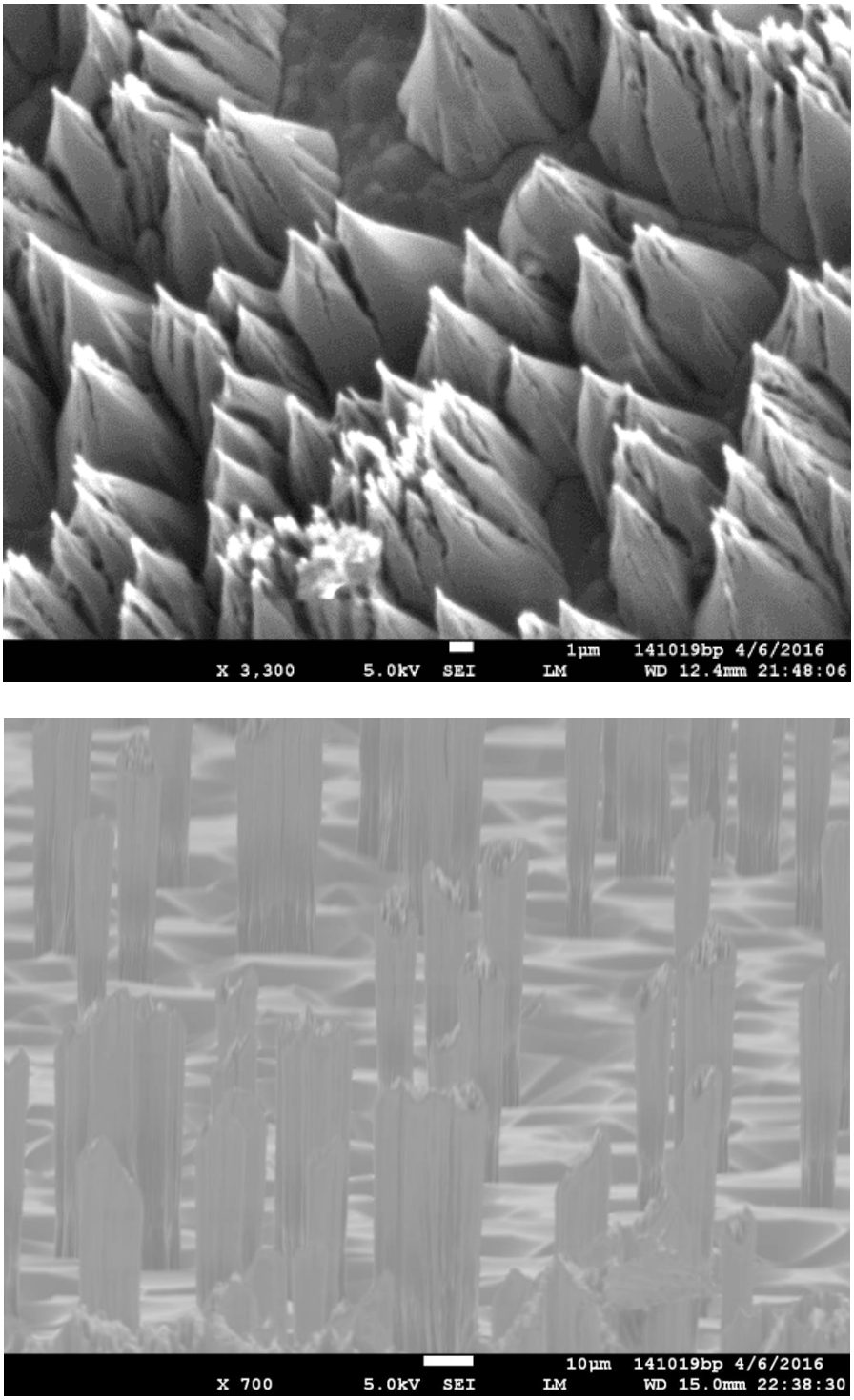

Figure 2.8. SEM images shows that intesity of SiC pillars increase if the SiC is expopsed to N_2 plasma, then SF_6 plasma.

2.3.3.2 Impact of N_2 on SiC pillars concentration

Exposing the SiC substrates to 10 minutes of N_2 plasma, and subsequently to SF_6, resulted in increased density of SiC pillars (refer to Figure 2.8). This etch could be used to control or vary SiC pillar density and the fabrication of nanostructures such as needle like or columnar structures [91,92].

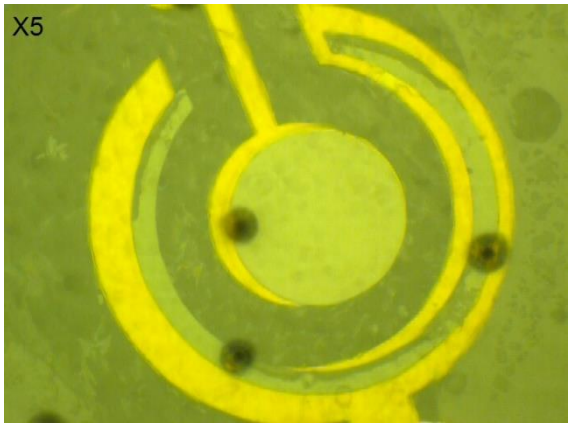

(a) Micrograph for LED-test structure with 3 SiC pillars.

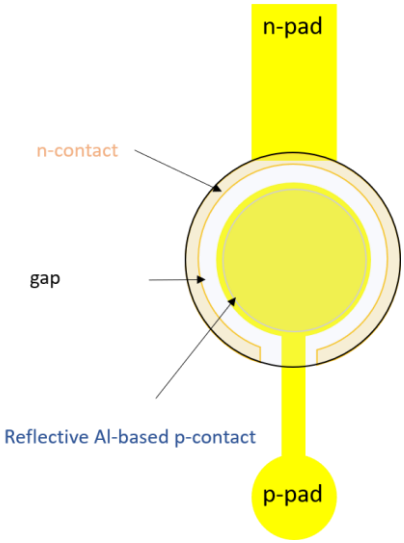

(c) Submount sketch. Gap = 30 µm.

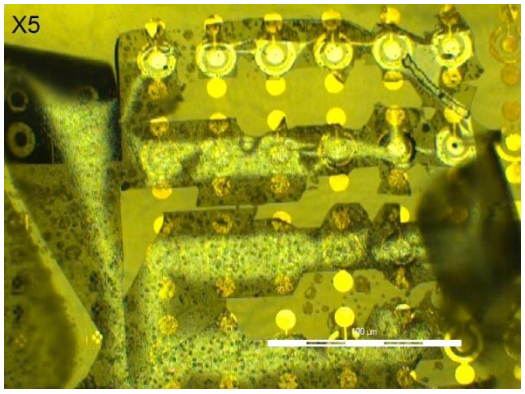

(d) Micrograph for an array of LED-test structure with 3 SiC pillars.

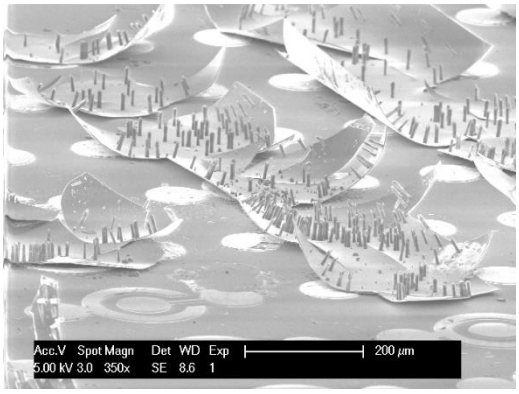

(e) SEM for an array of LED-test structure with 3 SiC pillars.

Figure 2.9. Micrographs for SiC pillars on test device structures in (a)-(e). (f) shows Top view of device of submount for Al based p-contact mirror TFFC LED. The SiC pillars are removed by optimizing the etch process.

(a) AlN transferred onto SiC (1.1 x 1.1 cm^2)

(b) AlN transferred onto Si substrate (1.1 x 1.1 cm^2)

Figure 2.10. 2 µm MOCVD grown AlN epi transferred (SiC pillars-free) into 1.1 x 1.1 cm^2 substrates (Au-Au bonded) with *no* micromasking defects.

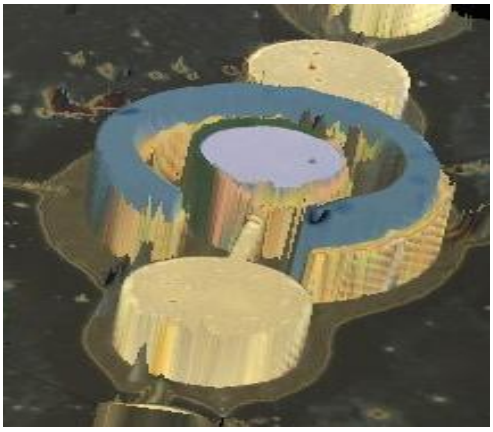

(a) Confocal microscope of a test structure shows n- and p- bonding pads and thin-film AlN/AlGaN epi.

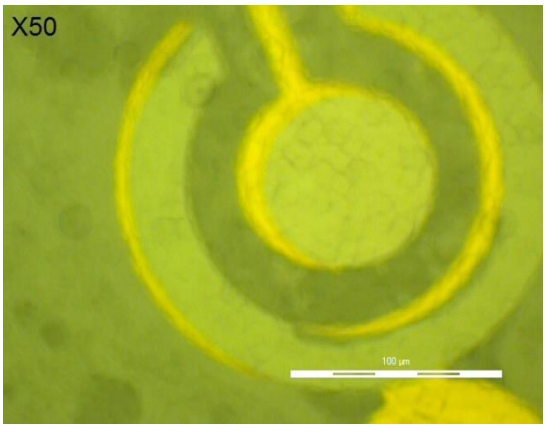

(b) Optical microscope of test structure (SiC pillars free).

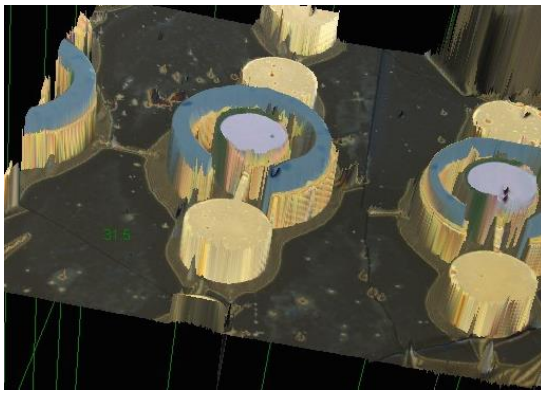

(c) Confocal microscope of array of LED test structures (SiC pillars free).

(d) Micrograph or microscope of array of LED test structure (SiC pillars free).

Figure 2.11. Micrographs for exposed AlN surface of test device structures (mimic LEDs but with large 30 µm gap between and an p-contact) without SiC pillars or any micro-masking defects using the etch process we developed.

2.4 Characterization of epi transfer for UV TFFC LEDs

The epi transfer quality was dependent on the bonding quality and strength. The metal bonding did not impact the IV characteristics (see Chapter 4 for more information). Furthermore, the metal-metal bond had negligible thermal resistance and we maximized the contact area to maximize heat transfer. We characterized the high-resolution X-ray diffraction (HRXRD) rocking curves and the photoluminescence (PL) of the epitaxial film before and after bonding and there was not change in AlN crystal quality.

Figure 2.10 below shows HRXRD (002) of the sample after SiC substrate removal and shows a FWHM of 300 arcseconds which was similar to the FWHM width before substrate removal. The peak PL emission was not changed before and after the epi transfer.

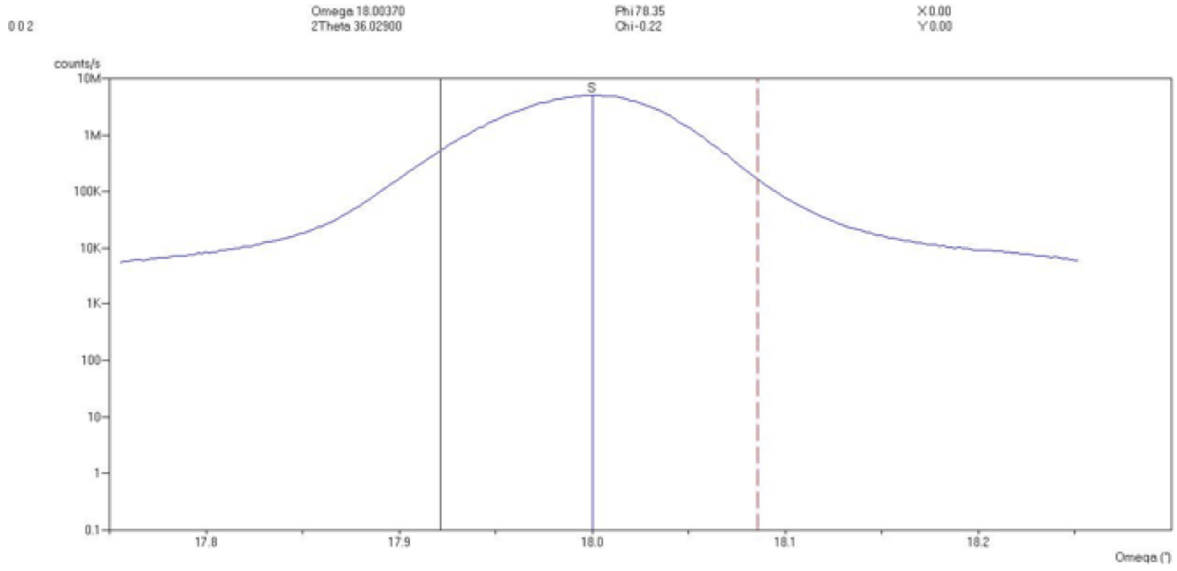

Figure 2.10. High-resolution X-ray diffraction (002) of the sample after SiC substrate removal shows an FWHM width of 300 arcseconds which is similar to the FWHM width before substrate removal.

2.5 Epi transfer and hetrointegration onto flexible substrates

Figures 2.11a and 2.11b shows the AlN or AlGaN epi can be transferred into flexible substrates for novel devices and systems integrations [93–100].

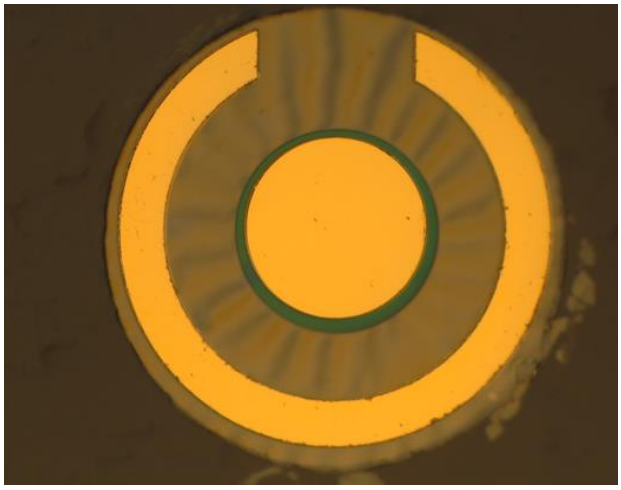

(b) optical micrograph shows wrinkling modes in suspended film across a 30 µm gap in suspended film.

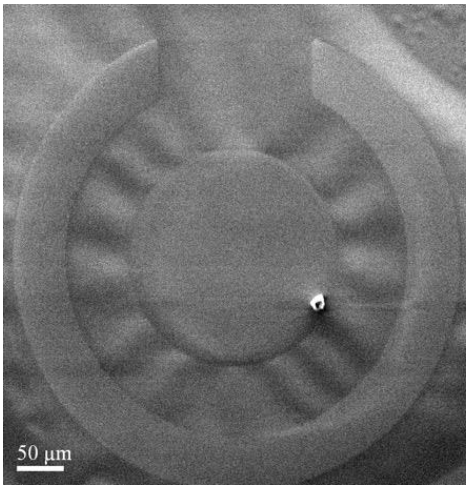

(c) SEM images shows wrinkling modes in suspended film across a 30 µm gap.

Figure 2.11a. Demonstration of epi transfer of a single mimic-LED test structure and hetrointegration into a flexible substrate (Nitto Denko tape). (a) Optical micrograph, and (b) SEM image of a mimic-LED test structure epitaxial layer (AlGaN/AlN/SiC), with 30 µm gap between n-pad and p-pad.

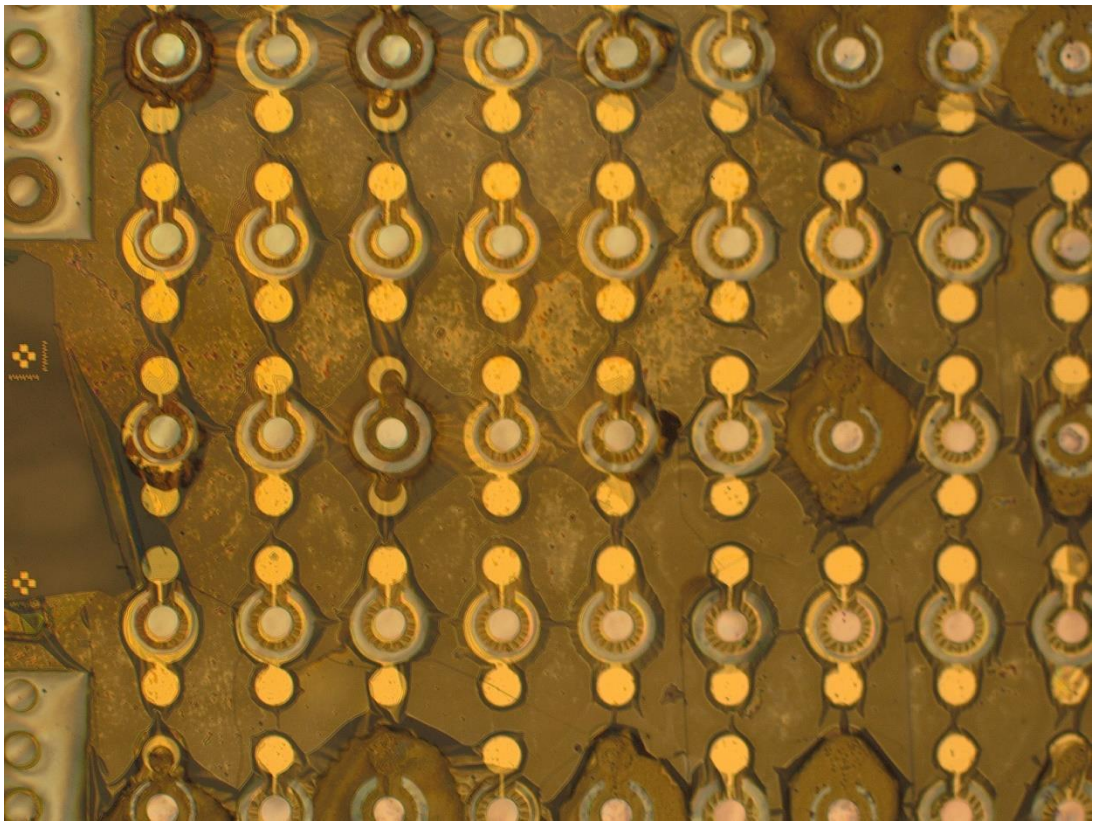

Figure 2.11b. Demonstration of epi transfer and hetrointegration of an array of devices into a flexible substrate (Nitto Denko tape). Arrays of mimic-LED test structures (AlGaN/AlN mesa structures) with exposed N-face AlN (RMS roughness < 1 nm). Notice that the test structures were misaligned by ~12 µm but within the 30 µm tolerance margin for the test structure. The alignment tolerance of the Fintech bonder was improved later from ~12 µm to less than 4 µm by calibrating the Finetech bonder before each wafer-to-wafer bonding.

Chapter 3: AlN roughening with KOH and MQW PL enhancement

"There is no royal road to geometry."

Attributed to Euclid (323-283 BC)

As explained in Chapter 2, the SiC substrate is removed partly by mechanical grinding, followed by a two-step ICP etches: a fast non-selective SF_6 etch followed by a slow but highly selective SF_6 etch of SiC over AlN to planarize the surface and stop at a smooth nitrogen-face (N-face) of pristine AlN. Thetexposed N-face AlN surface is then roughened with aqueous KOH, which generates hexagonal pyramids that are highly efficient in light extraction when combined with highly reflective p-mirrors, and low absorption p-GaN layer [2,101].

In this chapter, we discuss AlN roughening using KOH and its impact on the LEE of PL in MQWs by demonstrating a PL enhancement in an n-i-n structure: SiC/AlN/(n-AlGaN/MQW/n-AlGaN). We discuss the nitrogen face (N-face) roughening of AlN without light assistance and compare it to KOH roughening of N-face GaN without light assistance, as well as N-face GaN roughening with above-bandgap light assistance using photoelectrochemical (PEC) etching. We also, discuss the possibilities of PEC roughening of AlN. We show that the hexagonal cones are independent of TDD by roughening the AlN samples for (roughly) the same duration at three temperatures and then counting the densities of resulting AlN hexagonal cones (we later obtained similar cone densities with AlN grown using a TNSC SR4000 MOCVD). We end the chapter by showing 3.9X PL enhancement in an n-i-n structure featuring a reflective p-contact with an ultra-thin Pt layer.

3.1 AlN roughening with KOH (without above-bandgap light assistance)

KOH anisotropically etches N-face AlN and GaN without above-bandgap light assistance, but the N-face roughening of AlN is much faster than that of GaN. The reasons for this are unclear; N-face AlN has faster etch rates despite a higher band-gap (6.1 eV for AlN vs. 3.4 eV for GaN), which indicates that the thermalization of *electrons* and *holes* does not play a dominant role in roughening N-face GaN (which is unintentionally n-type doped by oxygen donors (as oxygen is not an active DX center in AlN).

PEC etching, which is band-gap selective, has been applied to make III-nitride VCSELs with epitaxial cavity length control [102–104] and is a promising technique to liftoff blue and green micro-LEDs [105,106]. Moreover, PEC etching was used to increase the LEE of thin-film blue LEDs by etching N-face GaN to roughen the surface of the LEDs [101,107]; however, PEC etching of AlN would be too fast for practical use when roughening AlGaN LEDs, however, we were able to roughen N-face AlN in KOH without above-bandgap light assistance.

To the best of my knowledge, before this study, AlN roughening has never been used to improve the LEE of UV-C LEDs below 300 nm. There have, however, been several attempts at creating TFFC LEDs with laser liftoff of the AlN buffer layer [20,108–113], but few paper showed any roughening of the exposed surface and, in those that did, the exposed n-AlGaN surface was etched (instead of AlN) which led to smaller improvements in LEE, device degradation, and leakage. For example, Zhou et al. [108] reported large-area (700×700 μm^2), vertically-injected thin-film LEDs grown on GaN-on-sapphire templates and reported that they operated LEDs with a double peak of 280 and 325 nm. The vertical n-contacts were deposited on the exposed n-AlGaN surface, covering part of the emission, and the n-AlGaN was then

roughened with PEC KOH using an arc lamp. Neither the etch rates nor the KOH concentration was reported. The spectra of the LED changed significantly due to the roughening, and the LED greatest power was at the new parasitic peak of 325 nm. The use of GaN as a buffer layer for an AlGaN LED epi also must have constrained the device's performance because of the high TDD that results from growing AlGaN LEDs on GaN-on-sapphire templates. Aoshima et al. [113] reported a 1.7X enhancement on Laser lift-off of AlN/sapphire for UV LEDs for an LED emitting at 343 nm, however, the LED used an underfill to limit cracks and fractures that were reported by earlier attempts of lift-off of AlN; however, the underfill could decay as it is exposed to UV radiation.

Etching N-face AlN instead of n-AlGaN lead to increased gains in LEE without impact the devices IV characteristics. Etching n-AlGaN increases the sheet resistance of the n-AlGaN layer and causes leakages. Furthermore, AlN has a lower refractive index than $Al_{0.6}Ga_{0.4}N$, which make AlN cones able to extract more light.

The etch rate of N-face AlN by KOH (without above-bandgap light assistance) was much faster than the etch rate of N-face GaN. N-face GaN etches in KOH at a relatively slow rate of ~ 0.7-1 nm/min in 1 M KOH [106]. This etch rate is very slow (comparable to or even slower than KOH etching of Al and AlD or PECVD-deposited SiO_2) and would require several hours to achieve optimal light extraction enhancement. The slow KOH etching of N-face GaN constrains the amount of etching possible because a long etching time could etch the LEDs' contacts and dielectric passivation layers. By comparison, PEC etching of N-face GaN is much faster [114], as it needs only a few minutes to optimally increase the light extraction form a thin-film LED [115]. In contrast, AlN etching without light assistance is very fast; its etch rate

is comparable to that of N-face GaN PEC (refer to Table 3.1 for a summary of etch rates and a comparison between AlN and GaN).

We did not employ PEC etching of AlN; however, considering that there could be different future applications for PEC etching of AlN and high Al-composition AlGaN, the main challenges for successful PEC etching of high-Al composition AlGaN are due to: the lack of light sources at very deep UV with high enough density, the fact that both water (i.e., KOH solution) and air absorb UV light below 230 nm, and the fact that air absorption will generate ozone.

3.2 N-face roughening of AlN in other solutions

We found out that N-face AlN etched anisotopically in dilute ammonium hydroxide, and in concentrated TMAH, albeit at a slower etch rate than 0.24 KOH (refer to figure 3.6). Furthermore, TMAH is industrially less convenient to deal with than KOH due to TMAH's toxicity, cost and handling. Therefore, KOH would be preferable for N-face AlN KOH roughening.

Table 3.1. KOH roughening comparison of AlN and GaN. (exact etch rates depend on many variables)

N-face AlN etch rate (c-plane)		**N-face GaN etch rate (c-plane)**		**Lateral InGaN MQWs**	
Natural	**Photons assisted (PEC)**	**Natural**	**Photons assisted (PEC)**	**Natural**	**Photons assisted (PEC)**
600-900 nm/min in 0.25 M KOH at room temperature.	Unknown Light (<230 nm) is absorbed with air, water. Also, light sources have limited intensity.	< 3nm/min in 1 M KOH at 25 °C [106].	20-50 nm/min [116]. 5000 nm/min[117].	No data	2400 nm/min in 1 M KOH and LED array [106]. 5000 nm/min in 2.22 M KOH and Xe–Hg lamp [118].

3.3 Experimental

AlN was grown on quartered 2-inch 6H-SiC substrates (SiCrystal AG) by MOCVD by Humberto Foronda in a Vecco MOCVD reactor (similar KOH etched AlN cones densities at 25 °C and 75 °C were later obtained with AlN grown by TNSC SR4000 MOCVD and without using a surfactant). The TDD was $1.5x10^{10}$ cm^{-3} as determined by plan-view TEM. The n-i-n structure (n-$Al_{0.6}Ga_{0.4}N$/MQWs/n-$Al_{0.6}Ga_{0.4}N$/$Al_{0.6}GaN$/AlN) was coated with a p-contact mirror (Pt/Al/Ni/Au deposited by e-beam). Then, the sample was bonded to a carrier wafer by Au-Au bonding. The substrate was thinned then removed by etching the SiC with a highly selective SF_6 etch to expose a pristine N-face AlN layer as described in Chapter 2 and elsewhere [14], [15]. Figure 3.1 shows the structures before and after KOH roughening. KOH (0.24 M KOH mixed with 1%, in volume, surfactant) etching was used to create hexagonal pyramids that are very efficient in surface light extraction when a reflecting p-mirror contact is used. The etching rate, AlN cones density, and the uniformity were investigated to understand the etching mechanism and to optimize the light extraction efficiency. The surfactant was used to make the etching more uniform but no improvement in uniformity were observed. Furthermore, photoluminescence emission measurements were used to describe the LEE enhancement in the PL of a KOH roughened n-i-n AlGaN structure (mimicking a thin-film LED).

3.4 Relationship between TDD and hexagonal cone density

Holes diffusion to the surface of N-face GaN is thought to be responsible for reducing the GaN and helping it oxidize and dissolve into KOH in an anisotropic manner [119]. The etched surface shows hexagonal cones bound by {10-1-1} facets. Some reports have indicated that

GaN roughening with KOH correlates with the TDD. This would be true if the etching of N-face GaN was dependent on light generated electron-hole pairs, as the strained areas around a TD are expected to trap the generated electron hole pairs. Although the PEC etching of GaN might be related to TDs, especially in light-limited regime, it is not the case for KOH roughening of AlN (or GaN) without light. Figures 3.3 and 3.3 shows SEM images of hexagonal cones of AlN after KOH etching for a fixed time at various temperatures. The average cones densities were roughly estimated from the SEM images by an image processing program (ImageJ) and are shown in Figure 3.4. We plotted the RDF of cones peak lattice in several top view SEM images and the RDF spectrum showed no correlation and varied across the surface of this sample or other samples (refer to Figure 3.5).

Figures 3.2, 3.3 and 3.7 show an exposed, pristine N-face AlN surface roughened with KOH. The wet etching of the N-face AlN result in nano-sharp hexagonal pyramids, similar to the N-face GaN hexagonal pyramids. Several studies indicated from cross-sectional TEM analysis that hexagonal pyramid are not related to the threading dislocations when etching in KOH without assistance from above bandgap photons (as in photo-electrochemical (PEC) etching) [120][121]. We simply show that TDD is independent of cones density by etching AlN at three different temperature and calculating the cones density. The cones densities that resulted from a 60 sec etch in [0.24 M] of KOH (and an added 1% volume of Tergitol which was unnecessary because it didn't seem to affect etching uniformity) were as follows: ~$3x10^9$ cm^{-2} at 25 ºC, ~$4x10^8$ cm^{-2} at 50 ºC, and ~$2x10^8$ cm^{-2} at 75 ºC (see Figures 3.3 and 3.4). The etch rate increased with temperature, and at higher temperature, the AlN pyramids size increased and their densities decreased. We show in Chapter 4 that the larger cones densities etched at 25 ºC result in better light extraction than the lower cones densities etched at 75 ºC.

3.5 Demonstration of PL enhancement

LEE enhancement is highly dependent on mirror reflectivity, as estimated by light extraction simulation using the ray tracing method [122,123]. Figure 3.1 demonstrates the LEE enhancement of PL for an n-i-n structure (n-$Al_{0.6}Ga_{0.4}N$/MQWs/n-$Al_{0.6}Ga_{0.4}N$/$Al_{0.6}$GaN/AlN) before and after KOH roughening. In this experiment, the mirror was made from Pt/Al/Ni/Au and was deposited by e-beam. The mirror mimicked a potential p-contact mirror for UV-C LEDs. In a typical UV-C LED, Pt or Ni makes ohmic contact with p-GaN. Al was used because it has the highest UV-C reflectivity of any metal. The Pt thickness was reduced to minimize light absorption; however, metal deposition by electron beam has a limited ability to deposit uniform ultrathin layers. Figure 3.1c shows the reflectivity of a Pt/Al/Ni/Au mirror (as measured with a Cary 500 UV-Vis spectrophotometer) for ultrathin layers of Pt at 286 nm; for a Pt thickness of 2.6 nm, the reflectivity was 85%, and for a Pt thickness of 0.26 nm, it was 90%. A Pt/Al/Ni/Au mirror with a Pt thickness of 0.26 nm was used to produce 3.9X PL intensity enhancement with p-mirror reflectivity of 90% at 286 nm, as shown in Figure 3.3d; no parasitic peaks were generated here or in LEDs processed in Chapter 4 and 5 unlike in the KOH PEC etching of exposed n-AlGaN in vertical, thin-film LEDs [108]. The observed PL intensity enhancement after roughening was due to both increased LEE, and increased laser pumping of the active region. After roughening, the LEE enhancement is determined by the mirror reflectivity at the emission wavelength and on the light absorption in the epitaxial structure. A slight red shift was observed as the AlN etch depth increased. This red shift may have originated from a reduction in the compressive stress of the epilayer as the AlN etch depth increased [121].

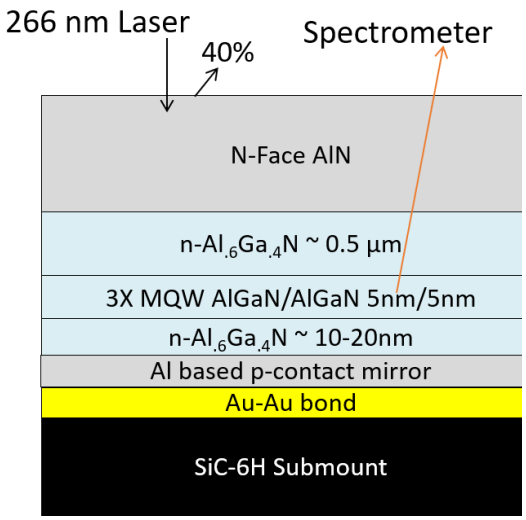

(a) Flip-chip bonded n-i-n strucutre before KOH roughening.

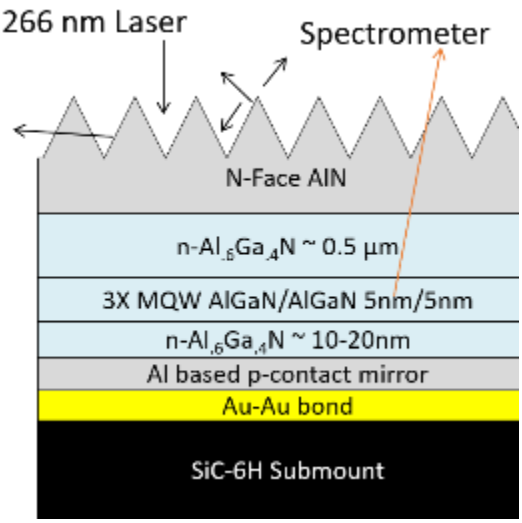

(b) Flip-chip bonded n-i-n strucutre after KOH roughening at room temperature for 40 sec.

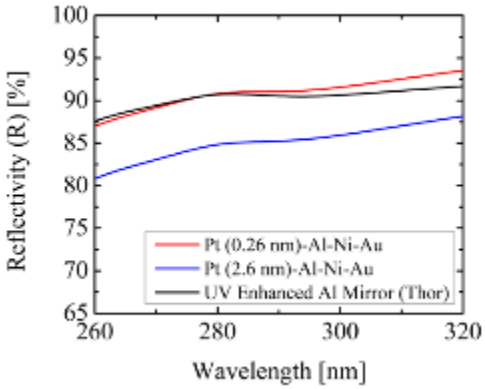

(c) Normal reflection from Al-based (Pt/Al/Ni/Au) mirror in air, at 12° AOI, for Pt=0.26 nm and 2.6 nm. (as measured with a Varian Cary 500 UV-Vis-NIR spectrophotometer.)

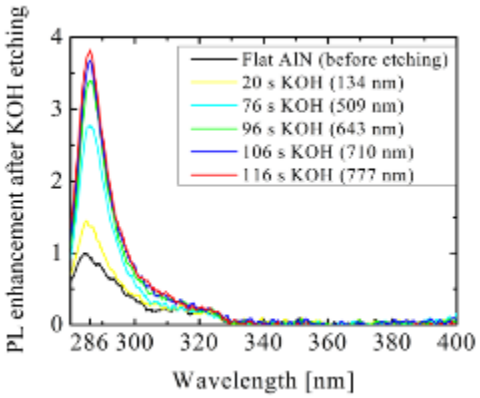

(d) p-mirror (Pt/Al/Ni/Au) with Pt=0.26 nm with a reflectivity of 91% at 286 nm results in a ~3.9X PL enhancement.

Figure 3.1 PL enhancement before and after KOH roughening of an exposed N-AlN surface (without above-bandgap light assistance). The n-i-n structure (n-AlGaN/MQWs/n-AlGaN/AlGaN/AlN) was bonded to a new carrier, and then the SiC growth substrate was etched with SF_6 to expose the N-face AlN.

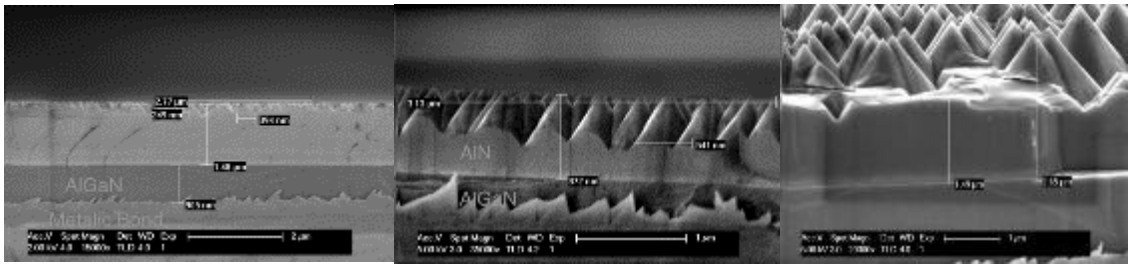

(a) (b) (c)

Figure 3.2. Cross-section SEM images that demonstrate the removal of SiC substrate, and the subsequent KOH roughening of the exposed pristine N-face AlN (grown using MOCVD) for high light extraction efficiency (LEE) UV LEDs. The KOH etched surface shows hexagonal cones bound by {10-1-1} planes.

(a) 250 nm hexagonal pyramids result of 40 s etch in 0.24 M aqueous KOH at ~ 25 ºC.

(b) 440 nm hexagonal pyramids result of 45 s etch in 0.24 M aqueous KOH at ~ 75 ºC.

(c) 900 nm hexagonal pyramids result of 60 s etch in 0.24 M aqueous KOH at ~ 75 ºC.

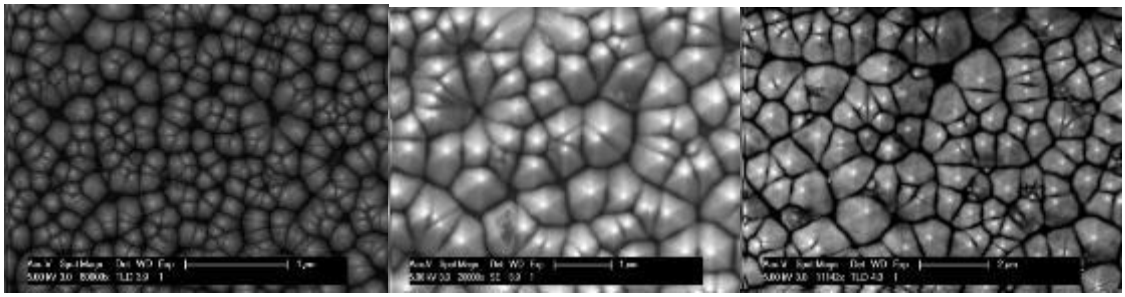

(a) (b) (c)

Figure 3.3. As the etch rate increases with temperature, pyramids size increase and their densities decrease. The cones densities (after 60 s etch in 0.24M KOH with 8% volume of diluted Tergitol) are estimated by ImageJ software to be:

(a) 3 x10^{9} cm^{-2} at 25 ºC. (b) 4 x10^{8} cm^{-2} at 50 ºC. (c) 3 x10^{8} cm^{-2} at 75 ºC.

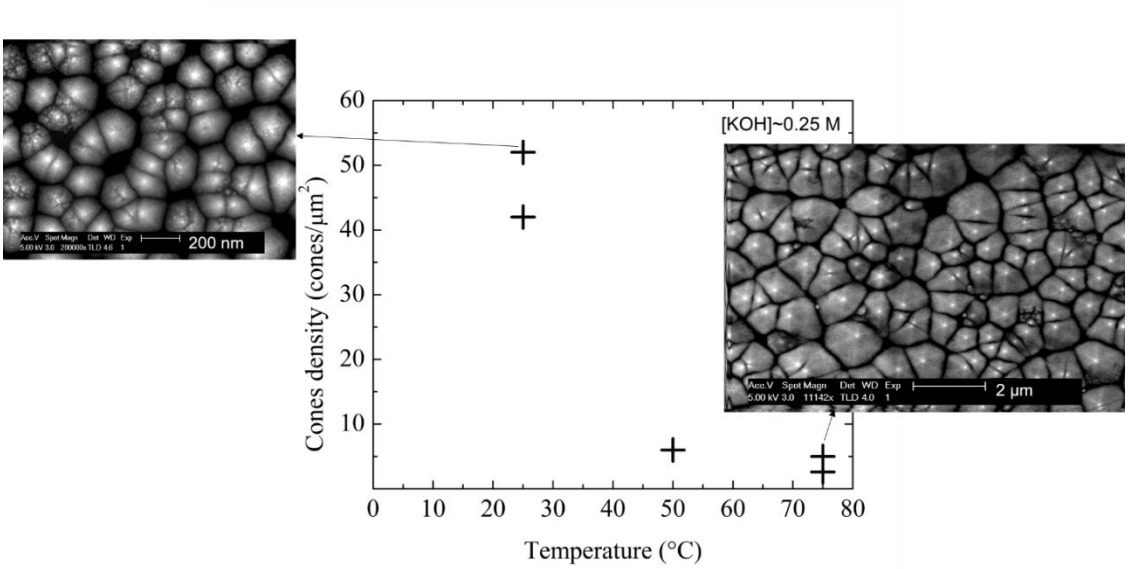

Figure 3.4. Impact of KOH temperature on the density of AlN cones (KOH [0.25 M] etch for 50 sec). The cones density is independent of the threading dislocations density (TDD) in AlN.

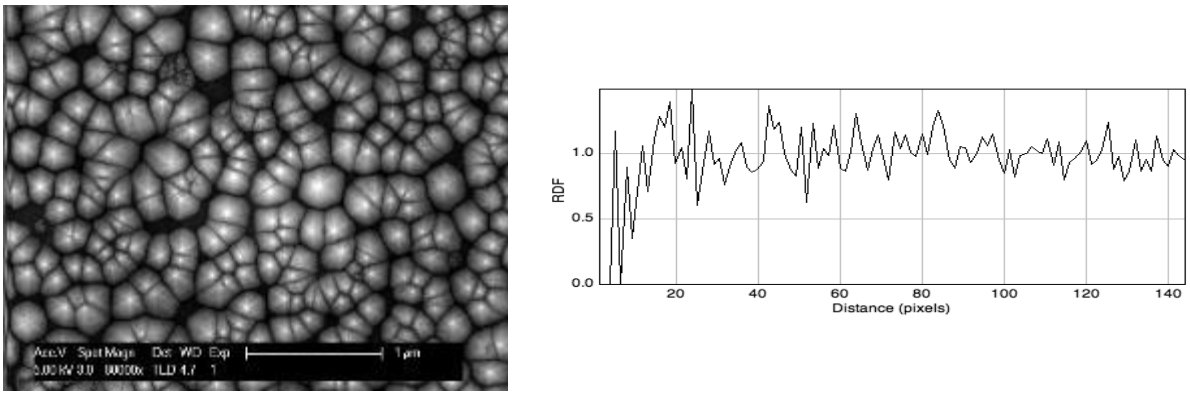

(a) AlN etched in [0.24M] KOH at 75 ºC for 40 sec.

(b) RDF of the AlN cones peak lattice showed no correlation and varied across the surface, both for this sample and for other samples.

Figure 3.5. The distribution of the KOH generated AlN hexagonal cones is random as indicated by several radial distribution function (RDF) of the cones' lattice (as estimated using ImageJ).

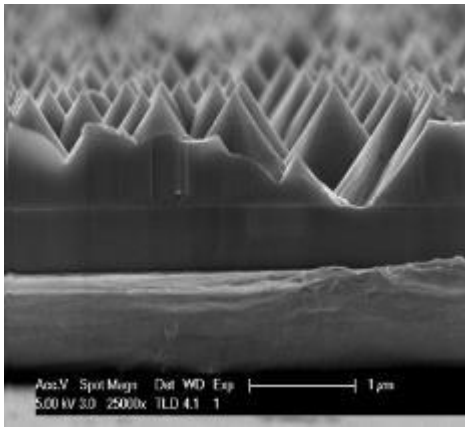

(a) KOH

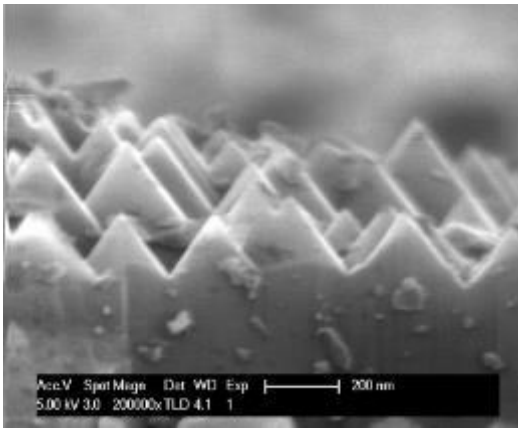

(b) TMAH

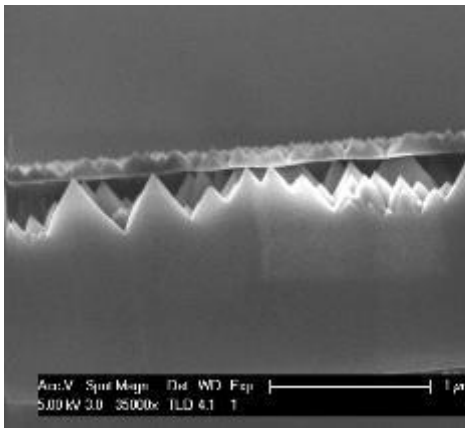

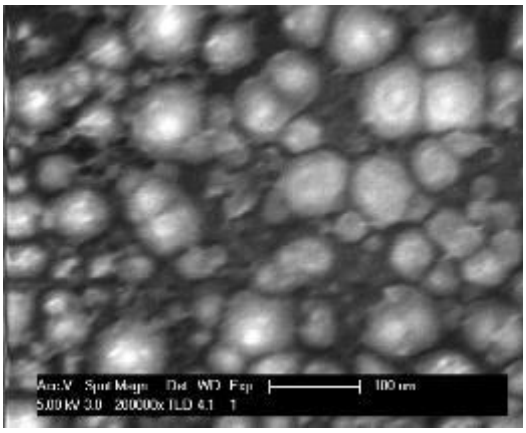

(c) Dilute Ammonium Hydroxide (75 ˚C)

Figure 3.6. (a) Anisotropic etching of N-face AlN in KOH (KOH roughening) exposes cones with a 58.4˚ angle between 0001 and 10-1-1; the cone tip angle is ~ 31.6˚. (b) Etching N-face AlN in TMAH exposes cones with a ~ 58.4˚ angle between the 0001 and 10-1-1 crystallographic plane; the cone-tip angle is 31.6˚. (c) Dilute ammonium hydroxide (at 75 ºC) was also found to generate hexagonal cones, although at lower etch rates than for KOH.

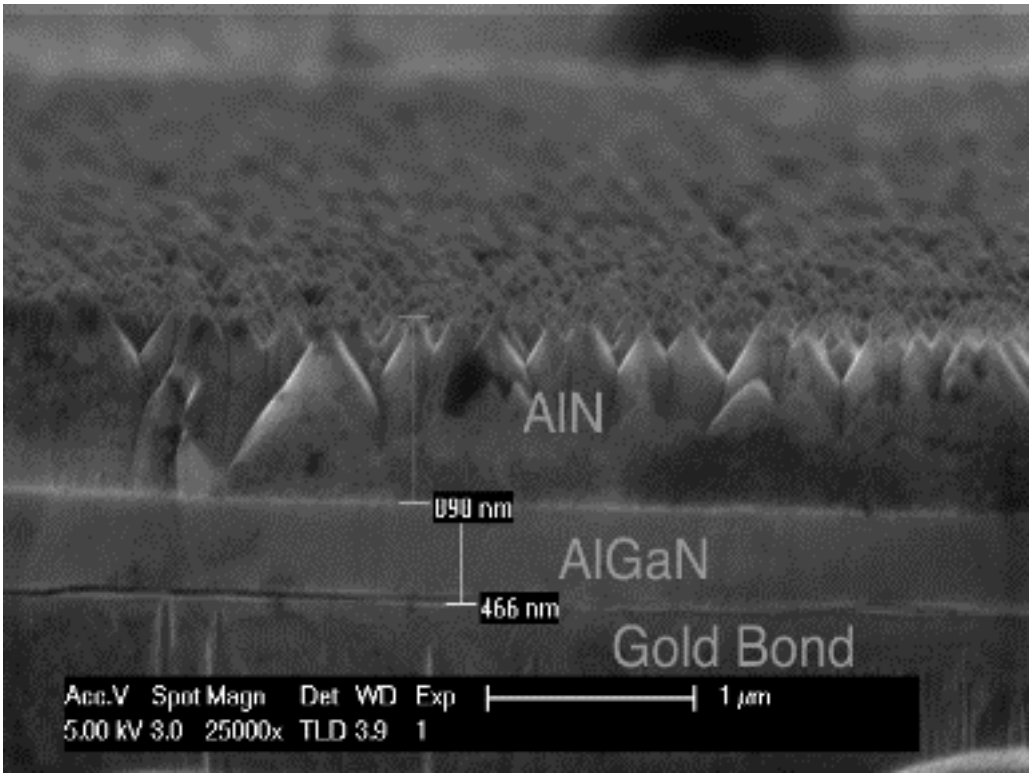

(a) SEM image of N-face roughened AlN. The KOH etched surface shows hexagonal cones bound by {10-1-1} facets.

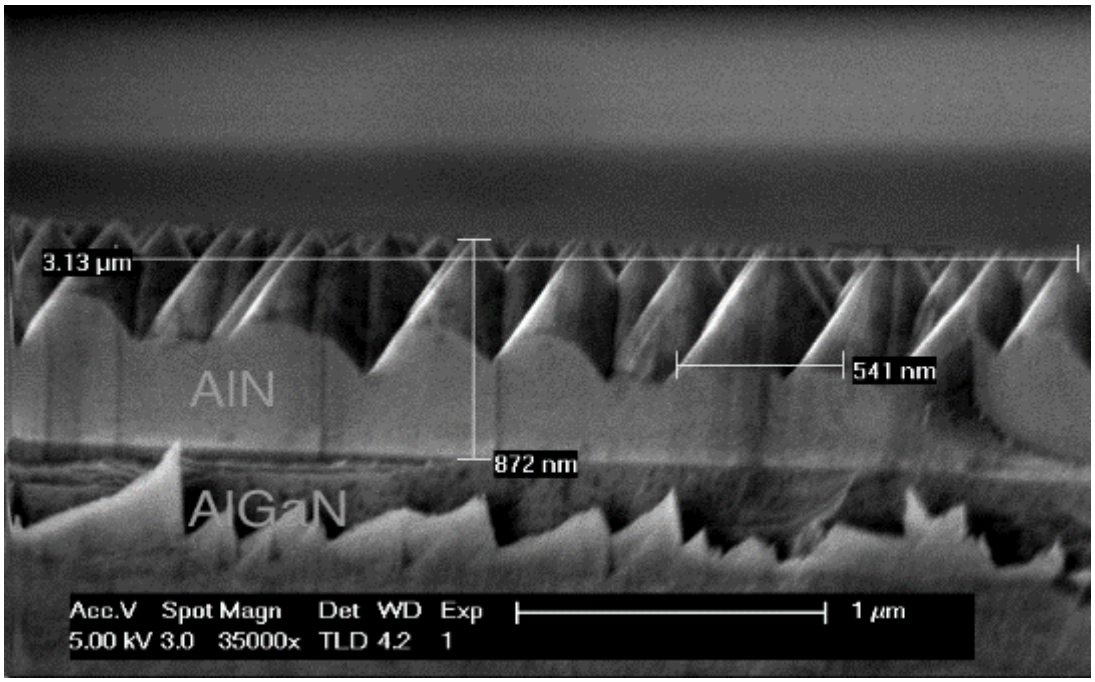

(b) SEM image of a 440 nm hexagonal pyramids as a result of a 45 sec etch in 0.24 M aqueous KOH at 75 ºC

Figure 3.7. SEM images of N-face roughened AlN.

Chapter 4: Development of 1st generation thin-film UV LEDs

"When something is important enough, you do it even if the odds are not in your favor."

-Elon Musk (1971-current)

In this chapter, we will discuss the development of epitaxy and TFFC LEDs for 310 nm and 298 nm emitters. At this phase, the AlN TDD was 10^{10} cm^{-2}, as these LEDs were made before the development of the thick AlN with 2D/3D buffer layers (which resulted in the TDD $\leq$ 10^{9} cm^{-2}) [64], and before the discovery of crack removal through SiC nitridation at a high temperature. The LEDs with 300 nm and 310 nm had AlGaN composition at 52% with specific n-contact resistivity of 1-5x10^{-4} **Ω**-cm^2. The p-GaN contacts were unannealed to preserve high reflectivity, but ohmic with 2/100/100/1000 nm Ni/Al/Ni/Au.

4.1 Development of ohmic n-$Al_{0.52}Ga_{0.48}N$ contacts

N-type conductivity is established in AlGaN by doping with Si (via disilane as the Si source). MOCVD process parameters such as temperature, pressure, III/V ratio, and gas flows were used to control intentional doping of AlGaN alloys. These parameters control the incorporation of Si, , incorporation of impurities such as oxygen, carbon, and other self-compensating acceptors (such as the formation of Al-vacancies, and DX centers), which affects the AlGaN layers' electrical, optical, and thermal properties [124]. At all Al-compositions for AlGaN, Al and Ga vacancies act as acceptors and compensate free electrons. The roles of O, Ge and Si as compensating DX centers were studied using density function theory (DFT); these studies took many years to get right as initial results contradicted reports by several groups on

low n-AlGaN resistivities for below 80% AlN content AlGaN (i.e., $x < 0.8$ for $Al_xGa_{1-x}N$), and a measured effective Si activation energy of around 15 meV below 80% AlN content AlGaN [125]. Subsequently, using hybrid functional calculations, Gordon et al. calculated that Si forms a DX center at AlN= 94% using a hybrid functional approach, and estimated that oxygen forms a deep-level DX center at AlN=61% AlN, but these centers are not active, so typical oxygen levels do not affect n-type conductivity [126]. Ge forms DX centers at lower AlN composition, AlN=52% [127], but it's unclear if these DX centers are active (i.e., trap electrons). Additionally, according to another hybrid density functional study by Gordon et al., S_N is a potential n-type S [128] dopant because it does not undergo a DX transition and has low formation energy and high solubility, however, there is currently no MOCVD process to dope AlGaN with Sulfur.

The best n-contacts for n-AlGaN contacts (AlN content =50-55%) reported in the literature are Ti-based or, more recently, V-based contacts. In this section, we discuss Ti-based and reflective Al-only contacts for n-AlGaN (AlN content =50-55%). We will discuss V-based contacts in the next chapter for higher AlN composition (AlN content=56-65%). The goal was to develop low specific contact resistivities for the LEDs using n-AlGaN grown by Humberto Foronda and Mike Iza at UCSB. We developed a Ti-based n-contact process with specific resistivity in the $1\text{-}5x10^{-4}$ Ω-cm^2 range, which was equivalent to the best results published in the literature on Ti-based n-contacts; however, our process avoided annealing the n-AlGaN at N_2/H_2 mixture, which was reported to result in ohmic Ti-based contacts but can potentially result in AlGaN:Mg and GaN:Mg passivation.

4.1.1 Plasma etching development for ohmic n-contact

Plasma etching was used to define the LED mesa and access the n-AlGaN. The plasma etching processes can impact the IV characteristics of the n-AlGaN contacts. Chlorine and silicon tetrachloride plasma etching of c-plane n-GaN typically improves the n-contacts [129]; however, it degrades high-composition n-AlGaN contacts. BCl_3 is used to make the etch rates more consistent, as it is thought to remove the Al_2O_3 [130]. We investigated the impact of BCl_3/Cl_2 plasma vs $BCl_3\backslash SiCl_4$ as shown in Figure 4.1. $SiCl_4$ plasma were reported by Adesida et al. to yield low specific resistivities [131], but $SiCl_4$ plasma has low AlGaN etch rates (25 nm /min at 200 W RIE bias). Cl_2 is used widely to etch InAlGaN alloys at more convenient rates (150 nm/min at 200 W RF bias). The process conditions investigated were annealing in N_2, annealing N_2/O_2 (non-ohmic, data now shown), and annealing at high vacuum (non-ohmic, refer to Figure 4.7). Non-annealed n-contact on $SiCl_4$-etched c-plane n-AlGaN were non-ohmic, whereas unannealed n-contact on $SiCl_4$-etched c-plane n-GaN etched in $SiCl_4$ were ohmic [129].

We found that with annealing at 800 °C in nitrogen, $SiCl_4$ etched contacts were ohmic, while Cl_2 etched samples needed longer annealing times to be close to ohmic, as shown in Figure 4.1. Others in the literature reported ohmic contacts with Cl_2 etched n-AlGaN after annealing in forming gas (H_2/N_2 mixture) [132,133]; the issue with annealing in forming gas is that it could lead to p-GaN and p-AlGaN passivation, increasing the voltage of the LEDs. It is expected that V-based contacts could have resulted in lower specific resistivities, but we only tried V-based contacts on higher-composition AlGaN, which will be discussed in chapter 5.

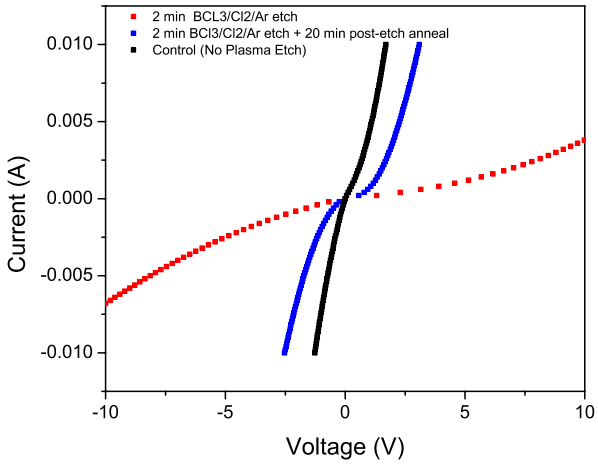

(a) IV of n-CTLM structure with 10 µm gap on Cl_2/Ar/BCl_3 etched n-AlGaN that was annealed at 800 °C. Cl_2 plasma resulted in worse contacts relative to non-etched n-AlGaN contact. Post-annealing the contacts for 20 min helped improve the contacts.

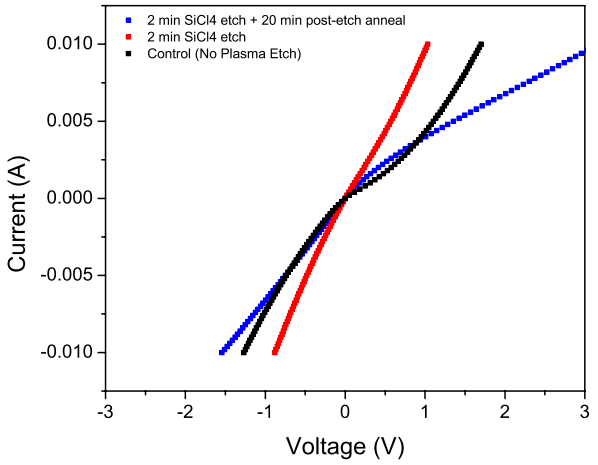

(b) IV of n-CTLM structure with 10 µm gap on $SiCl_4$/BCl_3 etched n-AlGaN that was annealed at 800 °C. $SiCl_4$ resulted in ohmic contacts. In contrast to Cl_2-plasma's contacts, post-annealing was not needed.

Figure 4.1. n-contact process development for AlGaN with x_{AlN}=52%.

Table 4.1. XPS measurements for O, N, Al and Ga fraction in a grown sample, compared to a grown and annealed and the other plasma etching

Element (%) in:	**as grown (not annealed)**	**as-grown**	**$SiCl_4$ etched** (annealed at 800 °C under N_2)	**Cl_2/Ar**
O	10.4	35.6	38.9	47.8
N	38.9	30.9	31.2	22.0
Al	30.8	19.6	13.4	20.8
Ga	19.9	14.0	16.5	9.4
Elements fraction				
N/(Al+Ga)	0.8	0.9	1.0	0.7
N/Al	1.3	1.6	2.3	1.1
N/Ga	2.0	2.2	1.9	2.3
Al/N	0.8	0.6	0.4	0.9
Al/Ga	1.5	1.4	0.8	2.2

Reduced nitrogen vacancy (donors) on the surface is thought to indicate high electron concentration on the surface. Selvanthan et al. reported ohmic Ti/Al/Mo/Au contacts on n-$Al_{0.2}G_{0.8}aN$ with a low specific resistivity of 4.5 x 10-7 Ω-cm^2. They reported that the N/(Ga+Al) fraction was reduced by 40% after $SiCl_4$ etching, from 1.76 before etching to 1.08. We conducted X-ray photoelectron spectroscopy (XPS) measurements on the surface of the n-$Al_{0.51}Ga_{0.48}N$ (with Tom Mates assistance, refer to Table 4.1); however, N/(Ga+Al) fraction increased slightly after $SiCl_4$ etching. N/(Ga+Al) surface fractions were: 0.8 as-grown, 0.9 after annealing at 800 ^oC under N_2, and 1.0 after $SiCl_4$ etching and annealing at 800 ^oC under N_2. The surface atomic ratios of N/Ga were comparable for both etches. On the other hand, Al/Ga and Al/N fractions decreased the most at the n-AlGaN surface etched by $SiCl_4$ (The Al/Ga and Al/N ratio for $SiCl_4$ were half of that with the Cl_2/Ar etch.); the decrease in the Al/Ga and Al/N fractions might indicate a decrease in Al vacancies (acceptors) which might explain the

improved resistance for the $SiCl_4$ etched contacts. However, it worth noting that XPS measurements might not be accurate enough to discuss concentrations changes in atomic N and Al vacancies on the surface.

4.1.1.1 Optimizing the ohmic n-contacts annealing temperature for AlGaN 50-55%

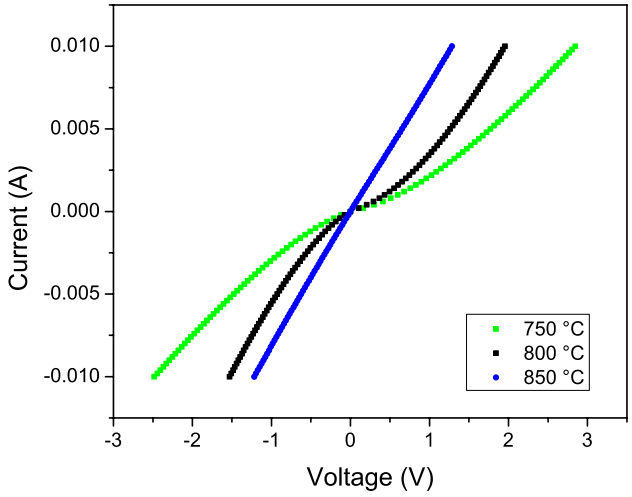

Figure 4.2. IV of n-CTLM structure with 10 µm gap on $SiCl_4/BCl_3$ etched n-AlGaN annealed at 750 °C, 800 °C, and 850 °C. The best anneal was at 850 °C.

The etched n-AlGaN sample was diced into three samples that were annealed at 750 °C, 800 °C and 850 °C (in N_2). The best Ti-based samples we obtained were ohmic contacts at 850 °C (refer to Figure 4.2). The specific resistivities were in the 10^{-4} Ω-cm^2 range (depending on the Hall electron concertation), which was equivalent to the lowest etched n-AlGaN *Ti-based* contacts reported in the literature.

4.1.2 Impact of Si flow on the specific n-contact resistance and n-AlGaN resistivity

To characterize the specific contact resistance after etching, circular transmission line method (CTLM) patterns [134,135] were deposited on the etched n-AlGaN surface (refer to Figure 4.3a). The IVs of CTLM patterns (refer to Figure 4.3b) were measured by a 4-point probe, and the data were fitted using the full CTLM equation as described by Asad Mughal in his PhD dissertation [136].

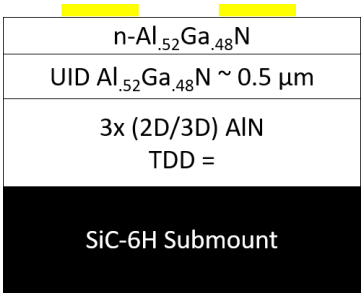

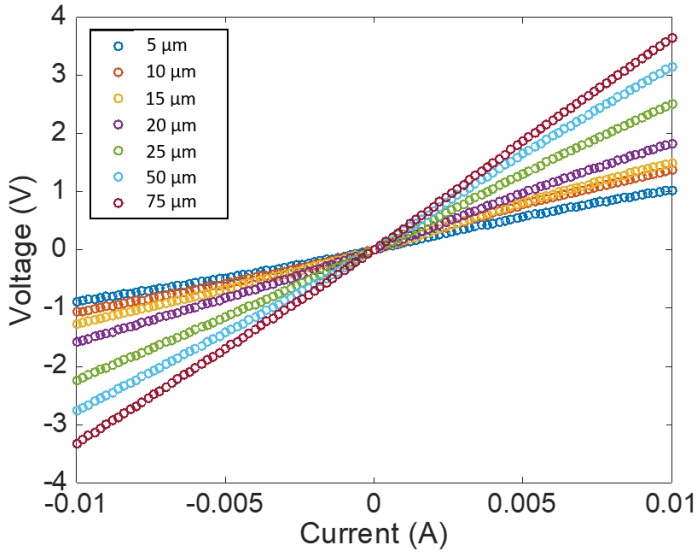

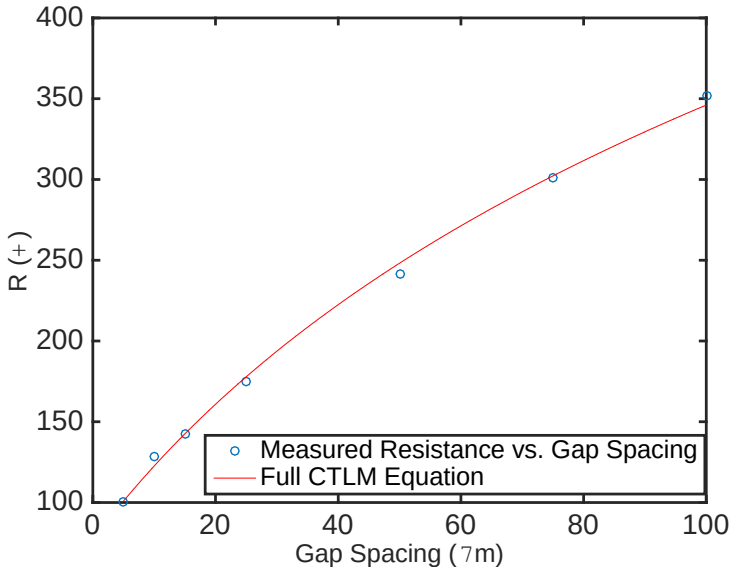

Figure 4.3. IV curves of CTLM structures for Ti/Al/Ni/Au (1-) contacts deposited on c-plane n-AlGaN after 850 °C annealing for 30 sec under N_2.

To maximize electron doping in n-AlGaN without causing self-compensation at too high an Si doping level, we ran an n-AlGaN series varying the Si flow: 100, 60, and 40 sccm. Table 4.2 shows that increased Si doping could result in compensating point defects. Under these n-AlGaN growth conditions, reducing the dislane flow increased the Hall electron concentration in n-AlGaN resulting in lower specific contact resistivity. The Hall electron density, Hall mobility, and resistivity were calculated from Hall measurements on the unetched surface. The best n-AlGaN resistivities we got for this AlGaN composition are summarized in Table 4.2. The specific resistivity decreased from 6.2 x 10^{-4} Ω-cm^2 to 4.6 x 10^{-4} Ω-cm^2 as the Hall electron concentration increased from 4.8 x 10^{18} cm^{-3} to 5.2 x 10^{18} cm^{-3}. The lowest resistivity achieved was 20 mΩ- cm, and the specific contact resistivity was 4.6 x 10^{-4} Ω-cm^2. While increasing the temperature is expected to reduce the amount of carbon and oxygen in AlGaN layers, increasing the temperature reduces the amount of Si incorporation and increases self-compensation [137–139].

Table 4.2: Impact Si flow on specific contact resistance and resistivity shows the limits of Si solubility in n-$Al_{0.52}Ga_{0.48}N$.

Disilane Si_2H_6 flow (sccm)	Hall Mobility (cm^2 V^{-1} s^{-1})	Electrons Hall density (cm^{-3})	Resistivity (mΩ-cm)	Specific contact resistance (Ω-cm^2)	Transfer length (μm)
40	60	5.2 x 10^{18}	20	4.6 x 10^{-4}	5.1
60	30	4.8 x 10^{18}	43	6.2 x 10^{-4}	6.5
100	Non-ohmic and rough surface				

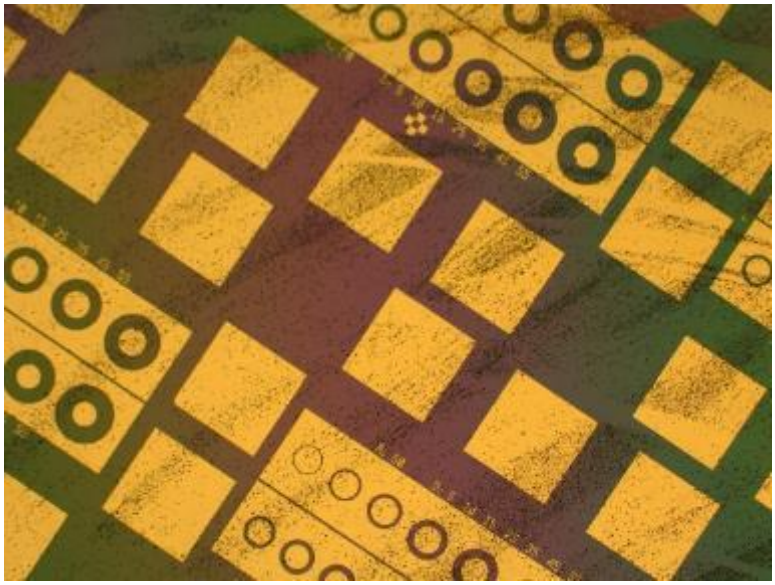

Figure 4.4 Micrograph for CTLM pattern on n-AlGaN doped at 100 sccm disilane flow had particles, rough surface, and non-ohmic contacts (inner circle radius in CTLM pattern is 50 μm).

4.1.3 Surface treatments

To determine the best surface treatment before n-contact metal deposition, the impact of buffered oxide etch (BOE), and HCl surface treatment before contact deposition were studied by comparing the IVs of a 10-μm gap CTLM structure. It was found that a HCl dip (1 min) yielded lower voltage than the BOE dip (1 min).

4.1.3.1 Impact of HCl vs BOE for $Al_{0.52}Ga_{0.48}N$

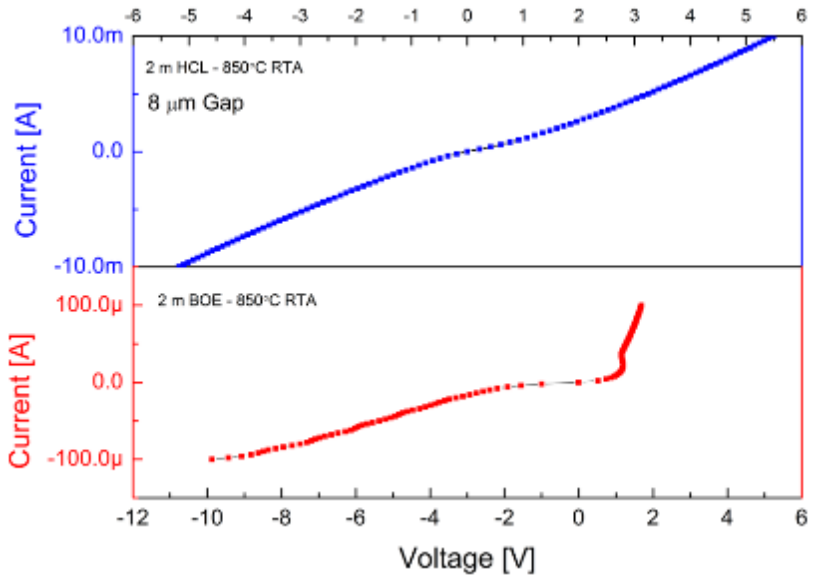

Figure 4.5: Impact of HCl and BOE surface treatment on the IV of 10 µm Gap CTLM.

Figure 4.5 compares the impact of HCl and BOE on the IV of a 10 µm gap CTLM. The surface treatment of HCl improved the contact performance, whereas the surface treatment in BOE added an additional voltage to the n-contacts. In the TFFC that we developed, the n-AlGaN surface touches BOE during the SiO_2 patterning step, which was a potential excess voltage source; however, the n-contacts' performance was recovered if the BOE surface treatment was followed by a subsequent dip in HCl for > 10 min.

Next, we investigated the impact of prolonged HCl exposure (refer to Figure 4.6). Additional exposure in HCl (10 min) reduced the voltage, especially at high currents. Interestingly, longer exposure to HCl (>10 min) lowered voltages at high currents and widened the contacts' optimum annealing temperature window; this is of practical importance because the n-AlGaN contact optimum annealing temperature increases slightly as the AlN composition increases.

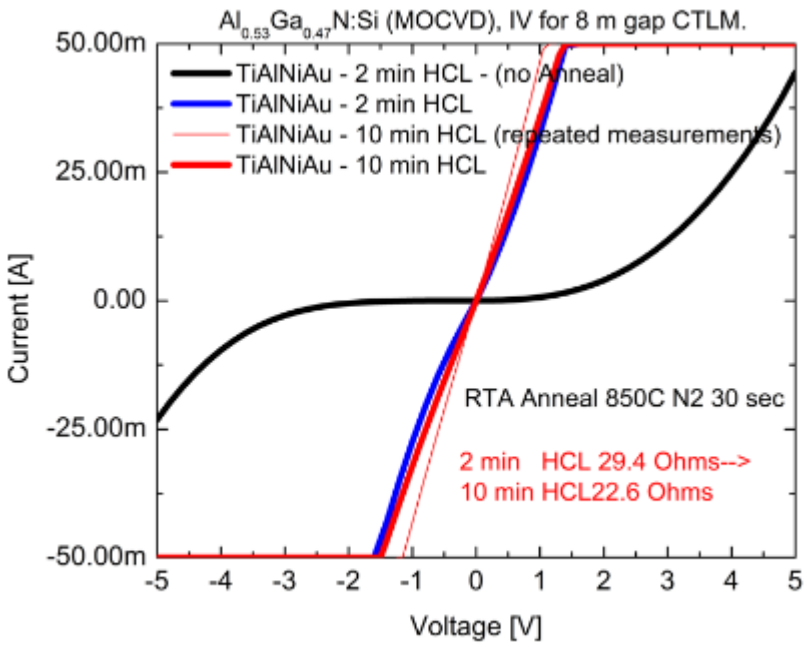

Figure 4.6. Impact of HCl surface treatment on the resistance of AlGaN:Si of 8 µm gap CTLM in the TFFC LED mask. Rapid thermal annealing at 850 °C yielded ohmic contact for $Al_{0.53}Ga_{0.47}N$.

4.1.4 Development of reflective n-contacts

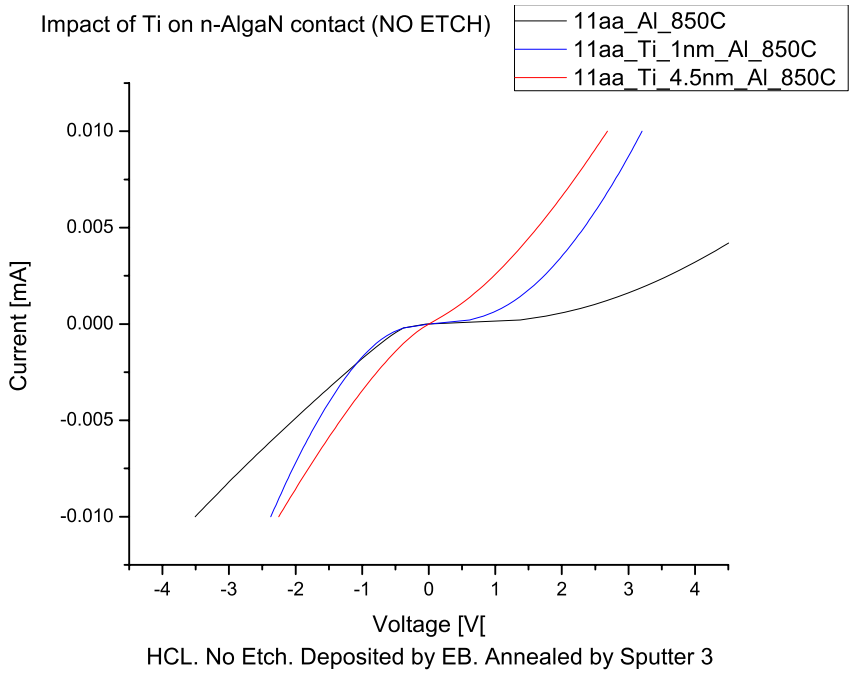

Figure 4.7. IV of three reflective n-contacts deposited with e-beam: Al only contacts and Ti/Al/Ni/Au with thin Ti of 1 nm and 4.5 nm. The anneal was carried out in an ultra-high vacuum inside a sputtering system at the highest available quartz lamp temperature of 850 °C (the actual anneal temperature was about 720 °C).

We attempted to develop *ohmic* and highly *reflective* contacts with Al only to help improve LEE [129]; however, the Al contacts were non-ohmic. Al-only contacts were developed for c-plane and semipolar GaN by Yonkee et al. without anneal, and with high vacuum anneal, respectively [129,140]. We tested several high-reflective n-contacts: Al contacts; and the regular Ti-based contacts (Ti/Al/Ni/Au). We attempted to develop Al contacts and Ti/Al/Ni/Au with ultra-thin Ti on unetched n-AlGaN (structure n-AlGaN/AlN/SiC), but the $SiCl_4$ etched contacts were non-ohmic. The n-contacts on a grown n-AlGaN surface were annealed in a high vacuum at 850 °C (the actual anneal temperature was about 720 °C) inside a sputtering system, and in a tube oven with ultra-low O_2 ppm (< 1 ppm). The IV curve in Figure 4.7 shows

the IV curve for the 10 µm gap CTLM for Al contacts, and for Ti/Al/Ni/Au with 1 nm and 4.5 nm Ti. Neither annealing of the Al contacts in ultra-high vacuum in a sputtering system nor in a tube-oven resulted in ohmic and reflective ohmic contacts; the Al contacts improved after the anneal, but were still highly non-ohmic. The 1 nm Ti had lower voltages than Al, but was still non-ohmic. The 4.5 nm Ti contact was almost linear, but slightly less linear than contacts with 10 nm Ti thickness . Annealing at higher temperatures might have yielded better results, but a lamp temperature of 850 °C was the maximum available (the actual anneal temperature was estimated to be ~720 °C.)

4.1.5 Impact of n-contacts annealing on the quality of bonding n-contacts with n-pads

After Ti/Al/Ni/Au n-contact annealing, which is needed to decrease the LED operating voltages, the n-contact needs fresh, soft Au instead of the alloyed contacts to bond the LEDs to the submount (in the case of Au-Au bonding). Redepositing the n-contact adds three issues to deal with: 1) increased processing steps to redeposit n-contacts; 2) an electrical issue: formation of a resistive thin oxide layer on the alloyed contact surface; and 3) a mechanical issue: alloyed contacts surfaces can be very rough and rigid.

To reduce the number of processing steps, we combined the 2nd n-contact re-deposition step with the p-contact that we didn't anneal to reserve high reflectivity (with 14 min HCl predisposition treatment). There was no difference in voltage before or after the new metal deposition with the HCl surface treatment. There was no need for ion milling to clean-up the oxide surface on alloyed contacts. The roughness of the alloyed contacts' surface was noticeably reduced by increasing the ramp up to 850 °C from 30 sec to 90 sec (refer to Figure 4.8).

(a) Ti/Al/Ni/Au as deposited by e-beam. (b) Annealed at 850 °C. Rapid anneal 30 sec.

Figure 4.8. Micrographs of part of the Hall and CTLM structure before and after annealing. It shows that the contacts' surface becomes rough after annealing. Changing the ramp-up time from 30 sec to 90 sec did not affect IV performance, but it reduced the roughness in the contacts, which makes the LED bonding more reliable.

4.2 p-AlGaN optimization

Pulsed-flow growth was used to grow AlGaN:Mg to enhance adatom surface mobility, reduce compensating defects and enhance p-type conductivity. Proper doping of GaN:Mg/AlGaN:Mg layer, improves injections into the active region, which improves the LED EL efficiency. High V/III ratio is thought to suppress the formation of nitrogen vacancies (V_N), which has low formation energies in AlGaN [141,142]; by optimizing III/V ratio, Kinoshita et al. [143] reported a record resistivity of 47 Ω-cm in $Al_{0.7}Ga_{0.3}N$:Mg, and Nilsson et al. [124] reported a resistivity of 60 Ω-cm in $Al_{0.6}Ga_{0.4}N$, in a hot wall MOCVD reactor (the lowest $Al_{0.6}Ga_{0.4}N$:Mg resistivities are ~6000X order of magnitude higher than the lowest n-AlGaN resistivities). Grading the Al-composition over a short range could result in increased 3D hole gas concentration, via polarization doping [26], however, we did not have time to

study this approach. Although the hole density is lower than the compensating oxygen impurities in AlGaN:Mg, proper doping of AlGaN:Mg resulted in a reduced series resistance for the diodes, as shown in Figure 4.9. The recipe for pulsed AlGaN:Mg developed by Mike Iza and two experiments were done to optimize the Mg in a UV LED structure (refer to figure 4.9).

Characterizing the AlGaN:Mg properties by CTLM and Hall structures is challenging because of the high ionization energy of Mg in AlGaN:Mg, which results in very low hole densities, lower than oxygen densities. Furthermore, CTLM and Hall measurements study lateral charge transport over +10 μm, while in LEDs the charge transports a very thin layer (50 nm or so) of p-AlGaN. Therefore, we decided to optimize the p-AlGaN through the IV of diodes even though growing working diodes proved challenging.

Additionally, minimizing the thickness of AlGaN:Mg should improve the hole injection, reduce and the series resistance. AlGaN:Mg thickness at 50 nm is fully depleted, with the depletion region between the p-GaN and n-AlGaN, contributing a small fraction of the resistance (< 4% for 300 nm UV LED). Reducing the AlGaN:Mg was possible from 100 nm to 50 nm, but once we reduced the AlGaN:Mg thickness from 50 nm to 10 nm, the LEDs were not rectifying and acted as a normal resistance. The 50 nm of AlGaN:Mg was grown over 30-periods (during each period, we supply 33 sec of NH_3, TMA, TMG, TMI pulses, followed by 2 sec of NH_3). This indicates that there is a minimum thickness (time) needed to dope and incorporate the Mg into AlGaN and GaN because of the Mg memory effect. Regardless of the ultra-fast MFCs, Mg needs to saturate the growth chamber and reactor walls before it starts to incorporate into the AlGaN and GaN. The pre-flow of the Mg source (Cp2Mg) prior to

AlGaN:Mg or GaN:Mg growth is critical for successful growth. , but it does not eliminate the Mg incorporation delay time and therefore limits the minimum p-AlGaN/p-GaN thickness.

It is worth noting that since the growth window of a low-resistance AlGaN:Mg layer is reported to be very narrow, we were very concerned about it when the LEDs turned out with dismal currents (<<1 mA at 20 V); however, the high resistance was usually due to a highly resistive n-AlGaN layer.

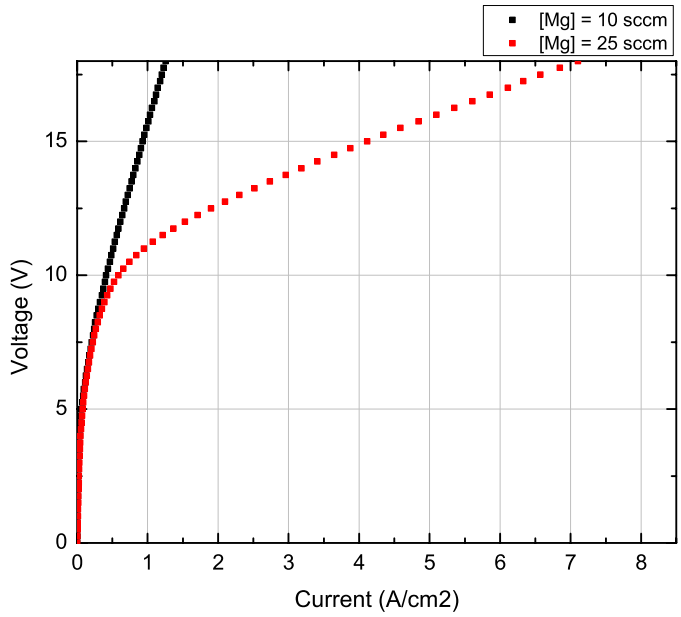

Figure 4.9. IV curves for two LEDs with pulsed doped AlGaN:Mg and 10 nm p-GaN. Increasing the Mg source flow from 20 to 25 sccm reduced the series resistance of the LED (with 10 nm p-GaN) diodes by 4.5X. Although holes density is estimated to be lower than oxygen impurities, optimizing Mg incorporation to increase holes densities in the AlGaN:Mg can still result in significant reduction of the diode series' resistance.

4.3 p-GaN

4.3.1 Choice of p-contacts for p-GaN

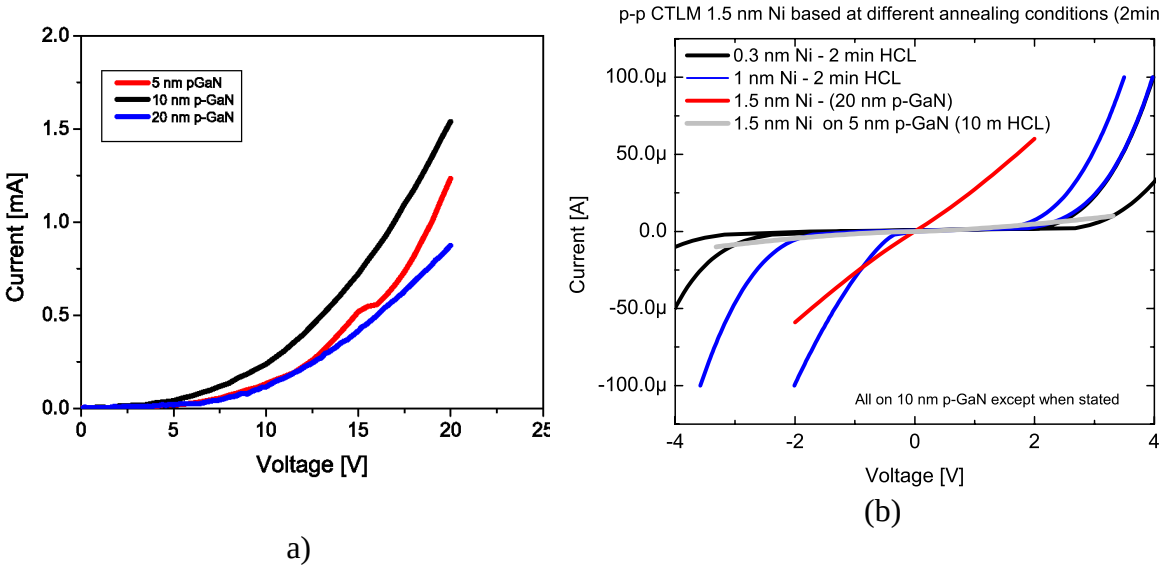

a) (b)

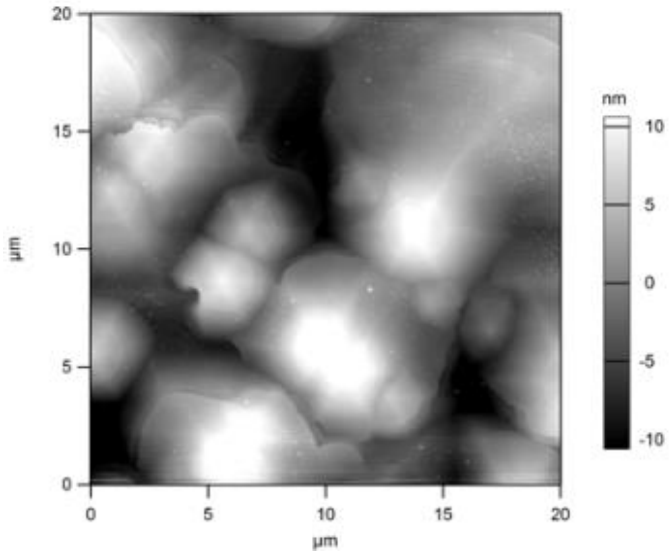

(c)

Figure 4.10. (a) IV for UV LED with the p-GaN series for 5, 10, 20 nm yielded surprising results: the p-contact resistance impact on series resistance was negligible because of highly resistive n-AlGaN, which dominated the series resistance of the diode. (b) IV for several p-CTLM structures on the p-GaN surface of UV LED on the right (diode turn on above 4 V) ruled out any problem with p-GaN. The IVs shows p-contact quality was good and the p-contact were ohmic at thick enough p-GaN (1.5 nm Ni on 20 nm p-GaN) or thick enough Ni (1.5 nm Ni on 5 nm p-GaN). (c) AFM of p-GaN surface shows island growths of 10 nm p-GaN.

The p-GaN MOCVD growth recipe was adapted from Ryo Tanaka, who optimized low-temperature p-GaN regrowth techniques for the junction barrier Schottky (JBS) diode. To decide on the p-GaN thickness, we considered the trade-offs between voltage efficiency and light extraction efficiency. The goal was to achieve a p-contact voltage efficiency of ~80% while maximizing the light extraction for the device. The resistance contribution from the p-contacts will decrease as the p-contact area increased. In the first-generation TFFC microLEDs, the p-contact area was limited (because of limited n-AlGaN sheet resistivity at the time) which resulted in less power output per μLED and increased voltage. Increasing the device areas should reduce the p-contact contribution. Figure 4.10a shows the IV of UV LED (refer to Figure 4.13) for a p-GaN series: 5 nm, 10 nm and 20 nm that had very low current of ~ 1 mA at 20 V, even though the LEDs with thicker p-GaN had lower p-contact resistivities; a typical suspect would be p-GaN contact or AlGaN:Mg. However, Figure 4.10b shows *lateral* transport of holes in CTLM structures; the IV curves shows p-contact had low contact resistivity at thick enough Ni (1.5 nm) on 20 nm p-GaN, and at thick enough Ni (1.5 nm) on 5 nm p-GaN. The culprit was not the hard-to-dope but thin AlGaN:Mg layer (50 nm), but the n-$Al_{0.52}Ga_{0.48}N$ layer sheet's resistivity. (This has been a recurring issue during our research on the TNSC SR-4000: n-AlGaN resistivity would increase suddenly if the reactor flow channels are not cleaned regularly, every 10-15 growths or so.) To avoid the recurrence of such problems (or mistakes in growth), we started checking the n-AlGaN resistivity before growing any LED series by growing an n-AlGaN/AlGaN/AlN/SiC and measuring the n-AlGaN's Hall electron concertation and Hall electron mobility to calculate n-AlGaN resistivity with ohmic indium dots (which is comparable to results from processed ohmic contacts but gives immediate

feedback). Once we fixed the n-AlGaN resistivity, the current at 7 V was 20 mA rather than ~ 1 mA or less at 20 V (refer to next section).

4.3.2 Impact of passivation on n-AlGaN, p-GaN and LED

The LED mesa plasma-etched side walls (especially LEDs with narrow mesa widths, such as 50 or 60 μm) need to be passivated by the deposition of a dielectric after the mesa etch. If the sidewalls of narrow LED mesas are passivated, most of the LEDs become leaky, perhaps because of side-wall conduction due to plasma etch damage. We studied the potential damage on a n-AlGaN surface or p-GaN surface to select the appropriate dielectric type among the options available in the cleanroom: PECVD SiN_x and AlD SiO_2. We did not consider sputtering SiO_2 because of reports that it could damage the p-GaN or p-AlGaN surface, but also because the other tools were more available in the cleanroom. However, sputtered SiO_2 was used on the LEDs if the passivation steps were delayed to post p-contact deposition without impacting the LEDs' voltages. The requirement on the dielectric type was that it does not etch in KOH during the time needed to roughen the N-AlN of the TFFC LEDs (20 sec -70 sec). The etch rate of ALD SiO_2 and PECVD SiN_x in KOH at room temperature was negligible (< 10 nm per hour).

The n-AlGaN surface did not suffer any noticeable damage after exposure to PECVD SiN_x or ALD SiO_2; however, the BOE etch through SiO_2 exposes the n-AlGaN surface but does not cause any additional voltage (as we explained earlier in this chapter) because the n-contacts' performance does not degrade by exposure to BOE; the n-contacts became ohmic after we dipped the samples in HCl for 14 min (>10 min).

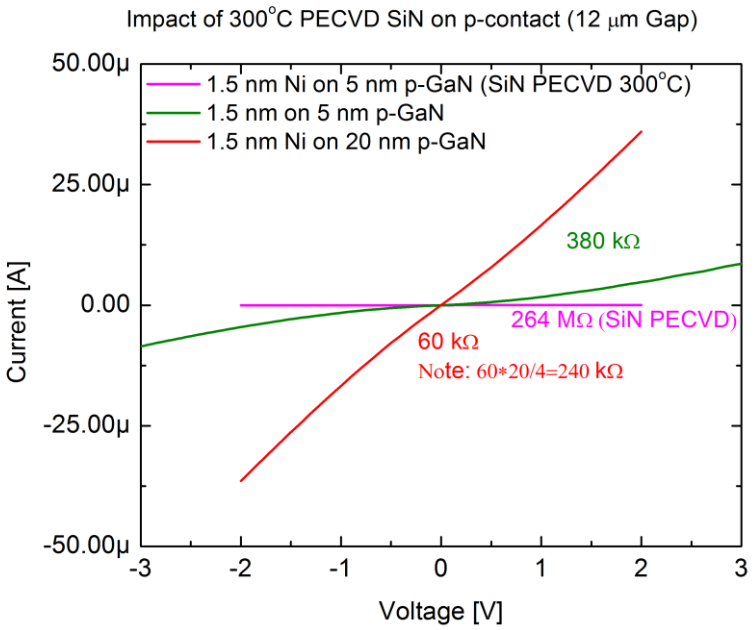

Figure 4.11. (a) Comparison between the IV of CTLM structure on a 5 nm p-GaN, as grown (green curve), and passivated by SiNx PECVD (pink curve). The red curve (a reference) is the IV of CTLM structure on a 20 nm p-GaN, as grown.

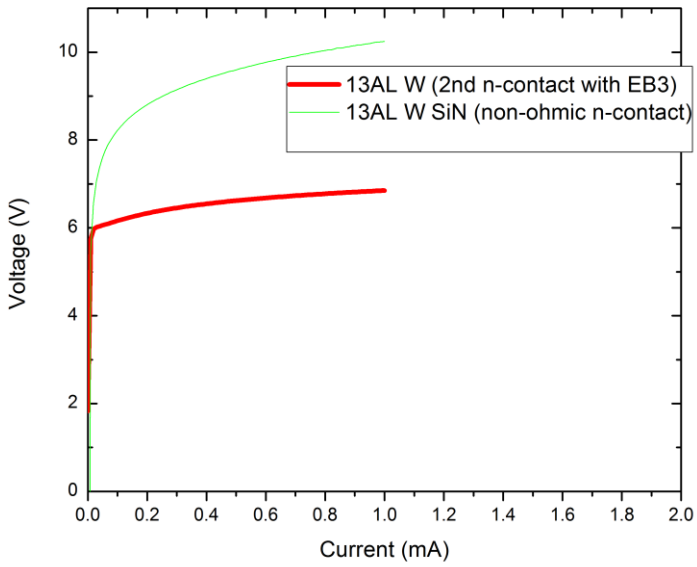

Figure 4.11. (b) Impact of PECVD passivation on p-GaN contact resistivity as captured by four volts of excess voltage LED IV.

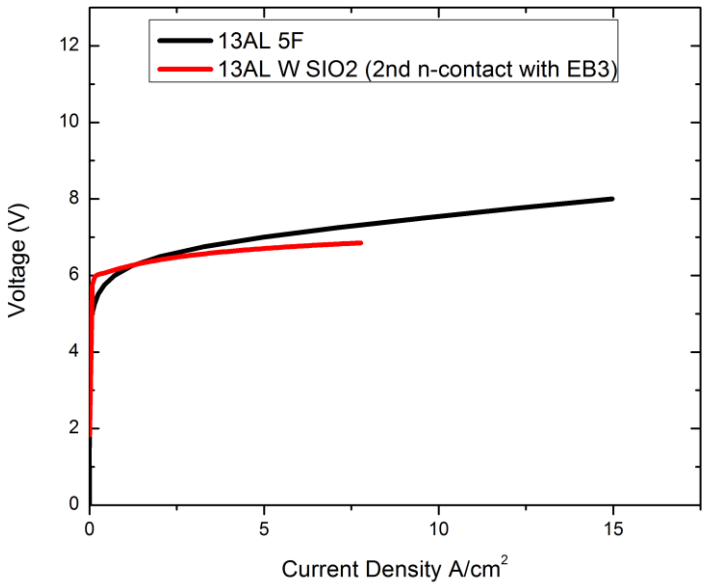

Figure 4.11. (c) Impact of ALD SiO_2 passivation on p-GaN contact resistivity as captured by LED IV. Without passivating the side walls of narrow mesas, most LEDs were leaky.

The p-GaN surface was damaged by exposure to PECVD plasma at the relatively high temperature of 300 °C, as shown by CTLM IV in Figure 4.11a and by LED IV in Figure 4.11b. In contrast, SiO_2 deposition by ALD did not yield additional p-contact voltage (refer to Figure 4.11c).

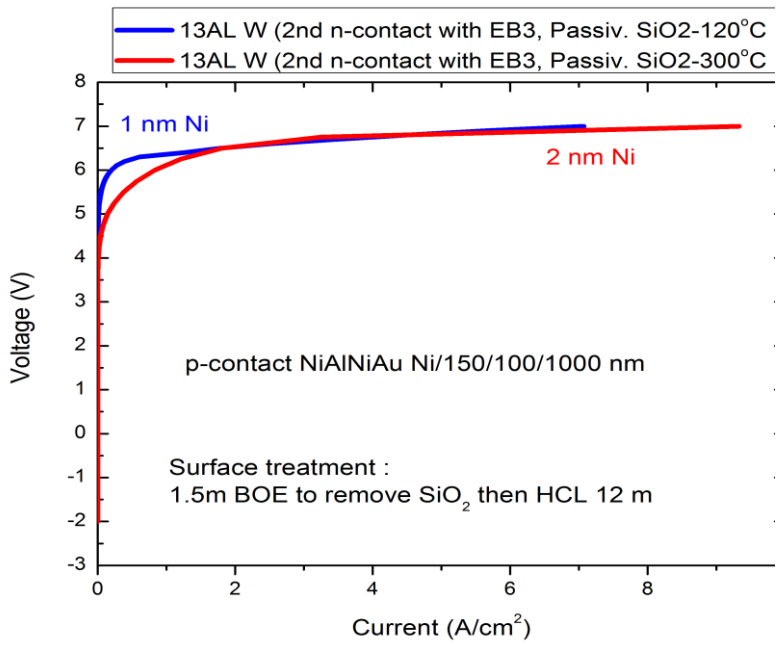

Figure 4.12. Impact of using thinner Ni (1 vs 2 nm) in the p-contact (Ni/Al/Ni/Au) on the UV LED IV characteristics.

Figure 4.12 shows the voltage impact of using thinner Ni (1 vs 2 nm) in the p-contact (Ni/Al/Ni/Au) on the UV LED IV characteristics (LED structure is shown in Figure 4.13). However, the variability among devices was higher in the case of 1 nm Ni deposited by e-beam, so for the first demonstration, we decided to go with 1 nm Ni. We conducted another Ni/Al/Ni/Au p-contact series with 1 nm Ni and 1 nm Pt for LEDs on top of 100 nm Al/100 nm Ni/1000 nm Au; however, the EL on those UV LEDs was too small to measure (< µW) due to high TDD (~1.5×10^{10} cm^{-2}) and non-optimal active region structure.

In UV LEDs, the hole injection is vertical over ~ 60 nm of AlGaN and GaN, so obviously, the massive *lateral* p-contact resistance *over several microns* (shown in Figure 4.10b) was only a guide to optimize and study the p-contacts. For the 1st generation of LEDs, we tried 2 nm and

1 nm Ni p-contacts LEDs using ohmic p-contacts (for Ni> 1.5 nm) as shown in Figure 4.10b, and ohmic n-contacts as shown in Figure 4.5 and 4.3.

4.4 TFFC LEDs

We demonstrated a 310 nm LED (6.2 mW/mm^2 at 45 A/cm^2) [72,144] and 297 nm LED (1 mW/mm^2 at 20 A/cm^2) on a highly dislocated AlN buffer layer 1.5 $x10^{10}$ cm^{-3} (refer to Figures 4.13 and 4.14). We optimized the KOH roughening at 3.5 °C, 25 °C and 75 °C (refer to Figures 4.15, 4.16 and 4.17). We found out that TFFC LED LEE is increased by 100% after the KOH roughening of the exposed nitrogen-face AlN (without light assistance) in TFFC LEDs with a 2/80/100/1000 nm Ni/Al/Ni/Au as p-contact to a 10 nm p-GaN layer. Although we conducted the demonstration on micro-LEDs with 0.013 mm^2 because of limited n-AlGaN sheet resistance at the time of mask design and processing, the TFFC LED area is actually scalable to larger LEDs areas (> 1 mm^2). The TFFC LED brightness and luminous flux directly scale with the LED emitting area [145].

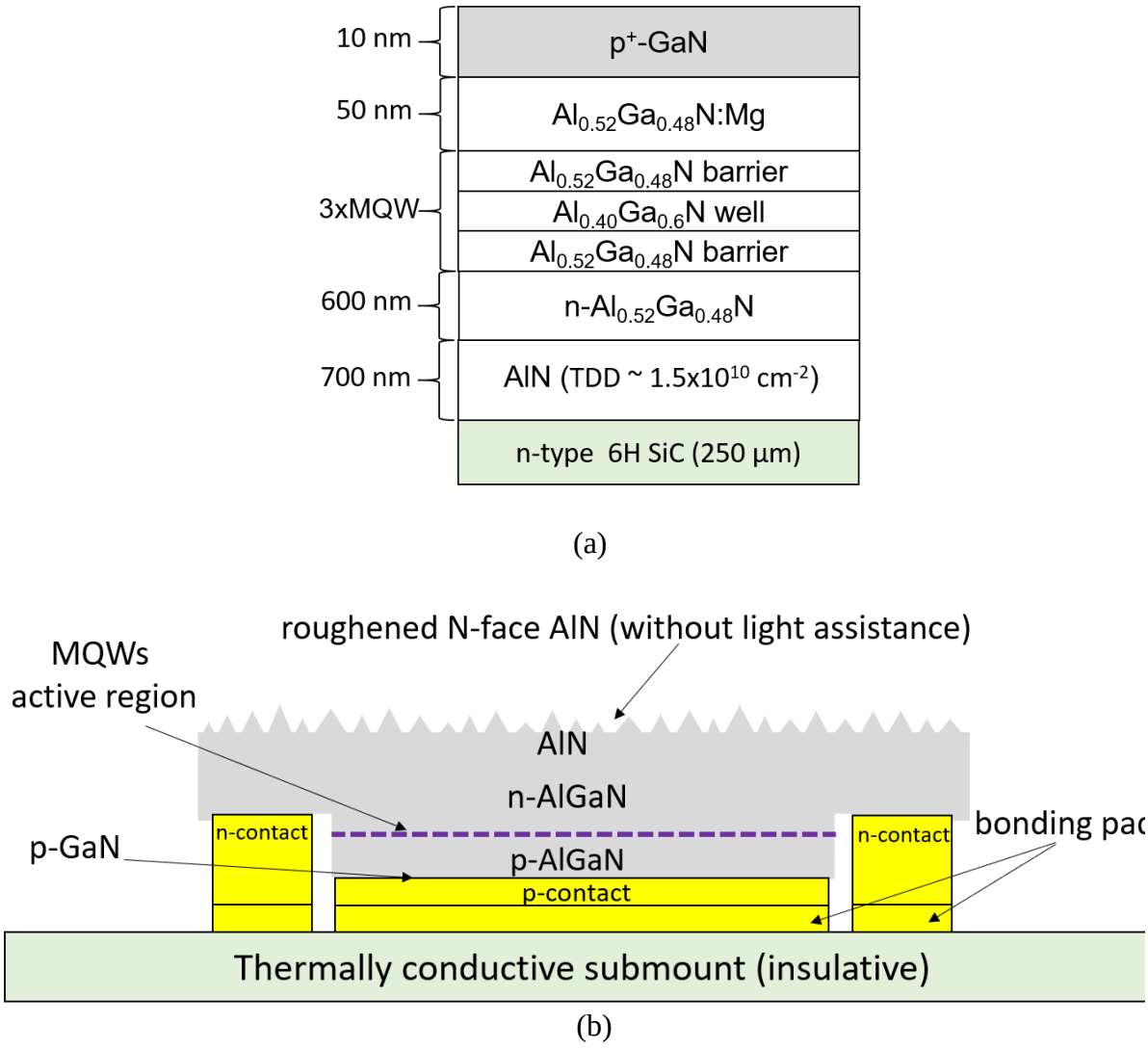

Figure 4.13. (a) epi structure of the UV AlGaN LED grown on SiC. (b) TFFC LED structure.

4.4.1 Experimental

The AlGaN LEDs were grown by metal-organic chemical vapor deposition (TNSC SR-4000 MOCVD) on the Si face of c-plane (0001) SiC substrate. The RMS roughness of the SiC substrates was < 1 nm. The MOCVD precursors used were ammonia, trimethylgallium (TMG), and trimethylaluminum (TMA). Disilane (SiH_4) and bis(cyclopentadienyl) magnesium (Cp_2Mg) were used for AlGaN n- and p-doping, respectively.

Fig. 4.13a shows the device structure, which consisted of six layers: an AlN buffer layer (700 nm), n- $Al_{0.52}Ga0_{0.48}N$ (600 nm), MQW active region (297 nm), p- $Al_{0.52}Ga0_{0.48}N$:Mg (50 nm), and p-GaN:Mg (10 nm). We did not use an electron-blocking layer in this structure because we did not observe any parasitic peak in the emission. The AlN buffer layers were grown on SiC substrates with TDD of $1x10^{10}$ cm^{-2}, as measured through transmission electron microscopy (TEM). After the growth, a thermal anneal at 850˚C for 3 min under N_2 was performed to activate the Mg-doped p-GaN and p-AlGaN. The samples were then dipped in boiling aqua regia ($HCl:HNO_3$ (3:1) at 120 ˚C for 3x10 min. The LEDs mesas were etched with RIE ($BCl_3/SiCl_4$) to access the n-AlGaN layer. The samples were then dipped in DI water for 1 min to remove etch residue, and in HF for 30 sec (to remove etch residue).

The LED sidewalls were not passivated but passivation is recommended as SiO_2 (50 nm) was deposited by atomic layer deposition. The SiO_2 was patterned with a buffered oxide etch (BOE) before n-contact and p-contact deposition as follows: BOE was used to pattern the SiO_2 (30 sec), then the samples were dipped in DI water (1 min) and in HCl (14 min).

The n-contacts (Ti/Al/Ni/Au) were deposited by electron beam. Then, the n-contacts were annealed at 850 °C and the CTLM measurements were performed to estimate the n-contact specific resistivity. Ni/Al/Ni/Au were deposited as p-contacts. Then, devices on the growth substrate were aligned wafer-to-wafer to a bonding substrate. The wafer-to-wafer (W2W) Au-Au thermocompression bonding was made using Finetech flip-chip bonder at 300 ˚C for 1 hr. The bonding substrate was made by patterning n- and p-pads (Ti/Au 20/1000 nm) on a highly thermally conductive substrate (n-type SiC substrate covered with 100 nm of low stress SiN). After bonding, the SiC growth substrate was mechanically thinned to 90 µm, followed by a two-step plasma etch using ICP SF_6 plasma: a fast SiC etch (40 µm/hr) and a slower SiC etch

(5 μm/hr), but with high selectivity (AlN etch rate is ~ 200 nm/hr); the details of the thinning and ICP SF_6 plasma etching were reported in Chapter 2. The highly selective etch accounts for any substrate non-uniformity within ~ 10-20 μm of total thickness variation. The μLED thin-films were packaged to TO-39 headers and measured in an integrating sphere.

The n- and p-type contacts were bonded to n- and p-metalized insulating submount by Au-Au thermocompression bonding. Then the growth SiC substrate was mechanically thinned and etched with a highly-selective SF_6 plasma that exposed a pristine ~700 nm AlN buffer layer.

4.4.2 Results and discussions

Figure 4.13a shows the microLEDs structure for the 297 nm μLED. Figure 4.13b shows a schematic of the TFFC microLEDs and Table 4.3 summarizes the structure of the 297 nm μLED. Figure 4.14a shows an SEM image of a packaged UV AlGaN thin-film flip-chip TFFC microLEDs (297 nm). The freestanding thin-film surrounding the LED is under tensile stress (concave-up thin-film).

The ideal turn-on voltage for UV microLEDs emitting at 297 nm is slightly below 4.17 V. The best commercial LEDs' forward voltages at 20 A/cm^2 are around 6.5 V (refer to table 4.4 for the voltage breakdown), however, UV-C LED operations will probably be at higher current densities and thus special attention need to be paid to series resistance. There is a tradeoff between p-contact resistance and light extraction. The voltage is dominated by p-contact resistance, n-contact resistance, and p-AlGaN series. (refer to Table 4.4 for the voltage breakdown). We were able to develop 297 nm microLEDs with ~6.4 V at 20 A/cm^2, yet because the n- and p- contacts area of the microLEDs were small, their excess voltage contribution to the μLED were high (28% and 56%, respectively). As a result, the voltage at high current density was high, 85.5 A/cm^2 are around 8.5 V.

Figure 4.14a shows an SEM image of a packaged UV AlGaN thin-film flip-chip TFFC microLED (297 nm), and Figure 4.14b shows a CCD image of a microLED EL emission (UV exciting AlGaN/AlN) at 2 mA. After roughening, the UV TFFC microLED power increased to 1 mW/mm^2 at 20 mA for LED in Figure 5.15b, and 1 mW/mm^2 at 60 mA in Figure 5.16b. Figure 4.19 shows an EL wavelength shift from 297 nm at 25 mA to 299 nm at 60 mA; and the FWHM was 14 nm at 25 mA.

KOH roughening was used to enhance the LEE from the TFFC microLEDs. Figures 4.15a, 4.16a and 4.17 shows that proper KOH roughening did not degrade the IV characteristics of the TFFC microLEDs. Figure 4.16b shows the impact of KOH roughening on the UV TFFC microLED power as a function of current. After 20 seconds of KOH etching the AlN buffer layer at room temperature, the LEE of the TFFC LED increased by ~100% after KOH roughening for 20 sec. As the smooth N-face AlN surface is roughened by etching in KOH [0.25] at room temperature, the LEE and the power increase but ultimately the marginal gains in LEE start to decrease gradually. KOH etching forms hexagonal cones that roughen the AlN surface and reduces its effective refractive index. The power levels after 20 sec of etching were only slightly higher than after 15 sec of etching. After a total of 26 sec of KOH etching, the microLED power dropped and the IVs became leaky. The AlN thickness in this LED was 650 nm. It seems that after 26 sec of etching, KOH starts etching into the n-AlGaN, affecting its sheet resistance, as well as beginning to etch into the active region, making leakage pathways.

We studied the LEE as function of cones density, size and KOH etch temperature (refer to Table 4.5). The maximum power enhancement obtained at 3.5 °C was 1.8X (after 129 seconds, refer to figure 4.15b), 2X at room temperature (after 20 sec, refer to figure 4.16b), and 1.1X at 75 °C (after 10 seconds). Figure 4.18 shows that the light extraction was enhanced by

roughening in KOH by 2X at room temperature with cones side length (~100–85 nm) smaller than EL wavelength, with density of 42–52 cones/μm^2, but only by 1.1X at 75 °C (cones side length ~440-360 nm and cones density of around 2-3 cones/μm^2); for long duration etches, depending on the AlN thickness, the etch starts to etch n-AlGaN and MQWs, and causes the LED to be leaky. The thickness of the AlN buffer layer was 600 nm with TDD of 1.5x10^{10} cm^{-2}. We were unable to grow thicker AlN at this point because the epi was cracking without the high temperature nitridation of SiC in H_2/N_2 mixture before AlN growth. The high TDD limited the IQE to below 0.1%, which impacted the power output of the microLEDs. Although we conducted the demonstration on microLEDs with 0.013 mm^2 because of limited n-AlGaN sheet resistance at the time of mask design and processing, the LED area is scalable to larger LEDs areas (> 1 mm^2). The TFFC LED brightness and luminous flux directly scale with the LED emitting area [145].

Table 4.3. Summary of the structure of 297 nm LED.

Structure	Description
TDD in AlN	1-2x10^{10} cm^{-2}
Active region	3x MQW
n-$Al_xGa_{1-x}N$	x=0 52%
n-contact (0.019 mm^2)	Ti/Al/Ni/Au
n-contact specific resistance	5x10^{-4} Ohm cm^2
$Al_xGa_{1-x}N$:Mg	x= 32%
p-GaN thickness	10 nm
p-contact (0.0129 mm^2)	Ni/Al/Ni/Au 2/150/100/1000 nm
p-contact specific resistance	1.5 x 10^{-3} Ohm cm^2
Power density at 20 mA	1 mW/mm^2
Enhancement of LED power after KOH roughening	~100% at KOH temperature of 25 °C

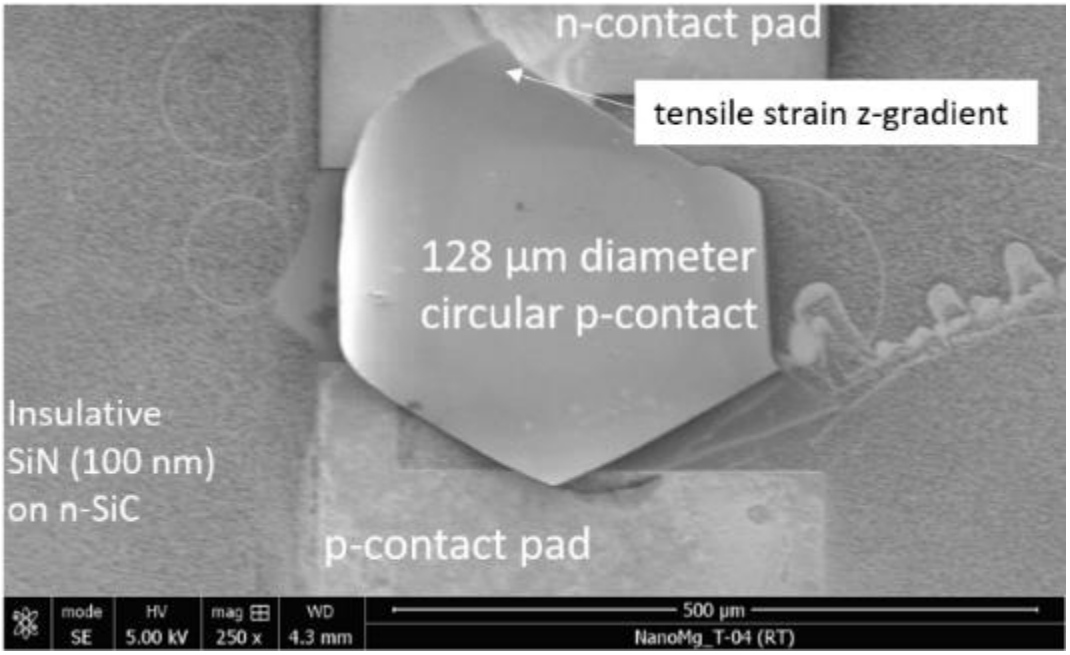

(a)

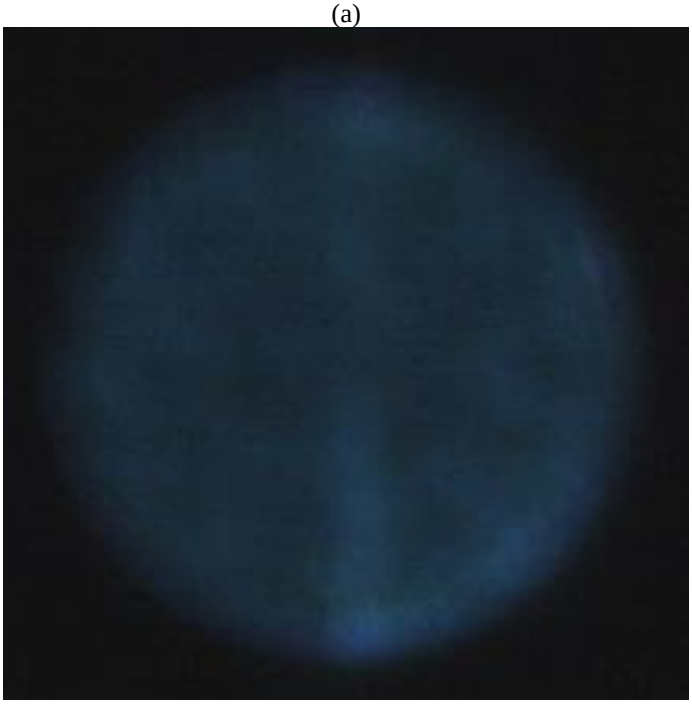

(b)

Figure 4.14. (a) SEM image of a packaged UV AlGaN thin-film flip-chip TFFC LED (297 nm). (b) CCD image of a UV LED of the EL emission (exciting AlGaN/AlN) at 2 mA.

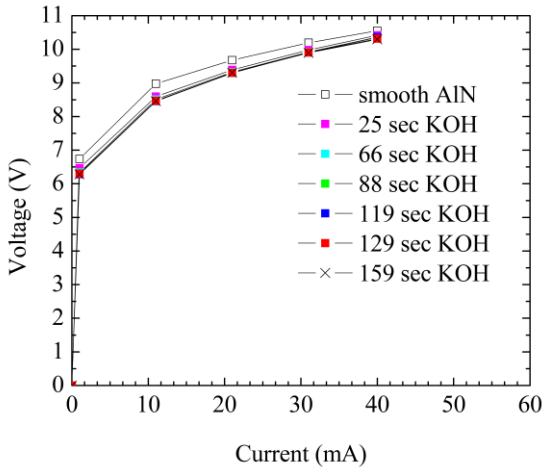

(a) TFFC LED (297 nm) IV at 3.5 °C.

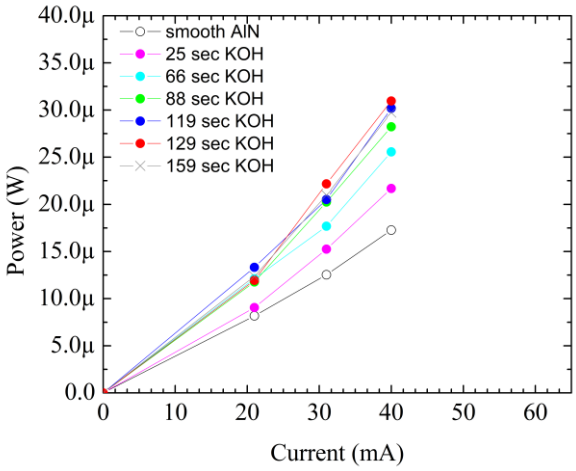

(b) Impact of KOH roughening (at 3.5 °C) on TFFCLED power output.

Figure 4.15 (a) IV of 297 nm TFFC LED (161030AL) under DC operation. (b) The LI characteristics of the 298 nm LED before and after roughening in [.25 M] KOH at 3.5 °C. The power was limited because of high TDD ~ $1.5x10^{10}$ cm^{-2} in the AlN buffer layer.

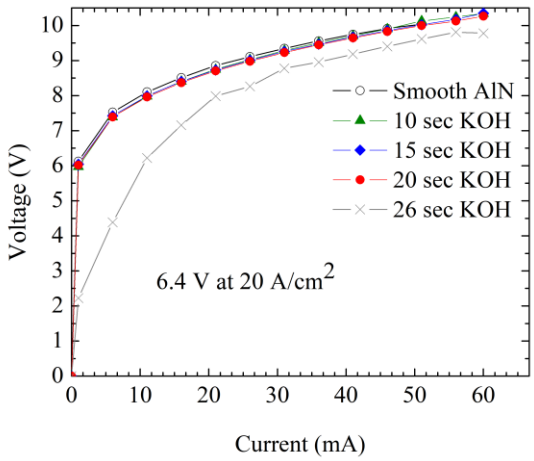

(a) TFFC LED (297 nm) IV during roughening at 25 °C. Voltage was 6.4 V at 20 A/cm^2.

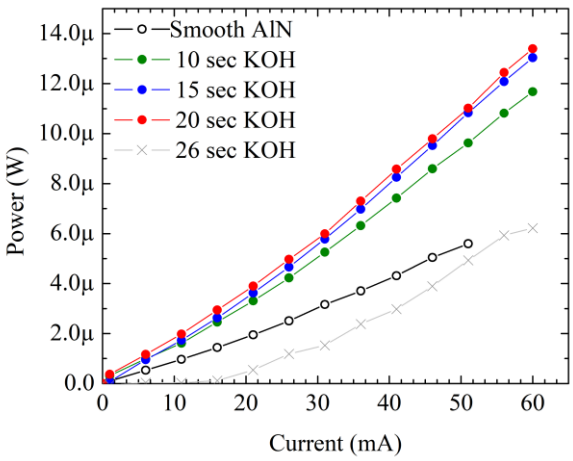

(b) Impact of KOH roughening (at 25 °C) on TFFC LED power output.

Figure 4.16 (a) IV of 297 nm TFFC LED (161030AL) under DC operation (5 sec integration time). (b) The LI characteristics of the 298 nm LED before and after roughening in [.25 M] KOH at room temperature 25 °C. The power was limited because of high TDD ~ $1.5x10^{10}$ cm^{-2} in the AlN buffer layer.

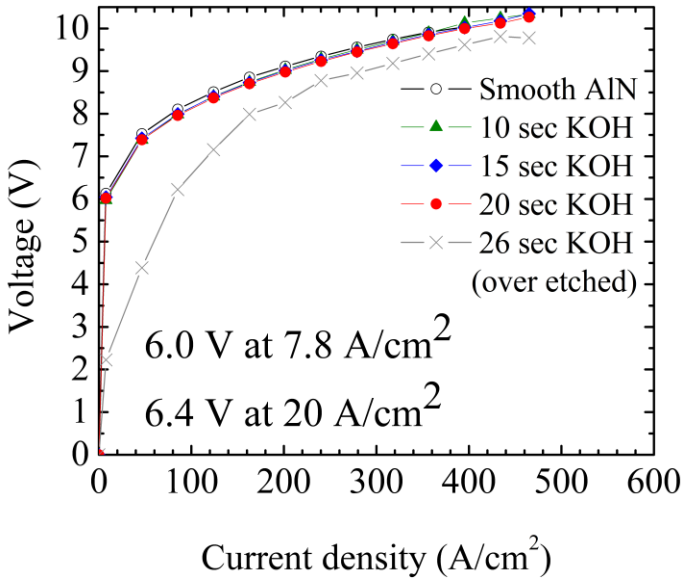

Figure 4.17 JV of 297 nm TFFC LED shown in Figure 4.16. KOH roughening was at room temperature 25 °C. Voltage was 6.4 V at 20 A/cm^2.

Table 4.4. Estimate of series resistance (excess voltage) contribution to TFFC LED in figure 4.16a.

Resistance contribution	**Specific contact resistance (Ω cm^2)**	**Resistivity (Ω-cm)**	**Thickness (μm)**	**Resistance (Ω)**
n-contact resistance	5 x 10^{-4}			2.6
p-contact resistance	1.5 x 10^{-3}			11.6
Total contact resistance				14.2
Layer resistance				
p-GaN (vertical)	-	5	0.01	0.039
p-AlGaN(vertical)	-	260	0.05	10.08
n-AlGaN (vertical)	-	0.02	0.3	0.0047
n-AlGaN (lateral)	-	0.02	10	0.0005
Total Transport resistance				*10.2*
Total LED resistance				**24.5 Ω (3 mΩ cm^{-2})**

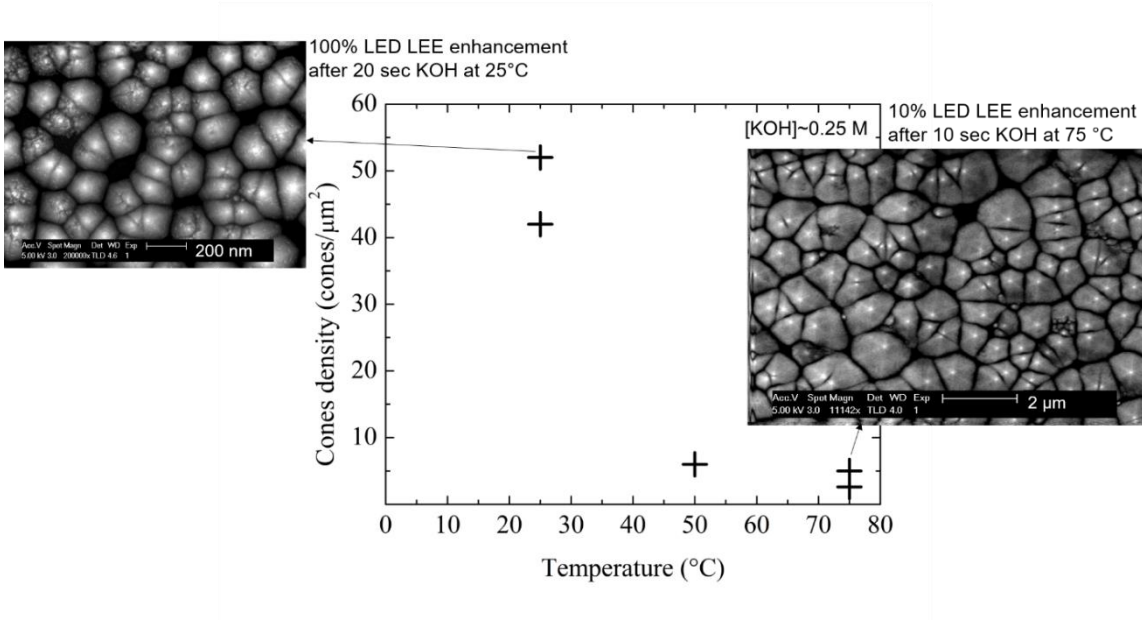

Figure 4.18. The inset shows an SEM image of roughened AlN surface.

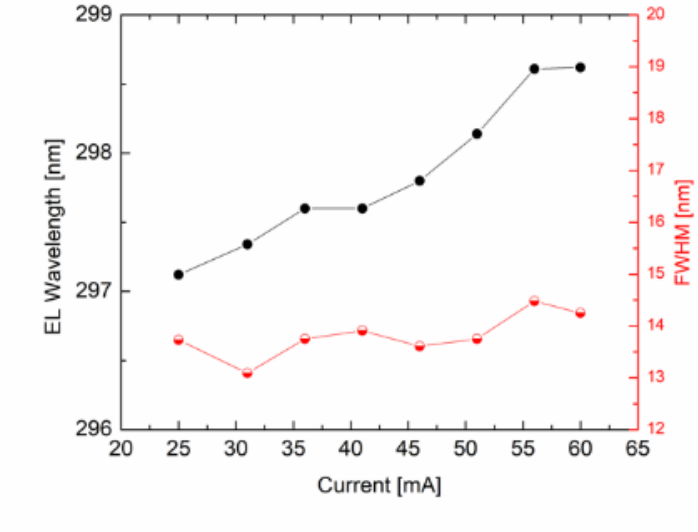

Figure 4.19. EL and FWHM of 297 nm TFFC LED as a function of current.

Table 4.5. TFFC LED LEE enhancement after KOH roughening at different temperature. The LEE enhancement depends on cones sizes and AlN/AlGaN etch depth.

Temperature (°C)	Etch time in [0.25 M] KOH	LEE enhancement after KOH roughening	KOH induced AlN hexagonal cones density	Average hexagon side length
3.5	129 sec	1.8X	--	--
25	20 sec	2X	42–52 cones/μm^2	~100–85 nm
75	10 sec	1.1X	2–3 cones/μm^2	~440-360 nm

4.4.3 Reasons the LEE was limited to 2X

The best results for LEE enhancement after roughening were only 100% (2x). There are several reasons for the light extraction being limited to 2X: p^+-GaN absorption, use of p-contact with 2 nm Ni, and bonding at 300 °C, and internal epi losses. Emission reflected from the p-contact for the first time has to travel (2x10 nm =20 nm) of p^+-GaN. Ga has an absorption coefficient of $1.5x10^5$ cm^{-1} at 275 nm [46], and p^+-GaN absorption will be even higher. In the next chapter, we show how to improve the light enhancement after KOH roughening of the TFFC LED to ~3X. These issues as well as ways to improve LEE further will be explored further in the next chapter.

Chapter 5: Development of 2nd generation thin-film UV LEDs

"If you want to be inventive, you have to be willing to fail…patience, persistence, and obsessive attention to detail."

Jeff Bezos

Thin-film technologies have yet to be developed for AlGaN LEDs [20,25,48,72,108–111,113,146]. Thin-film architecture results in higher surface brightness than bulk (volumetric) LEDs and enables better extraction of oblique TM emission from AlGaN quantum wells. Furthermore, lateral thin-film flip-chip (TFFC) LEDs avoid light absorption losses by a top n-contact or by the wire-bonds and allow for direct, dense integration into chips (without wire-bonding). The emission from thin-film blue LEDs is Lambertian after surface roughening [2,147], which is also applicable to UV TFFC LEDs and means that luminous flux and brightness directly scale with the LED emitting area [145].

5.1 Growth of UV-C LEDs

We will describe our efforts to optimize the different LED layers: AlN, n-AlGaN layer, active region, AlGaN:Mg, and p-GaN layers. The results for n-contacts and p-contacts are summarized in Table 1. Abdullah Almogbel, Christian Zollner, Humberto Foronda and Mike Iza's work on AlN and AlGaN growth on SiC was key to the progress of 2nd generation thin-film UV LEDs. I will briefly describe the key advances that led to the development of the AlN buffer layer: crack-free thick 2D/3D AlN buffer layers with TDD < $1x10^9$ cm^{-2}.

5.1.1 AlN buffer layer development milestones

5.1.2 Reducing AlN TDD

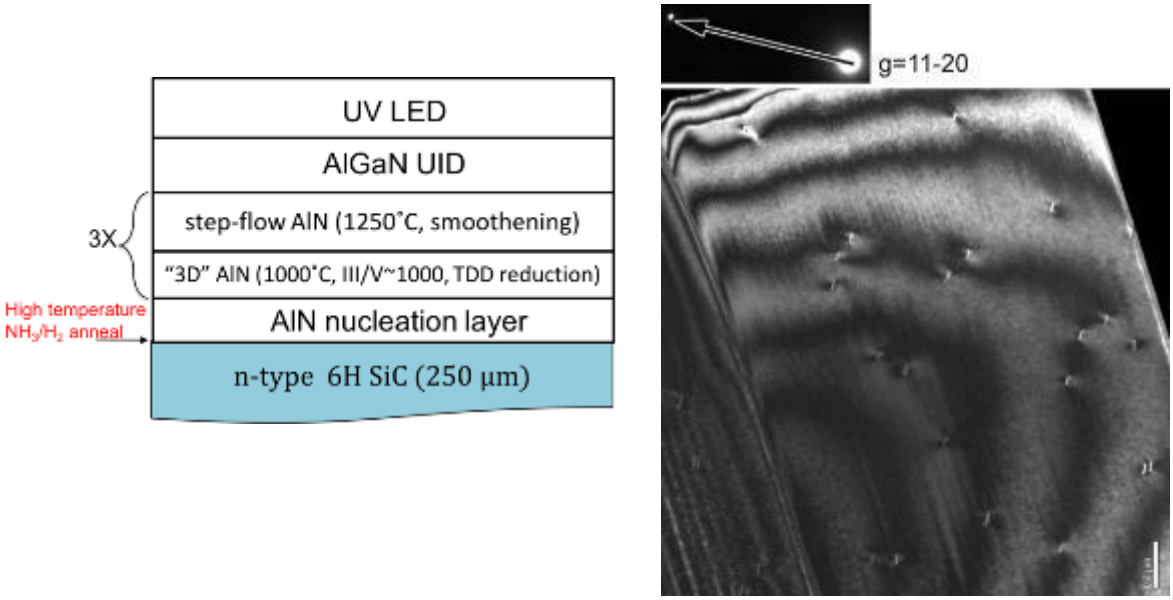

(a) AlN superlattice buffer layer technology

(b) TEM Dark field image taken with g = <11$\underline{2}$0> showing threading dislocations density (TDD) of $8x10^8$ cm^{-2} in AlN.

Figure 5.1. (a) AlN 2D/3D buffer layer technology reduces threading dislocations to $8x10^8$ cm^{-2} as measured by plane-view TEM shown in (b). The AlN superlattice consists of a thin interlayer grown at an intermediate temperature (IT) and a smooth step-flow high temperature (HT) layer. The thin "granular" or "3D" IT interlayer (70 nm, 1000 °C) reduces threading dislocations by TD-TD annihilation and fusion reactions. The thick HT layer (700 nm, 1250 °C) smooths the AlN surface. The details of 2D/3D AlN growth are reported in Foronda et al. [64]. This figure is adapted with permission from SaifAddin et al. [25].

Despite the closet lattice match between AlN and SiC, the AlN nucleation layer starts with a 3D growth on a standard untreated SiC substrate with TDD > 10^{10} cm^{-2}. Figure 5.1a shows the AlN 2D/3D buffer layer technology. The AlN 3D/2D buffer layers were grown at 1000 °C and 1250 ˚C, respectively; the growth details are discussed in Foronda et al. [64] and a future publication by Zollner et al. By growing three iterations of 2D/3D AlN, the TDD in

the AlN buffer decreased from >1x10^{10} cm^{-2} in the initial 3D layer to less than 1x10^{9} cm^{-2} as measured by plane-view TEM (refer to Figure 5.1b). The 3D layers function as TD-reduction filters by twisting and tilting the TD; the 2D layers act as smoothening layers. Increasing the AlN buffer layer thickness was challenging because the AlN tended to crack under tensile stress caused by thermal tensile mismatch or threading dislocations inclinations (TD inclinations) [148]. Cracks were avoided in the LEDs described in this chapter by annealing the SiC at 1250 °C in the NH_3/H_2 mixture (refer to Figure 5.2).

5.1.3 Crack-free thick AlN and AlGaN on SiC

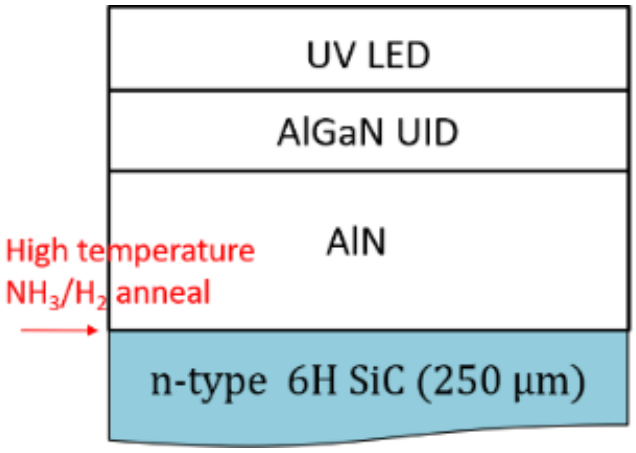

Figure 5.2. Pre-growth nitridation of SiC in NH_3/H_2 at T >1200 ˚C removed the cracks from thick AlN and AlGaN layers.

The lattice mismatch between AlN and SiC induces compressive stress during MOCVD growth, but the thermal expansion coefficient (TCE) mismatch at the AlN growth temperature (1200 °C for 3D AlN and 1200 °C -1250 °C for 2D AlN) generates tensile stress upon cooldown. Additionally, TD inclinations generate tensile stress [148]. Growing thick

AlN was necessary to lower the TDD using the 3D/2D AlN buffer layer method; however, the thicker the AlN and AlGaN, the higher the tensile stress.

SiC high temperature NH_3/H_2 annealing reduces thermal tensile stress in AlN epitaxy (refer to Figure 5.2 and SiC nitridation patent [61]). This pre-growth annealing enables the growth of thick 3D/2D AlN and thick AlGaN (with low TDD) without tensile stress (TCE or TD inclinations) inducing cracks. The LEDs reported in this chapter had thick AlN (~3.2 μm) and thick AlGaN (0.6 and 1.1 μm).

5.2 AlGaN growth

AlN on SiC is an insulating buffer layer. Moreover, although Si diffuses into AlN [149], it stays insulative when thick enough, and Si does not diffuse into AlGaN (confirmed by SIMS).

The calibrations needed to design the LED layers are summarized in Figure 5.3 and Table 5.1 The AlGaN composition was calculated using a reciprocal space maps (RSM) model that determines AlGaN composition and lattice relaxation relative to AlN. The RSM for the (105) reflection of AlGaN and AlN were measured using a high-resolution X-ray diffractometer (PANalytical X'Pert PRO MRD). The thickness for AlN and AlGaN were measured by Filmetrics (a spectral reflectance measurement system) and SEM. The thicknesses of AlGaN MQWs and EBL were extrapolated from measurements of thick AlGaN layers. The LED structures reported in this chapter were grown at 1175 °C for MQW and n-AlGaN; 1175 °C and 1050 °C for AlGaN:Mg; and 950 °C for p-GaN. We found out later that MOCVD grown n-AlGaN at 1050 °C had 4x less resistivity but these low-resistivity n-AlGaN layers were not incorporated in the LEDs discussed in this dissertation. Furthermore, we discuss reflective n-contacts developed for Ammonia MBE grown n-AlGaN (by Jianfeng Wang) which was found

to have ohmic n-contacts with very low specific contact resistivities but these n-AlGaN layers were not incorporated to any LEDs discussed in this chapter .

To grow the UV LED structures, we obtained the calibrations of the Al content x in $Al_xGa_{1-x}N$ as functions of TMG and AlGaN growth rates at various Al content in the AlGaN (at the chosen growth temperature) to grow the LED structures. The Al composition decreased as TMG flow increased at a constant temperature. At the same TMG flow, the Al composition was varied by adjusting the TMG flow.

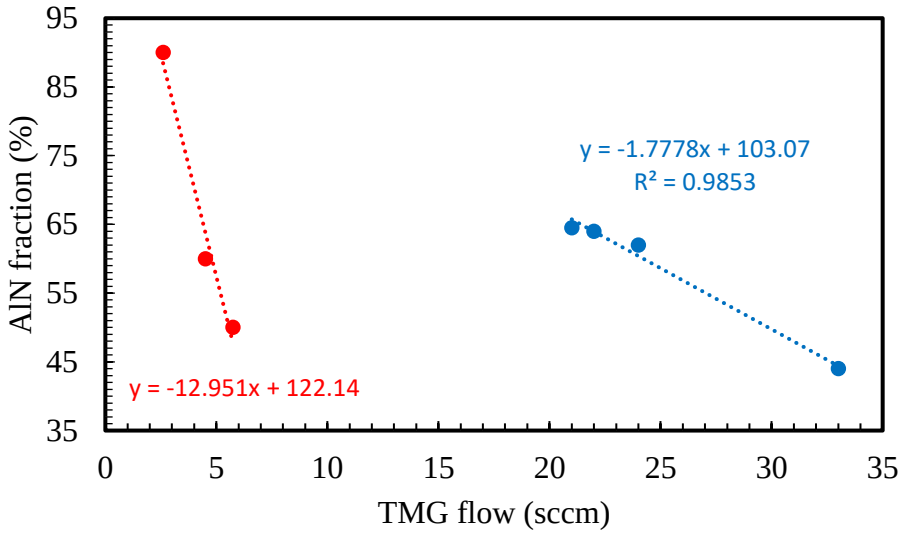

Figure 5.3. AlGaN composition as a function of TMG flow at 1175 °C (blue) and 1050 °C (red).

Table 5.1 Growth rate of AlN at different compositions at fixed temperature (1175 °C). (The AlN growth rate data were obtained from Abdullah Almogbel).

AlN composition (%)	AlGaN growth rate (Å/s)
50%	0.48
60%	0.4
70%	0.3
80%	0.28
90%	0.25
AlN (2D)	10
AlN (3D)	15

5.3 n-AlGaN contacts process development

Low specific-contact resistivities are needed to develop LEDs with low voltages, and the n-AlGaN resistivity needs to be small enough to increase current spreading lengths and reduce current crowding. We will discuss how we optimized the process for a low n-contact specific resistance with the best n-AlGaN samples grown by Abdullah Almogbel and Christian Zollner.

5.3.1 Impact of n-AlGaN growth temperature

Making an n-contact to a ~5 eV band-gap material ($Al_{0.62}Ga_{0.38}N$) is challenging due to the lack of low work function metals/alloys at the device operating temperature. In this section, we summarize the work we have done on optimizing the Vanadium (V) n-contact process [150,151] to reduce the n-contact resistance and maximize the LEE.

Stacia Keller et al. had shown that reduced growth temperature and high III/V ratios reduce n-AlGaN resistivity, despite increased residual oxygen and carbon concentrations at low temperatures [152–154]; however at some point the structural quality of n-AlGaN and its surface morphology degrades. The lowest n-AlGaN resistivity results were for n-AlGaN grown at 1050 °C and 950 °C (the surface morphology at 950 °C reduced LEDs EL); however, all of the UV LED results in this chapter are based on a 4X more resistive n-AlGaN that was grown at 1175 °C (refer to Figure 5.4). The resistance increased at 1175 °C compared to 1050 °C, due to increased compensating point defects with carbon and oxygen ruled out because of low levels as confirmed by SIMS done by Chris Zollner. Thermodynamically speaking, growing hotter than 1050 °C results in higher concentrations of compensating defects, such as group III vacancies (Ga or Al) [155,156].

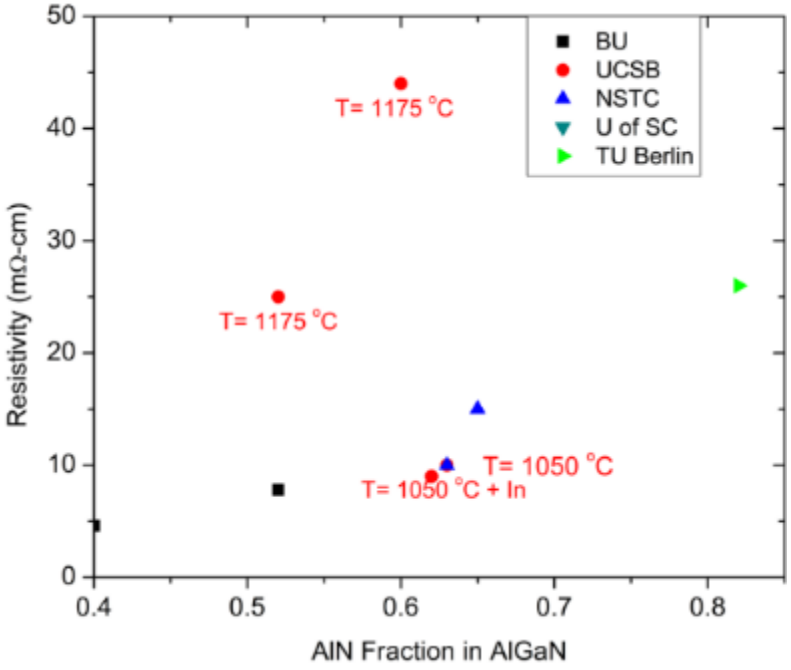

Figure 5.4. Impact of temperature on n-AlGaN (AlN content = 62-65%) resistivity (Ω-cm). UCSB data were roughly estimated by Hall via non-ohmic contacts as RF measurements were not possible because the SiC growth substrate were n-type (these data were compiled with the collaboration of Abdullah Almogbel and Chris Zollner). The LEDs presented in this chapter were grown using AlGaN grown at 1175 °C and had a resistivity of 62.5 mΩ-cm (low electron density of about 2×1018 cm−3 with an electron mobility of 50 cm2/V s). The low n-type carrier density resulted in non-ohmic contact and their series resistances (excess voltage contribution) were very high. In contrast, the MBE grown AlGaN had 10X higher electron density (2×1019 cm−3), and ohmic n-contacts (refer to Figure 5.6).

5.3.2 n-contacts for MOCVD $Al_xGa_{1-x}N$ (x_{Al} = 58-70%)

5.3.2.1 V-based contacts

BCl_3 is known to etch a thin oxide layer and eliminate the dead time problem of etching AlGaN or AlN [130] and so is CF_4 [157]. CF_4 is less aggressive and functions similarly to BCL_3 with similar levels of roughness [158]; however, BCl_3 was chosen over CF_4. We studied

the n-contact process on n-$Al_{0.6}Ga_{0.4}N$ etched with $BCl_3/SiCl_4$ and $BCl_3/Cl_2/Ar$. Contrary to the results of the Ti-based n-$Al_{0.52}Ga_{0.48}N$'s n-contact, $BCl_3/SiCl_4$ etching of $Al_{0.6}Ga_{0.4}N$ did not result in better V-based n-contacts than when etched with $BCl_3/Cl_2/Ar$.

We developed two n-contact stacks for ~58-70%% AlGaN. The contact stacks consisted of V/Al/V/Au, and V/Al/Ni/Au. The contacts were annealed in an N_2 atmosphere at different temperatures to find the optimal conditions; both contacts had similar electrical and mechanical (bonding) performance; however, V reflectivity at 280 nm was 50% (Ti reflectivity is slightly less at 48%) and Ni reflectivity at 280 nm was 20%. Therefore, V/Al/Ni/Au will have lower reflectivity than annealed V/Al/V/Au. Additionally, because the optimal anneal temperature for V/Al/V/Au contacts was lower than V/Al/Ni/Au, we choose to use V/Al/V/Au in the TFFC LEDs.

The n-contacts for AlGaN, grown by MOCVD, improved progressively as the electron concentration (determined by Hall measurements) increased while we reduced the growth temperature, but no ohmic contacts were obtained with MOCVD grown AlGaN at the growth conditions we used (refer to Figures 5.5 a, 5.5b, and 5.5c). Low temperature (1050 °C and 950 °C) n-AlGaN had much lower resistivity and higher electron concentration but it was not high enough to get an ohmic contact with the V-based n-contact process. n-AlGaN grown at 950 °C did not result in any measurable light emission from the diodes. Increasing the TMA flow from 5 sccm to 10 sccm helped to further reduce the resistivity (perhaps because of reduction in compensating vacancies ratios), but an ohmic contact was still not achieved. The LEDs presented in this chapter were grown using AlGaN grown at 1175 °C and had a resistivity of 62.5 mΩ-cm (low electron density of about 2×10^{18} cm^{-3} with an electron mobility of 50 cm^2/V s; refer to Figure 5.4). Ohmic contacts are achieved when the carriers tunnel through the

potential barrier between the metal and the n-AlGaN, when the depletion region is sufficiently narrow at uncompensated high doping concentrations. The low n-type carrier density resulted in non-ohmic (rectifying) n-contact (refer to Figures 5.5 a, 5.5b, and 5.5c). In contrast, the MBE grown AlGaN had 10X higher electron density (2×10^{19} cm^{-3}), and ohmic n-contacts (refer to Figure 5.6). Several groups have reported ohmic n-contacts for AlGaN (AlN content =58%-65%), including prior work at UCSB [150,152,159,160]; the reason we did not obtain high enough electron concentration for n-contacts on AlGaN (AlN content =58%-65%) grown by MOCVD was probably due to low V/III ratio because increasing the V/III rate is thought to reduce the formation of compensating vacancies [152,154].

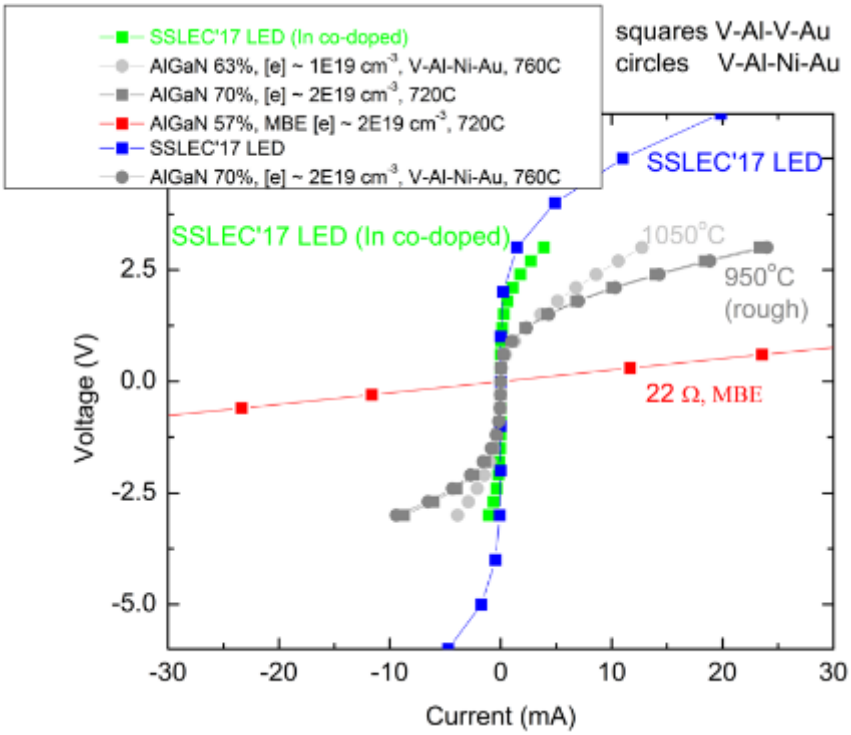

Figure 5.5a. IV for n-CTLM V-based n-contacts for several etched n-AlGaN in LEDs (8 μm gap) compared to the IV for the best MOCVD grown AlGaN and MBE grown n-$Al_{0.58}Ga_{0.42}N$ (2-pt probe measurements).

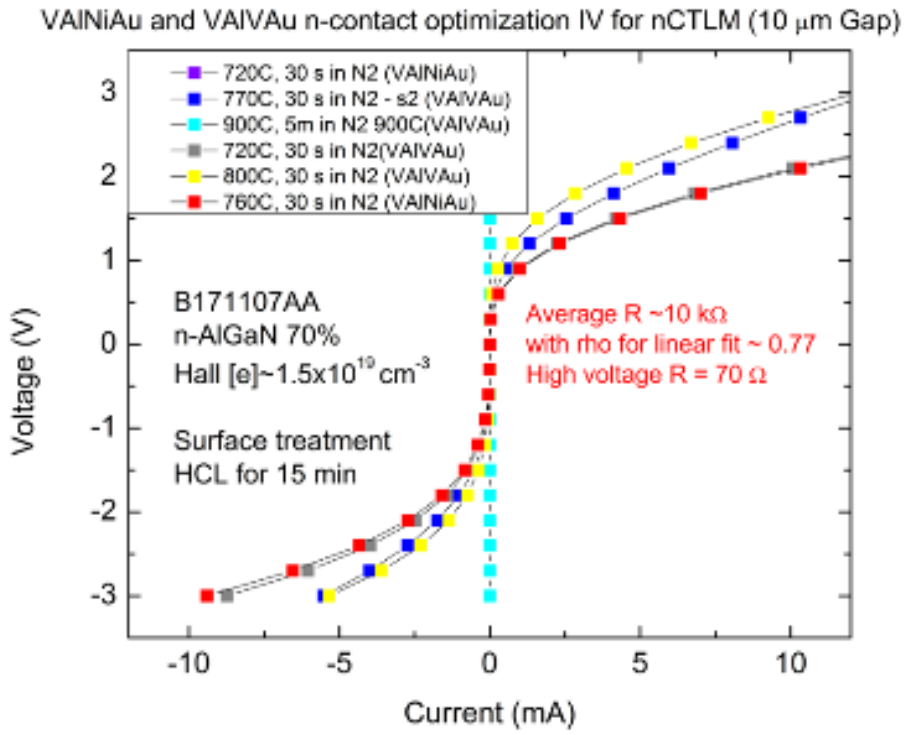

Figure 5.5b. MOCVD grown n-$Al_{0.7}Ga_{0.3}N$ with V-based n-contacts annealed at various conditions to find the optimal conditions for this sample with an electron density estimated to be ~ $1x10^{19}$ cm^{-3}. Relative to lower n-AlGaN with lower electron concentrations, The IV performance improved significantly with annealing, however, no ohmic contacts were obtained.

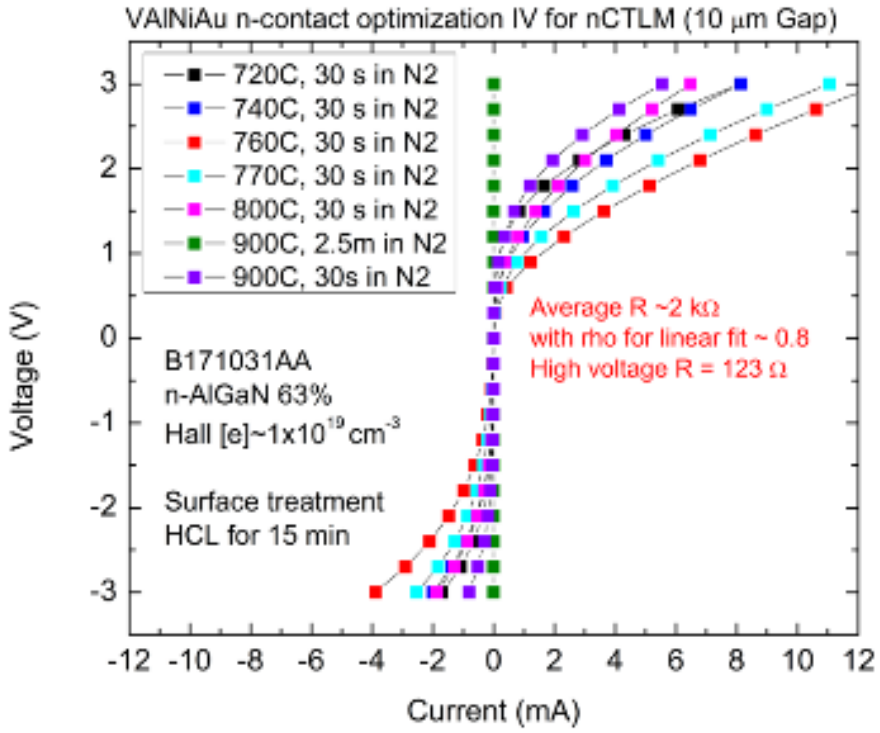

Figure 5.5c. MOCVD grown n-$Al_{0.63}Ga_{0.37}N$ with V-based n-contacts annealed at various annealing conditions to find the optimal conditions for this AlGaN sample with electron hall density estimated to be ~ $1x10^{19}cm^{-3}$. The IV performance improved significantly with anneal, however, no ohmic contacts were realized.

5.3.3 n-contacts for MBE grown $Al_xGa_{1-x}N$ (x_{Al} = 58%)

AlGaN was grown by Jianfeng Wang using MBE on AlN/SiC that Chris Zollner grew by MOCVD, and Aluminum content was measured by RSM to be 58%. In a parallel study, Bastien Bonef measured the aluminum content to be 59% using atom prob tomography (APT). The AlGaN grown by MBE had ohmic contacts with low specific contact resistivity ~10^{-6} Ω-cm^2 (refer to Figure 5.6 for the epi structure and n-contacts studies). In UV LEDs with n-contacts with resistivities of ~10^{-6} Ω-cm^2 , the contribution from the n-contact resistance becomes negligible (<0.1%) even if the n-contact area was 10X smaller than usual.

Additionally, we demonstrate reflective n-contacts (V (1 nm)/Al (150 nm)/V (20 nm)/Au (300 nm)) with low specific contact resistivity on -n-AlGaN grown by MBE. These contacts are an important stepping stone to realizing high EQE and WPE tunnel junction thin film UV LEDs.

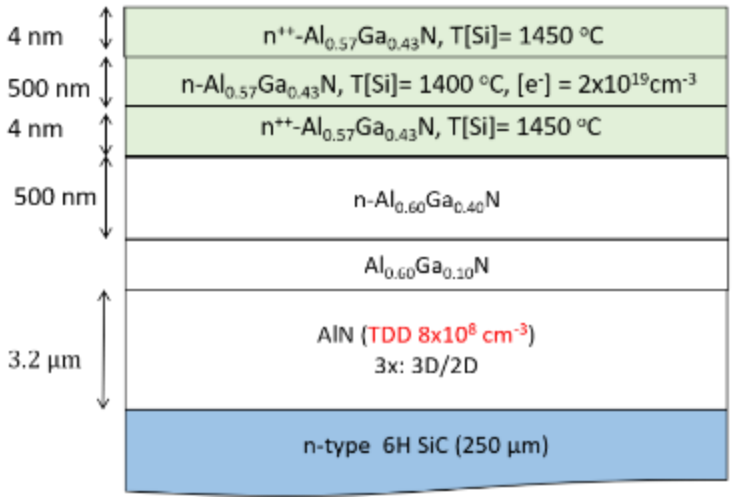

(a) Schematic of the n-AlGaN samples grown on SiC. The AlN buffer layer is insulating.

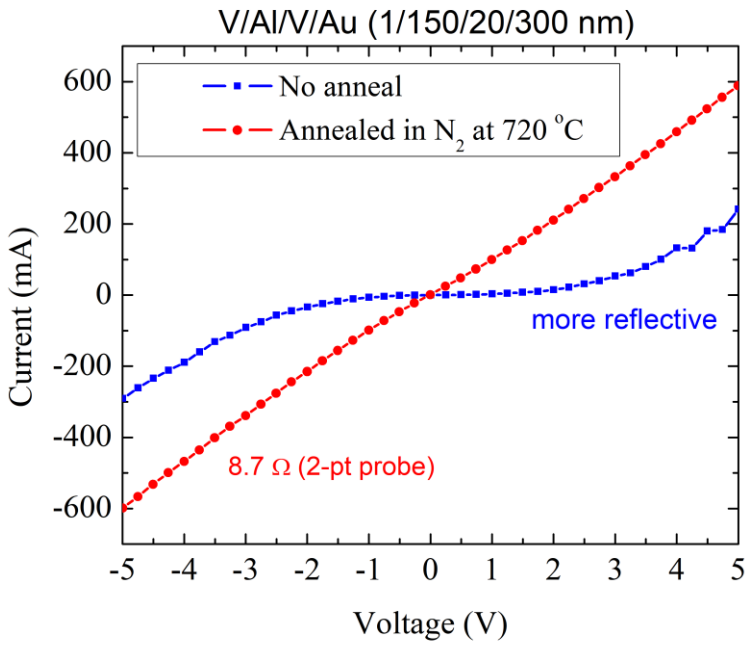

(b) IV for 10 μm gap CTLM with 1/150/20/300 nm V/Al/V/Au n-contacts. IV was non-ohmic before annealing (but highly *reflective*), as shown on the left. The contacts became ohmic with low specific contact resistivity after optimized annealing as shown on the right.

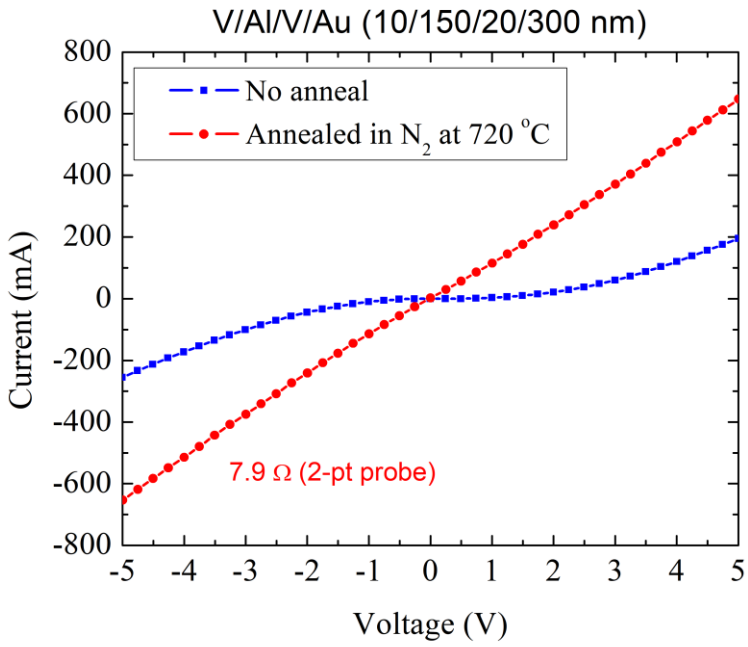

(c) IV for 10 μm gap CTLM with 10/150/20/300 nm V/Al/V/Au n-contacts. IV was non-ohmic before annealing (but less reflective than figure 5.6b), as shown on the left. The contacts became ohmic with low specific contact resistivity after optimized annealing as shown on the right.

Figure 5.6. Development of reflective n-type contacts for n-$Al_{0.58}Ga_{0.42}N$ grown by MBE. In tunnel junction LEDs, these contacts will inject electrons into the top, and bottom contacts. The n-contact specific contact resistivities was in the range of 10^{-6} Ω-cm^2 after annealing at 720 °C with 14 min HCl pre-treatment.

5.4 Active region optimization

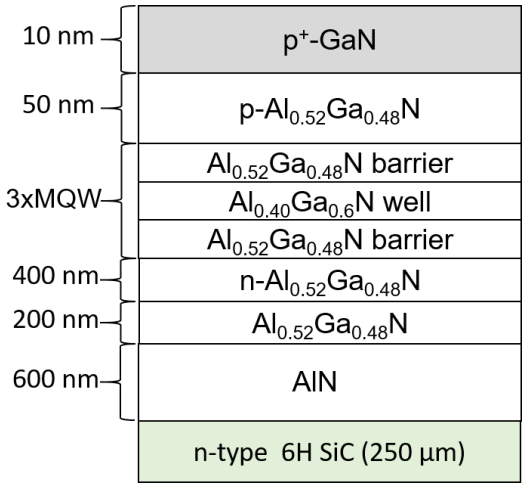

(a) 280 nm LED structure without an EBL.

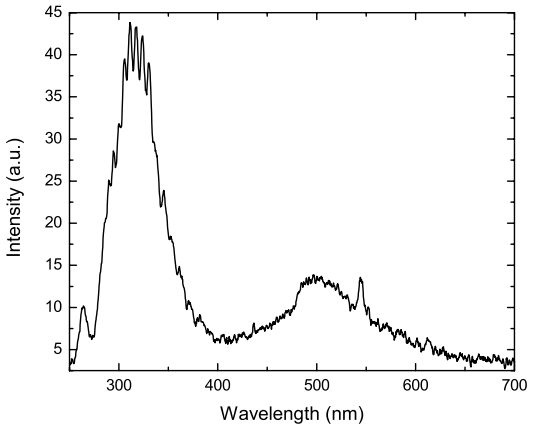

(b) EL emission shows 280 nm LED MQW peak, parasitic peak at 330 nm and SiC UV fluorescence (400-600 nm).

Figure 5.7. 280 nm LED without EBL and with absorbing cladding layer (tail absorption coefficient $>10^3$ cm^{-1}).

Figure 5.7a shows an LED structure designed to emit at 280 nm LED. Figure 5.7b shows the EL emission: 280 nm LED MQW peak, parasitic peak at 330 nm and SiC UV fluorescence (400-600 nm). The large parasitic peak at 330 nm is thought to be due to radiative recombination (band-to-deep-level radiative recombination) between electrons and holes in the AlGaN:Mg layer because of electrons flowing from the MQW region into the AlGaN:Mg. Adding a thin EBL should block electron overflow and help confine electrons for radiative recombination in the first well in the active region [161].

Additionally, the barrier and cladding composition were too low to confine the electrons, and $Al_{0.52}Ga_{0.48}N$ has significant absorption at 280 nm. Absorption data in the literature indicate that the tail absorption coefficient is $>5x10^3$ cm^{-1} [162,163]. To improve the 280 nm

LED active region radiative efficiency and reduce self-absorption, we added an EBL and to increase the barrier and cladding composition to higher than $Al_{0.60}Ga_{0.40}N$.

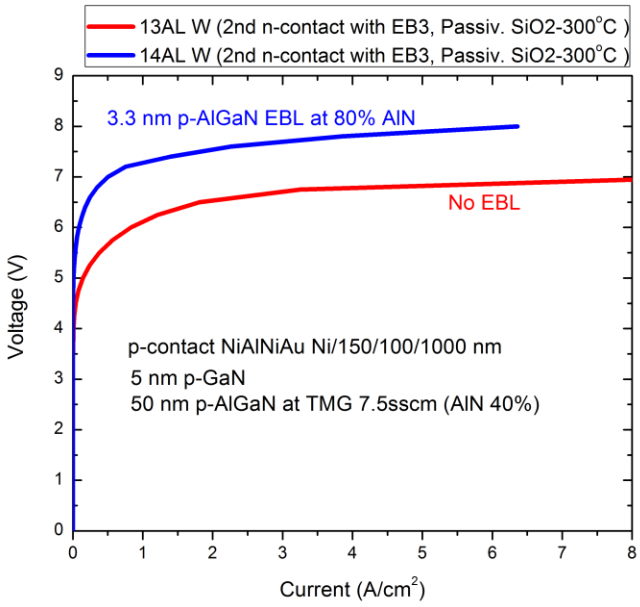

Figure 5.8. Impact of EBL on parasitic emissions shows an increased voltage. We decided to reduce the thickness of the EBL to 2.8 nm.

We eliminated the parasitic emission by adding an EBL. Adding a thick 3.3 nm EBL resulted in a ~1 V increase in turn-on voltage and excess voltage (refer to Figure 5.8). Therefore, we reduced the thickness of the EBL to 2.8 nm, which resulted in almost no increase in the turn-on voltage.

The 4X-MQWs were optimized by running a well series (nominally, 1.5 nm, 2 nm, 2.5 nm, and 3 nm) with a 7.5 nm barrier. The optimized LED structure is shown in Figure 5.9. With Abdullah Almogbel assistance, we optimized the 4X-MQWs by observing the EL emitted at high currents from around indium micro-dots (120-140 µm in diameter) that were used as p-contacts) in AlGaN:Mg grown at 1175 °C. In one series, the barrier was 7 nm and the wells thicknesses series (nominally) were: 1.75 nm, 2 nm, 2.5 nm, 2.75 nm, and 3 nm. We also ran a similar series with 9 nm barriers. We obtained the highest EL for both barriers at a well

thickness = 2.75 nm (nominal thickness as estimated from AlGaN growth rates in Table 5.1). Increasing the MQW's 7-nm-barrier further to 9 nm did not impact the EL intensity (there was no observable difference in indium-dots EL testing in with: 7 nm, and 9 nm barriers); however, the EL intensity was very sensitive on the MQWs' well thickness. The impact of the AlGaN:Mg growth temperature on the LED EL efficiency is discussed in the next section.

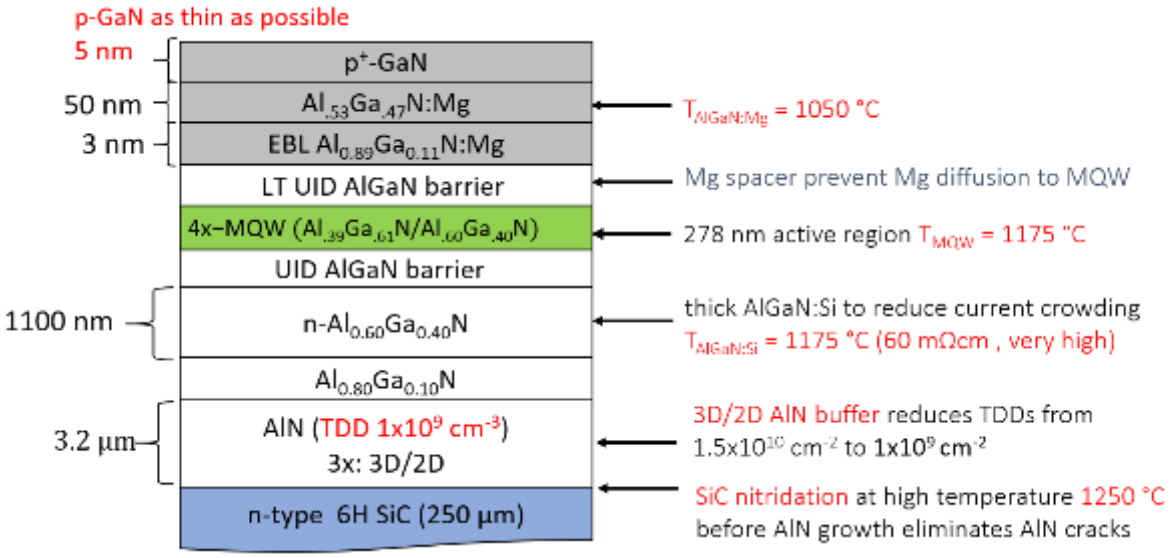

Figure 5.9. The structure of the 278 nm LED. The 265 nm LED had a similar structure except for: 1) a 200 sccm TMI flow was added in the active region growth; and 2) the n-AlGaN thickness was 550 nm (due to a scripting error but it emphasized the importance of low n-AlGaN sheet resistance).

5.5 p-AlGaN development

5.5.1 p-AlGaN growth temperature impact on EL efficiency

The 2nd generation LEDs were initially optimized at AlGaN:Mg grown at 1175 °C because we, initially, thought the AlGaN:Mg will have a higher holes concentration at 1175 °C than at 1050 °C. Increasing the growth temperature of AlGaN:Mg was thought to reduce carbon and oxygen incorporation at some MOCVD growth conditions. However, the Mg doping profile near the MQWs active region was found to be influenced by the growth temperature of the AlGaN:Mg and that Mg diffuses further toward the active region at 1175 °C than at 1050 °C (the LED structure is shown in Figure 5.10).

We grew three LEDs with similar structure to investigate the impact of varying the AlGaN:Mg layer growth temperature as shown in Figure 5.10a. The Mg doping densities were kept the same (~$1x10^{19}$ cm^{-3}) in AlGaN:Mg by adjusting the Cp_2Mg_2 flows. Two LEDs were grown with AlGaN:Mg at 1175 °C with Mg spacer of 9 nm and 19 nm, and both of these LEDs had very low power. The third LED was grown with AlGaN:Mg at 1050 °C with a Mg spacer of 19 nm and had ~500X more power than the LED with AlGaN:Mg grown at 1175 °C (refer to Figure 5.9b).

We measured the Mg and Ga atoms concentrations using a secondary ion mass spectrometer (SIMS) system (refer to Figures 5.10c and 5.10d). The sample surface was bombarded with a 2 keV Cs^+ ions beam with high depth resolution (~2nm) and the emitted secondary ions were collected and analyzed by mass spectrometry (with the assistance of Tom Mates).

The Mg doping profile depended on the AlGaN:Mg growth temperature and their diffusion into the MQW impacts the EL efficiency. The SIMS Mg profile shows a diffusion of

the Mg atoms into the first well of the MQWs when the AlGaN:Mg was grown at 1175 °C despite the use of a Mg-spacer (refer to Figure 5.10c) and the processed LED power had very low (refer to Figure 5.10b). However, when the AlGaN:Mg was grown at 1050 °C, the Mg was contained in the Mg spacer layer (refer to Figure 5.10d) and the processed LED had high power (refer to Figure 5.10b). The same LED structure to the latter was grown with AlGaN:Mg grown at 1175 °C, but the LED EL intensity was very low.

It is worth noting that a similar problem was observed for InGaN LEDs, where the GaN:Mg growth temperature affected the active region EL efficiency. Researchers have proposed Mg diffusion into the active region as a reason for the EL efficiency decay. Also, high temperature growth was thought to affect the InGaN active composition. To address this problem, visible GaN:Mg LEDs are grown at reduced temperature, so they do not damage the InGaN active region.

Kohler et al. (refer to Figure 5.10e) have shown that the Mg diffusion coefficient in $Al_{0.1}Ga_{0.9}N$ is higher than GaN, especially at growth temperatures above 1000 °C [164]; the Mg diffusion in higher Al-composition AlGaN is expected to be higher than in $Al_{0.1}Ga_{0.9}N$. The reason for the increased Mg diffusion in AlGaN is not clear. Mg diffusion across the AlGaN lattice is not expected to be substitutional thermodynamically. We suggest that the Mg diffusion process defects assisted, particularly threading dislocations.

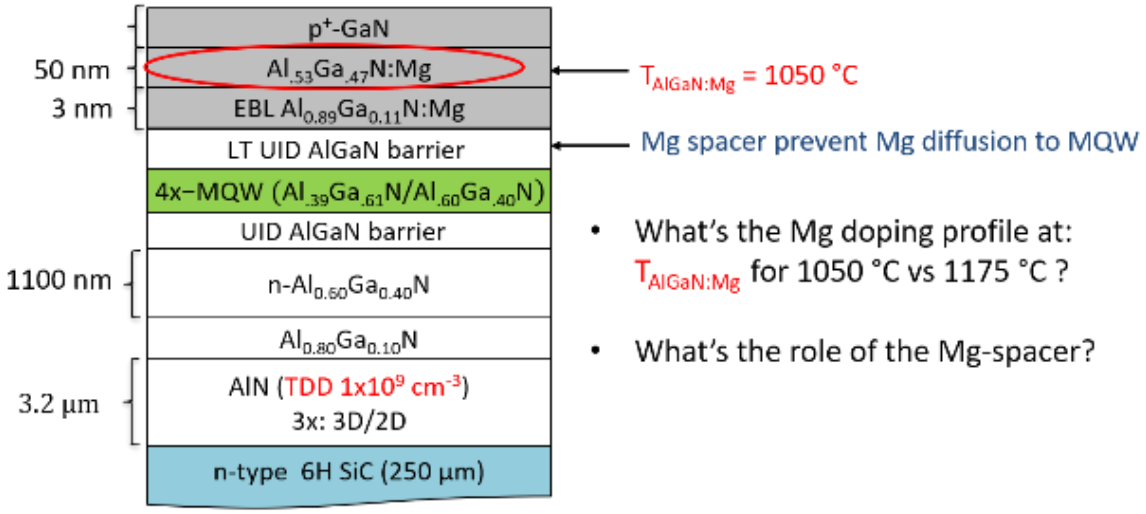

Figure 5.10a. LED structure used to study the impact of the AlGaN growth temperature impact om Mg diffusion and EL efficiency.

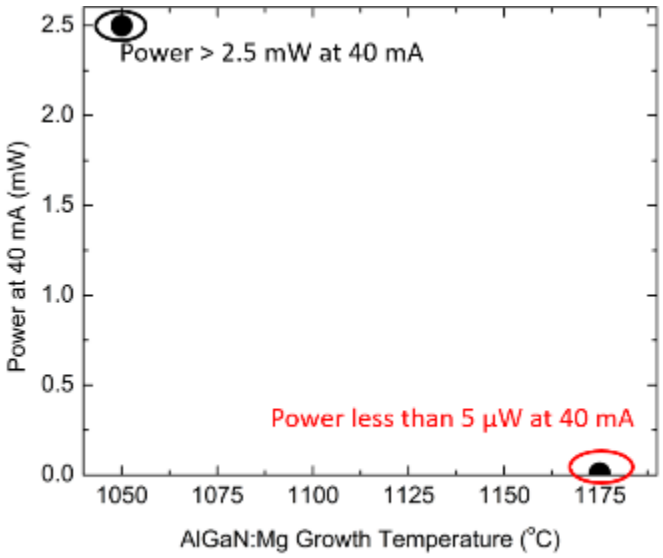

Figure 5.10b. Mg:AlGaN growth temperature impact on the LED power output.

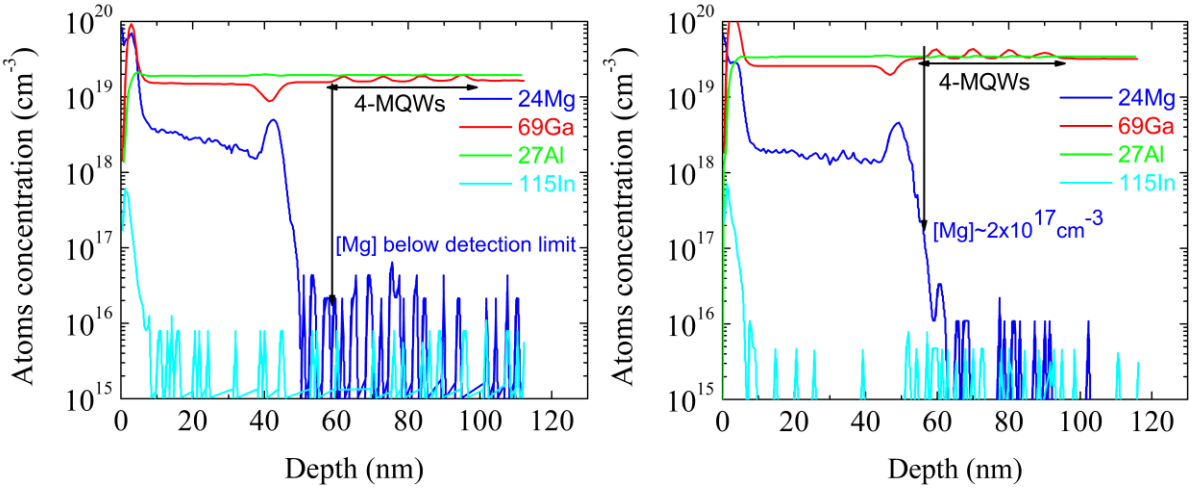

(c) 1050 °C AlGaN:Mg (High power LEDs)

(d) 1175 °C AlGaN:Mg (Very low power LEDs < 5 µW at 40 mA)

Figure 5.10. AlGaN:Mg growth temperature impacts the Mg doping profile near the MQWs active region and impacts the EL efficiency.

5.6 p-GaN development

p-GaN is the primary source for holes in AlGaN LEDs because of the low efficiency of Mg ionization in AlGaN with AlN ~ 60%. In this section, we continue the discussion of the p-contact development in Chapter 4. For the LEDs grown in this chapter, LEDs were grown with 5 nm, 3 nm and 0.5 nm p-GaN to attempt to maximize LEE. The LEDs with 3 nm and 0.5 nm p-GaN were too thin to establish (with the n-AlGaN layer) a depletion region, that only conducts currents in the forward bias direction. Most of the IVs of the diodes with 3 nm and 0.5 nm p-GaN were like the IVs of non-linear rectifying n-contacts.

5.6.1 p-contact reflectivity

The p-contact constitutes most of the area of the LED and is directly beneath the MQW. The reflectivity of the p-contact is of paramount importance to light extraction [122,146]. The p-contacts were deposited by e-beam, and the reflectivity measurements were done by a UV-

Vis spectrometer (Cary 500). The reference mirror used was a UV-enhanced mirror from Thor Labs.

5.6.1.1 Impact of diffusion barrier on p-contact reflectivity

It is expected that a diffusion barrier is needed to separate the aluminum (the most reflective metal below 400 nm) and gold (used in Au-Au thermocompression bonding) in the p-contacts, since intermixing reduces the p-contact reflectivity. The binary phase diagrams of Ni and Pt with Au indicate that Ni and Pt could be excellent diffusion barriers for a p-contact (Ni/Al/barrier/Au). We deposited 100 nm of Ni and Pt with an e-beam and tested the bonded p-contact reflectivity. Figure 5.12a shows that, after 300 °C Au-Au bonding, Ni performed better than Pt as a diffusion barrier, but e-beam deposited Ni was not a perfect diffusion barrier at 300 °C. It is possible that sputtered Ni could be denser and would work as a better diffusion barrier. With 200 °C Au-Au bonding, there was no drop in the reflectivity of the bonded p-contact reflectivity with Ni as a diffusion barrier.

5.6.1.2 Impact of temperature on p-contact mirror reflectivity

The p-contact was deposited by e-beam on a sapphire substrate. Then, the samples (Ni/Al/Ni/Au/DSP sapphire) were annealed in air (without bonding) at 300 °C, and at 200 °C to mimic an actual LED bonding. Figure 5.11a shows how the air/metal reflectivity were measured by Cary 500. Figure 5.11b shows that the p-contact Ni/Al/Ni/Au (0.3/100/100/1000 nm) reflectivity was observed to decrease after bonding at 300 °C, but not at 200 °C

Au-Au thermocompression bonding is normally conducted at temperatures >300 °C [85]; however, it was observed that conducting a 5 min bond at 275 °C and then bonding at 200 °C for 1 hr yielded acceptable bonding quality and better reflectivity (the impact of the bond at 275 °C for 5 min on reflectivity was not measured; however, diffusion is a time- and heat-

dependent process, so the impact of 275 °C for 5 min on reflectivity could be minimal, but it is worth checking for further device optimization). Therefore, to protect the p-contact reflectivity from Au diffusion, we considered Ni as a diffusion barrier.

Figure 5.11c shows the reflectivity of a bonded p-contact Ni/Al/Ni/Au (1/100/100/1000 nm) to: as deposited p-contact, Al, and MgF_2/Al. The MgF_2 was deposited by e-beam at 500 °C (actual temperature was 300 °C) and the refractive index (n) at 275 nm was 1.4, as measured by ellipsometry (M2000DI Variable Angle Spectroscopic Ellipsometer, J.A. Woollam Co., Inc.); MgF_2 deposited by e-beam at room temperature is reported to be flaky. The bonded p-contact to had similar reflectivity to as deposited p-contact, without damage. In contrast to the bonded p-contact reflectivity at 275 nm (80% for Ni =0.3 nm and 75 for Ni=1 nm), the MgF_2/Al had very high reflectivity: >97.5% close to normal incidence, and close to 100% for incident angles greater than the total internal reflection angle (TIR) as the reflectivity simulation shows in Figure 5.11d.

Transparent tunnel junction can enable even higher LEE TFFC LEDs with (perhaps) good voltage efficiencies. Employing the MgF_2/Al with a tunnel junction in a UV LED is expected to improve the LEE to above 80%, as estimated form ray tracing simulations [118]. The MgF_2/Al omnidirectional mirror can be employed in tunnel junction UV LEDs with 500 nm n-AlGaN as a current spreading layer to enable lateral injection of electrons by a mesh of reflective n-contact (1/150/20/300 nm V/Al/V/Au), which had low specific contact resistivity ($\sim 10^{-6}$ Ω-cm^2).

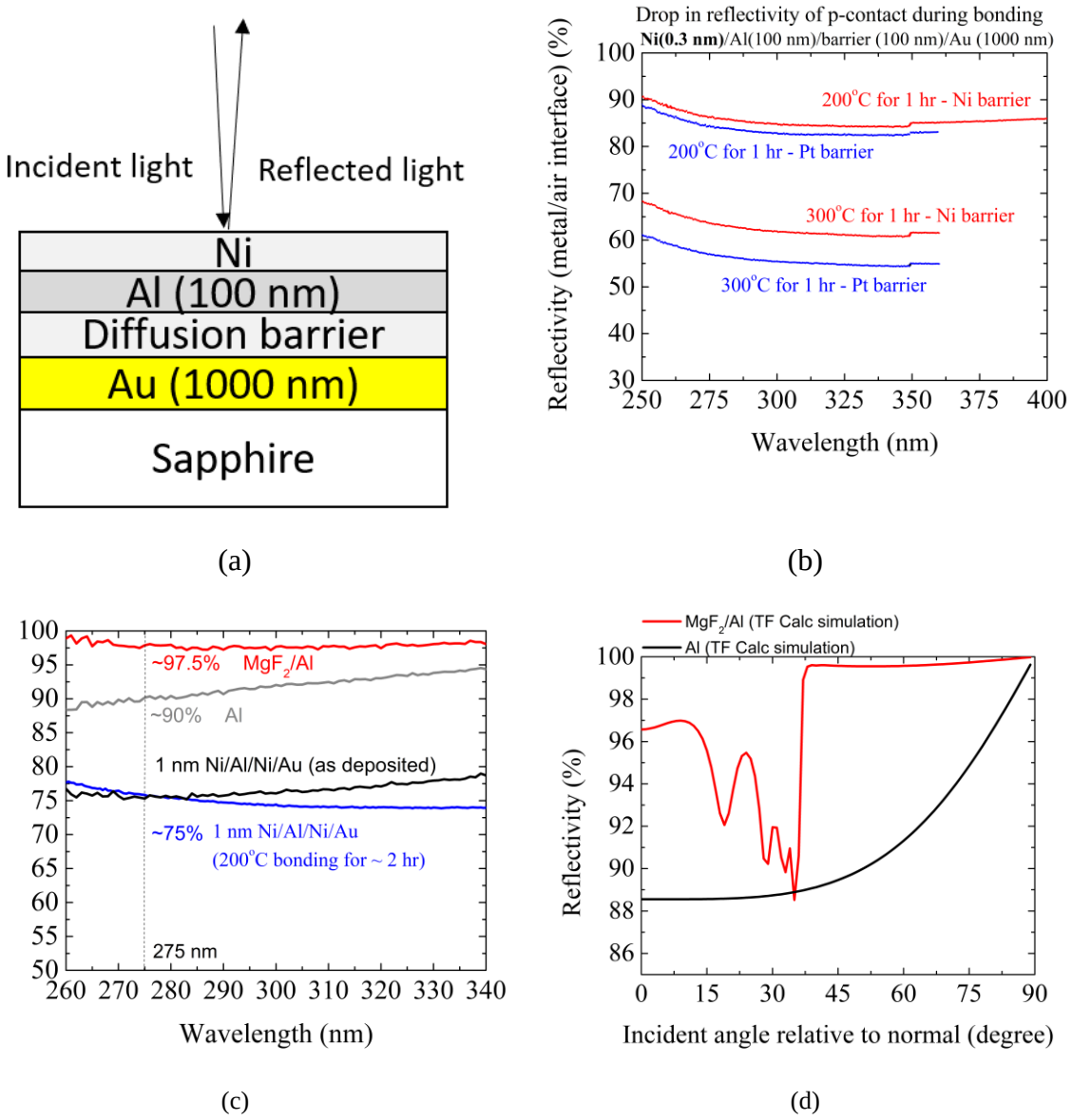

Figure 5.11. (a) Schematics for the p-contact Ni/Al/diffusion barrier/Au that is deposited on a sapphire substrate. The reflectivities were measured by Cary 500, using Thorlabs UV-enhanced mirror as a reference.(b) The measured reflectivity vs wavelength for the the p-contacts: Ni/Al/Ni/Au and Ni/Al/Pt/Au. The reflectivity data shows that Ni performed better as a diffusion barrier during bonding at 200 °C and 300 °C. (c) The reflectivity the p-contact Ni/Al/Ni/Au (1/100/100/1000 nm) was compared to: as deposited p-contact, Al, and MgF_2/Al (d) Simulation for reflectivity (at 275 nm) as a function of incident angle for the MgF_2/Al layer that was measured in (c). The simulated reflectivity was close 100% when the light incident angle was greater than the total internal reflection (TIR) angle at the n-AlGaN–(MgF_2/Al) interface.

As described in Chapter 2, we attempted to use In/Au bonding to improve the bonding adhesion and the LEDs thermal sinking [104], however, the bonding conditions used (5 min bonding, and 2 μm of In) caused the bonding layer to spread by +10 μm and short the n- and p- contacts. In/Au (with shorter bonding time (30 sec) and a thinner layer of In) or Sn/Au could be used to improve the TFFC LEDs bonding adhesion and thermal sinking, but without damaging the p-contact reflectivity. Furthermore, the p-contact area could be increased.

Table 5.2 Summary for n-contact results for 297-310 nm LEDs and 297-264 nm LEDs vs InGaN blue LEDs.

Materials	**n-contact specific resistivity** ρ_c^n (Ω-cm^2)		**p-contact specific resistivity** ρ_c^p (Ω-cm^2)	
GaN (450 nm LEDs)	Ti/Au Al/Au	10^{-4}-10^{-6} 10^{-6} [140]	Ni/Au(annealed) Pd/Au	10^{-4}-10^{-5} 10^{-4}
$Al_{.32}Ga_{.58}N$ (297-310 nm LEDs)	Ti/Al/Ni/Au	1-5x10^{-4}	Ni/Al/Ni/Au 1/100/100/100 (non-annealed)	1.5x10^{-3} (10 nm p-GaN)
$Al_{.53}Ga_{.47}N$	Ti/Al/Ni/Au	1-5x10^{-4}	Ni/Al/Ni/Au 1/150/100/100 (non-annealed)	2x10^{-3} (5 nm p-GaN)
$Al_{.62}Ga_{.48}N$ (264-280 nm LEDs)	Ti/Au V/Al/V/Au	10^{-3} 10^{-6} (MBE)	Ni/Al/Ni/Au 1/150/100/100 (non-annealed)	10^{-3} (5 nm p-GaN)

5.7 TFFC LED Experimental

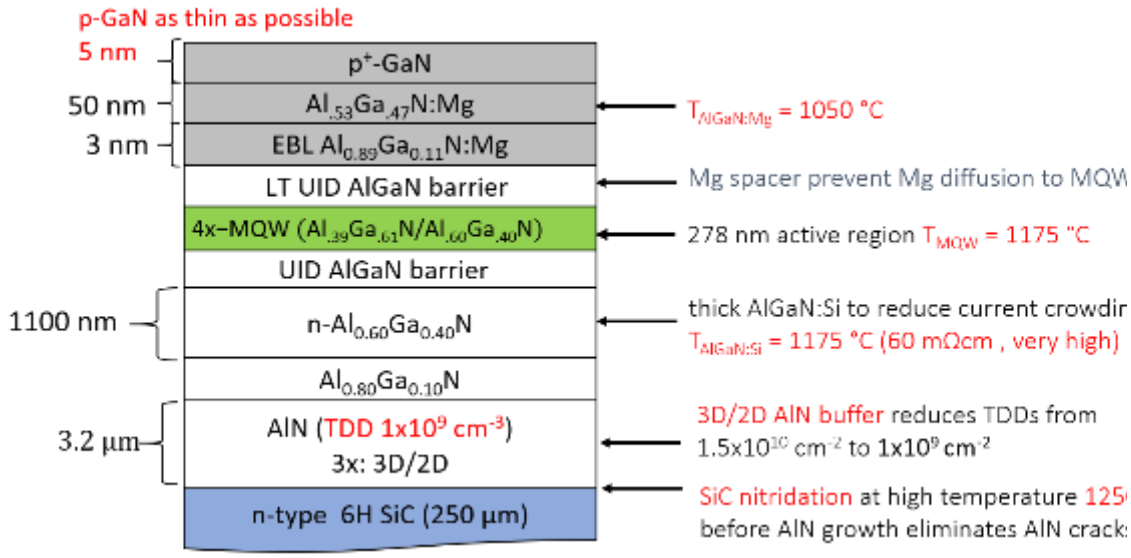

Figure 5.12. The structure of the 278 nm LED. The 265 nm LED had a similar structure except for: 1) a 200 sccm TMI flow was added in the active region growth; and 2) the n-AlGaN thickness was 550 nm (due to a scripting error but it emphasized the importance of low n-AlGaN sheet resistance).

In this section we briefly discuss two LEDs with the similar structure, and both LEDs have 5 nm p-GaN. The first LED had a peak emission at 278 nm, and the second LED had a peak emission at 265 nm. The n-AlGaN thickness for the 278 nm was 1100 nm LED and the n-AlGaN thickness for the 265 nm LED was 550 nm (instead of 1100 nm because of a scripting error, however, it highlighted the importance of having low sheet resistance of n-AlGaN to improve uniform current spreading). The n-AlGaN resistivity for both n-AlGaN were both about ~ 60 mΩ-cm. The high sheet resistance of n-AlGaN (which had low electron density~ $2x10^{18}$ cm^{-3}, obtained from Hall measurements) resulted in highly non-ohmic contact that made a significant contribution to the LEDs" excess voltage.

The fabrication process of these TFFC UV LEDs was discussed earlier in this chapter and in Chapter 2, and they are also discussed (in detail) in a paper published in Semiconductor Science and Technology [73]. Figure 5.13a shows a schematic of the different LED geometries that were processed. Figure 5.13b shows the submount layout for a 0.1 mm^2 and 0.33 mm^2 LEDs.

5.8 Discussion and analysis

The p-contact areas were 0.0324 mm^2 and ~0.1 mm^2 (0.093 mm^2). The n-contact area was maximized for the 0.032 mm^2 to improve mechanical adhesion and to reduce the contribution of the n-contact specific resistance. The yield for the TFFC LEDs from the 0.032 mm^2 was ~90%, but the yield for the ~0.1 mm^2 LEDs was about 50-60% due to the limited n-contact area in the interdigitated geometry. Figure 5.15 shows an SEM for a TFFC LED. An additional "haircut" lithography can be done around the thin-film LED by either: 1) etching a larger and deeper mesa around the LEDs mesa (into 80% of the AlN thickness); or, alternatively, 2) conducting a non-contact lithography after FC and substrate removal can etch away the excess area around the LED active area by KOH (which etches N-face AlN).

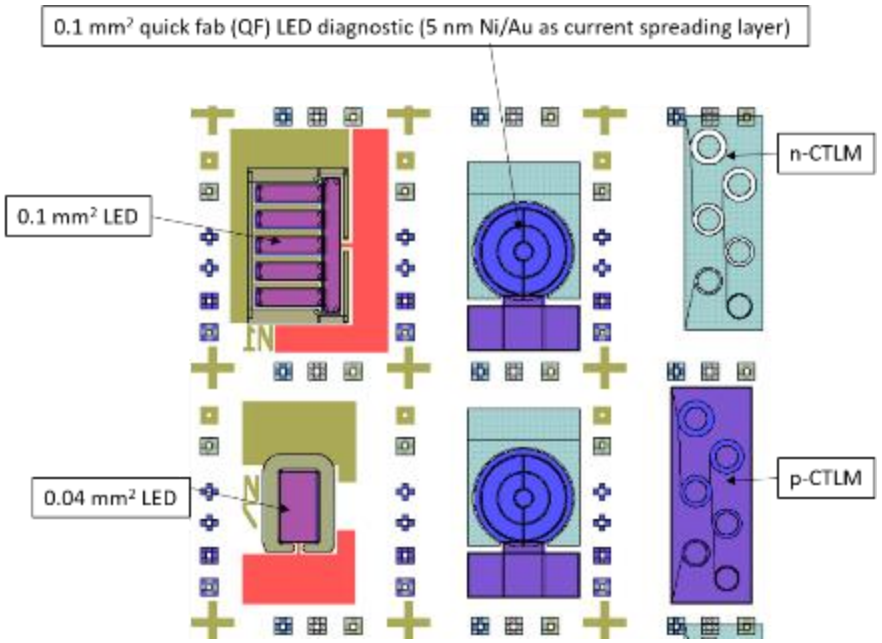

(a) Layout TFFC LEDs overlayed on the n- and p- bonding pads, and the diagnostic strucutres layout: (quick fab (QF) LED and n-CTLM and p-CTLM).

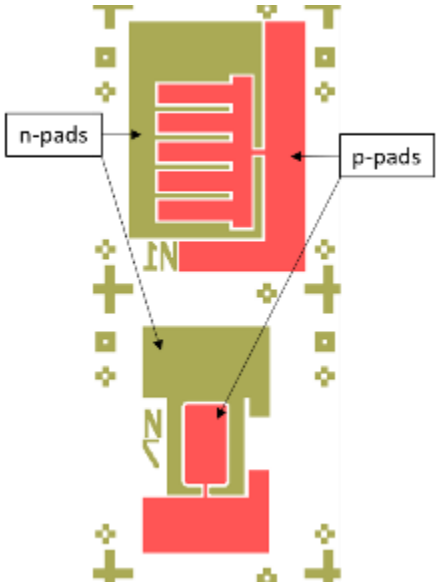

(b) layout of n- and p- bonding pads.

Figure 5.13. TFFC LEDs mask layout for 0.0324 mm^2 and ~0.1 mm^2 (0.093 mm^2).

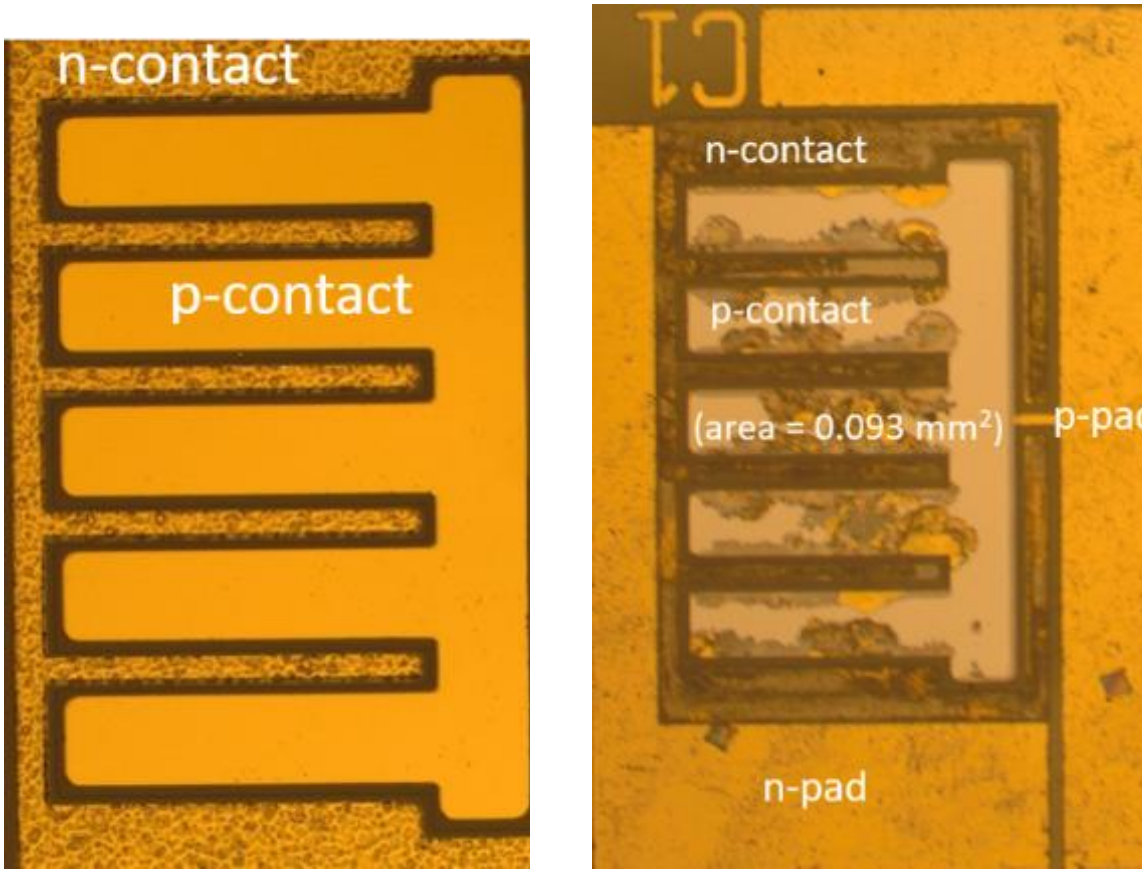

(a) (b)

Figure 5.14. Micrograph for ~0.1 mm^2 (0.093 mm^2). LED: (a) processed LED before bonding and flip-chip. (b) TFFC LED after substrate removal and seeing through the exposed pristine AlN layer. The bonding marks indicate areas where the LEDs are bonded mechanically. Gaps could affect thermal performance. The Ni/Al fractional coverage of the p-contact (because of gold diffusion) could reduce the p-contact reflectivity.

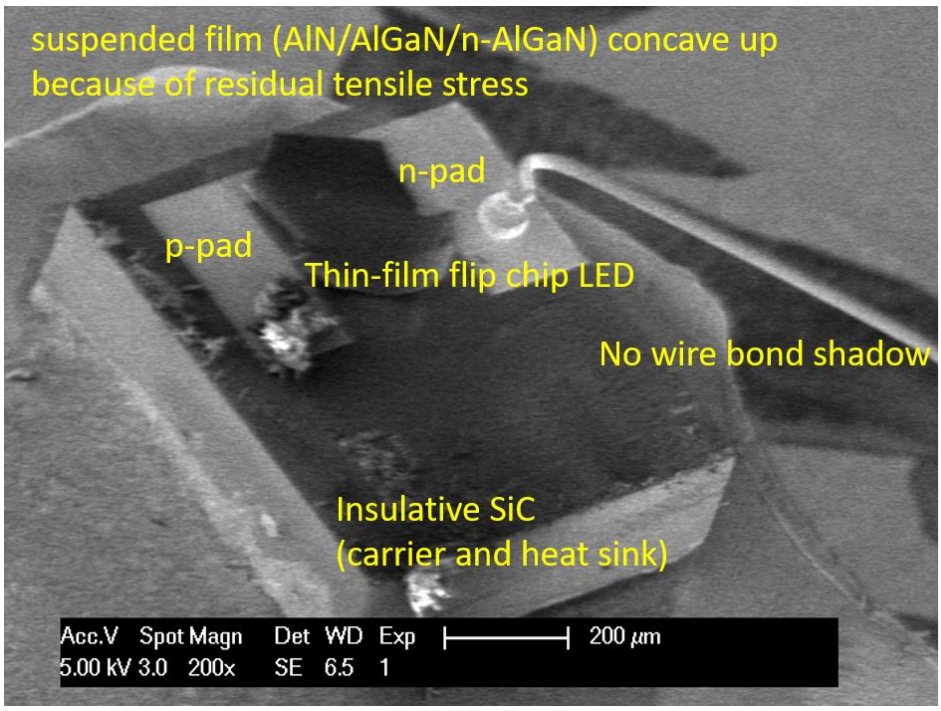

(a)

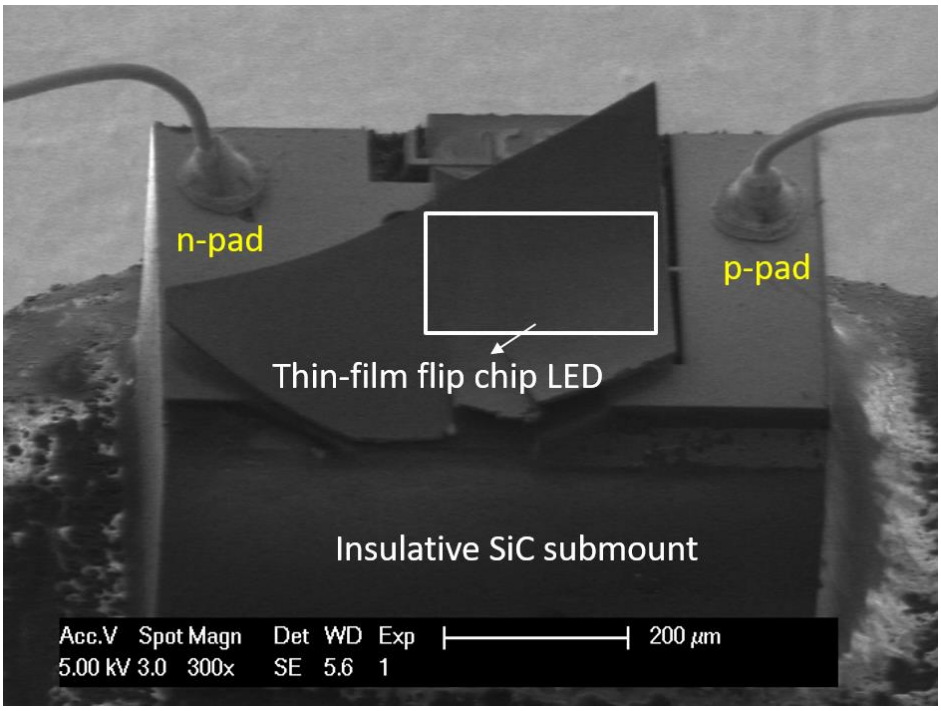

(b)

Figure 5.15. SEM for two TFFC LEDs with 0.0324 mm^2 in p-contact area.

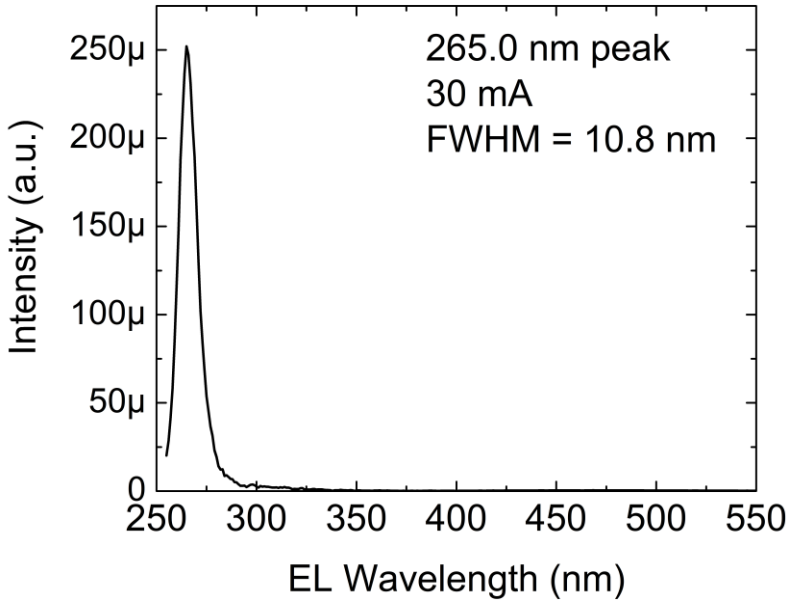

(a) The EL peak emission is 265 nm at 30 mA (92.6 A/cm^2).

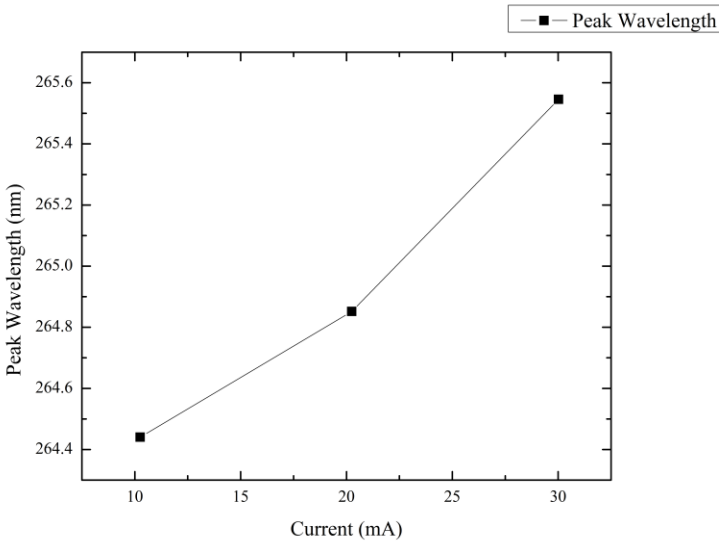

(b) The El peak emission is 265 nm at 30 mA (92.6 A/cm^2).

Figure 5.16. EL spectra and peak EL emission from 265 nm LED with 0.0324 mm^2 in p-contact area.

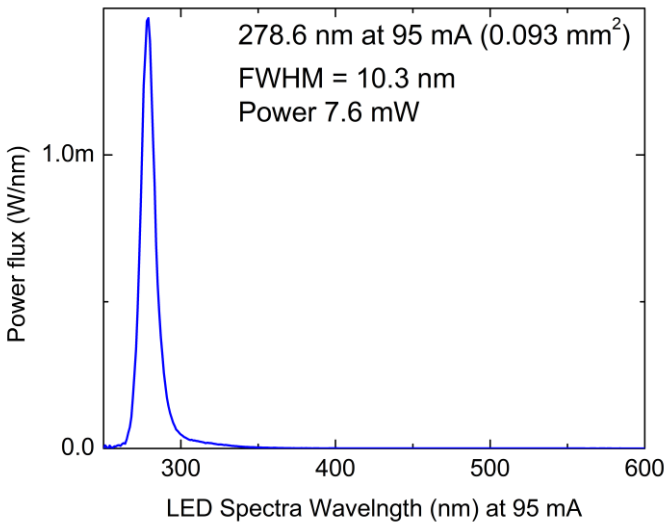

Figure 5.17. EL emission from the 278 nm LED with ~0.1 mm^2 (0.093 mm^2). in p-contact area.

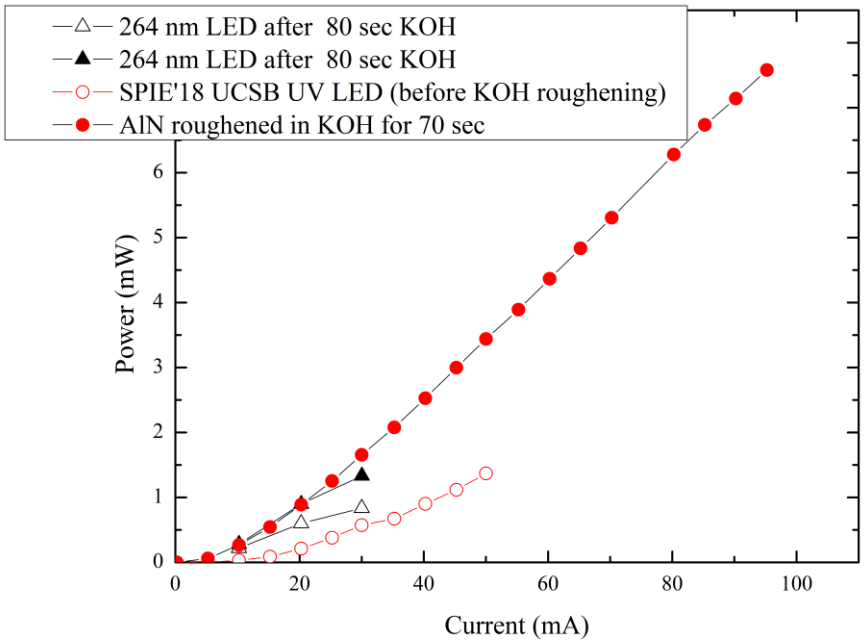

Figure 5.18. The light output of TFFC LEDs: 278 nm LED (AlN TDD~ 10^9 cm^{-2}, 0.093 mm^2) and 265 nm LED (AlN TDD~ $8x10^8$ cm^{-2}, 0.0324 mm^2).

A sample of the EL emission for the 265 nm LEDs and 278 nm LEDs are shown in Figures 5.15 and 5.16, respectively. Figure 5.18 shows the light output for both LEDs as a function of current. The 265 nm LED (with 550 nm thick and 60 mΩ-cm^2 n-$Al_{0.60}Ga_{0.4}N$) and 278 nm LEDs (with 1100 nm thick and 60 mΩ-cm^2 n-$Al_{0.60}Ga_{0.4}N$) operating current was limited to 30 mA, and 100 mA, respectively. The operating current was limited due to current crowding (non-uniform lateral current injection) as a result of high sheet resistivity of n-AlGaN. Thermal droop was not observed at low currents in the 278 nm LED, however, the Au-Au bonding might be need to be replaced with InAu or Sn/Au bonding to improve thermal sinking at higher currents densities [104].

Figure 5.19 shows a sketch for TFFC LEDs that feature vertical hole conduction through the p-contact and lateral electron conduction through the n-contact. As the voltage drops across the n-AlGaN layer (non-equipotential surface), the current distribution drops and is given by the following [165,166]:

$$J(x) = J(0)exp(-\frac{x}{L_{sp}})$$

where x is the lateral distance from the n-contact, and L_{sp} is the electron current spreading in the n-AlGaN below the active region and is given by the following [165,166]:

$$L_{sp} = \sqrt{\frac{(\rho_c^p + \rho_l^p t^p)t^n}{\rho_l^n}}$$

Here, ρ_c^p is the p-contact specific resistance, ρ_l^p is the p-AlGaN layer resistivity, ρ_l^n is the n-AlGaN layer resistivity, t^p is the p-GaN and p-AlGaN thickness, and t^n is the n-AlGaN thickness. L_{sp}^p is independent from n-contact specific resistance and is plotted in Figure 5.20 for t^n equal to 1000 nm, and 500 nm. When $\rho_c^p >> \rho_l^p t^p$, as in these LEDs, (.01 Ω-cm^2 >> 10 Ω-cm^2*0.05*10^{-4} cm):

$$L_{sp} = \sqrt{\frac{(\rho_c^p + \rho_l^p t^p) t^n}{\rho_l^n}} \sim \sqrt{\frac{\rho_c^p}{\rho_l^n} t^n}$$

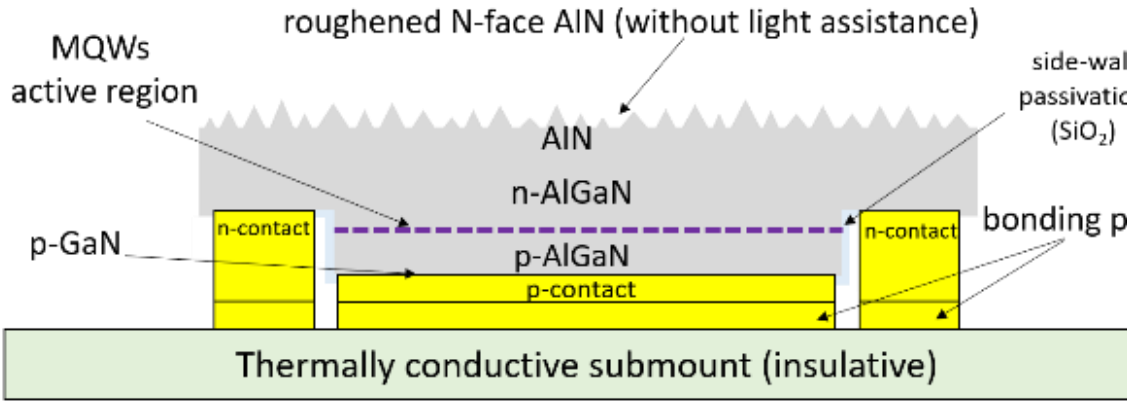

Figure 5.19. Sketch of lateral UV TFFC LED.

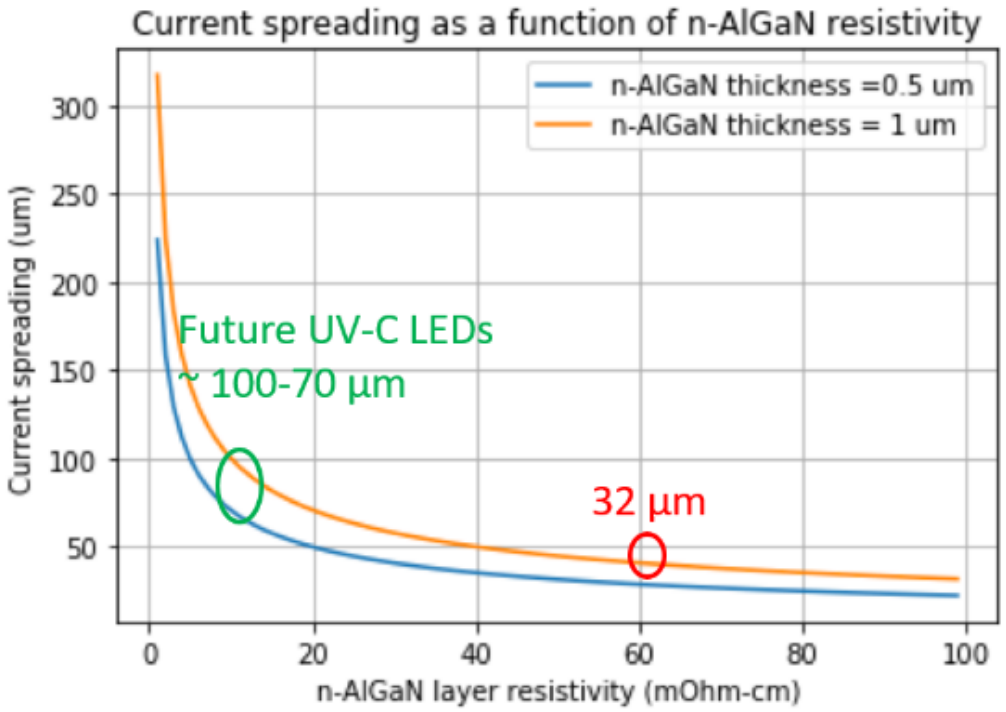

Figure 5.20. Current spreading as a function of n-AlGaN resistivity for two thicknesses: 0.5 µm and 1 µm. The 278 nm LED had 1.1 µm n-AlGaN. The 265 nm LED had 0.5 µm.

The uniform current density *J* (dividing the total current by the LED p-contact area) does not reflect the actual LED current density *J(x,I)* if the current is crowded, where ***x*** is the current injection distance from the n-contact and *I* is the LED current. Moreover, the current crowding becomes worse as the current increases. Current crowding causes non-uniform current injections and non-uniform thermal heating, limits EQE, limits maximum operating current, induces premature device failures, and limits the LEDs lifetime. [167]

The width of the mesas in the 0.1 mm^2 LEDs structures was ~ 58 µm. The distance between the edge of the n-contact and the center of the mesa was 12 +58 µm/2 = 41 µm. The equation above estimates that the current spreading (from each side of the mesa) is about 32 µm for the 1100 nm n-AlGaN LED (278 nm) and ~ 25 µm for the 550 nm n-AlGaN LED (265 nm). Therefore, the current spreading in the 278 nm LED was causing non-uniform current injection into the 0.1 mm^2 LEDs, and the LEDs currents were limited prematurely to around ~100 A/cm^2 due to current crowding. The current crowding in the 0.1 mm^2 LEDs was more severe because of the increased sheet resistivity of the thinner 550 nm n-AlGaN, and the LEDs were limited to around 30 mA. The width of the mesa in the 0.0324 mm^2 LEDs structures was ~ 58 µm, and the distance between the edge of the n-contact and the center of the mesa was 12 +128 µm/2 = 76 µm which made the 0.0324 mm^2 LEDs even more affected by current crowding.

Figure 5.21a shows the LIV for the TFFC LED after roughening. The voltage was 11.7 V at 20 mW with a series resistance of 16 Ω. Most of the excess voltage was due to the high resistance of the non-ohmic n-contact. The contribution of the n-contact to the voltage was estimated to add 4.1 V (16 Ω, 73%), whereas the p-contact resistance added 1.4 V (~5.4 Ω, 25%), and the p-AlGaN layer series resistance added 0.11 V (~0.5 Ω, 2%). The n-AlGaN contact resistance from the n-contact (ρ_c^n) was given by

$$R_{n-AlGaN} = \frac{\rho_c^n}{Area_{n-contact}}$$

$R_{n-AlGaN}$ is proportional to the n-AlGaN specific n-contact resistance (ρ_c^n) and inversely proportional to the n-contact area ($Area_{n-contact}$), which means that increasing the n-contact, will reduce the contribution of the n-contact resistance, yet, this will be at the expense of reducing the utilization efficiency of the epitaxial material.

Figure 5.21b shows the EQE peaked at 1.8% at 95 mA and the PCE peaked at 0.6%. The EQE and PCE did not peak at a low current density which might indicate high Shockley-Read-Hall (SRH) recombination in the active region, and possibly high current crowding due to limited n-AlGaN conductivity. Figure 5.21b shows that the 278 nm TFFC LED EQE was superior to some commercial LEDs that also suffer from low IQE active region. Figure 5.22 compares the light output between the 278 nm TFFC LED (0.1 mm^2) and several commercial ~278 nm LEDs procured at UCSB, and between 278 nm TFFC LED. The key to UCSB's superior results is the improved LEE, which is estimated to be 30 %.

TFFC LEDs are expected to extract TM emissions more efficiently than bulk FC LEDs because they don't require sidewall roughening to increase LEE, and because of improved LEE of TE and TM emissions. For example, Ryu et al. showed that the LEE of TM emissions in roughened AlGaN thin-film LEDs was significantly higher (>6X) than in bulk AlGaN FC-LEDs, using FTDT simulations [39]. Estimating the LEE in unroughened TFFC LEDs is challenging; for example, ray-tracing simulations by Keraly et al. estimate 13% LEE for each single-pass extraction (6 bounces for full extraction) [122]; however, wave optics simulations by David et al. estimate 31% LEE for each single pass extraction (3 bounces for full extraction) [123]. We discuss our LEE estimates for TFFC LEDs elsewhere [74].

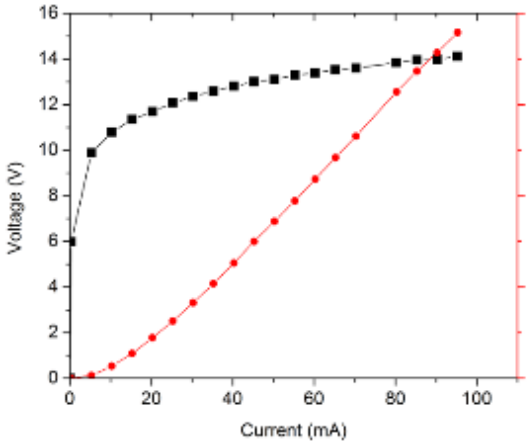

(a) L-I-V characteristic for 278 nm TFFC LED. The p-contact area is 0.093 mm^2. The voltage is high because of non-ohmic n-contact.

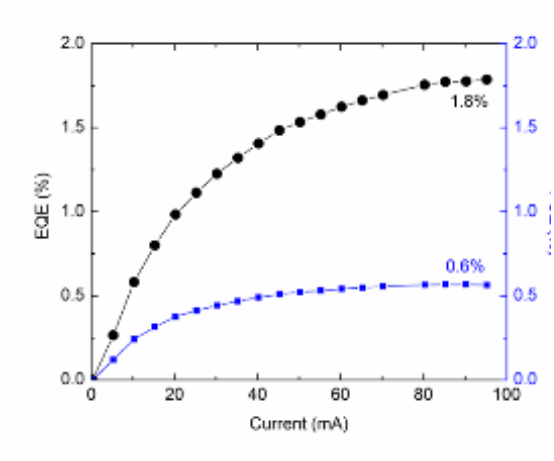

(b) External quantum efficiency (EQE) and power conversion efficiency (PCE) as a function of current for 278 nm TFFC LED.

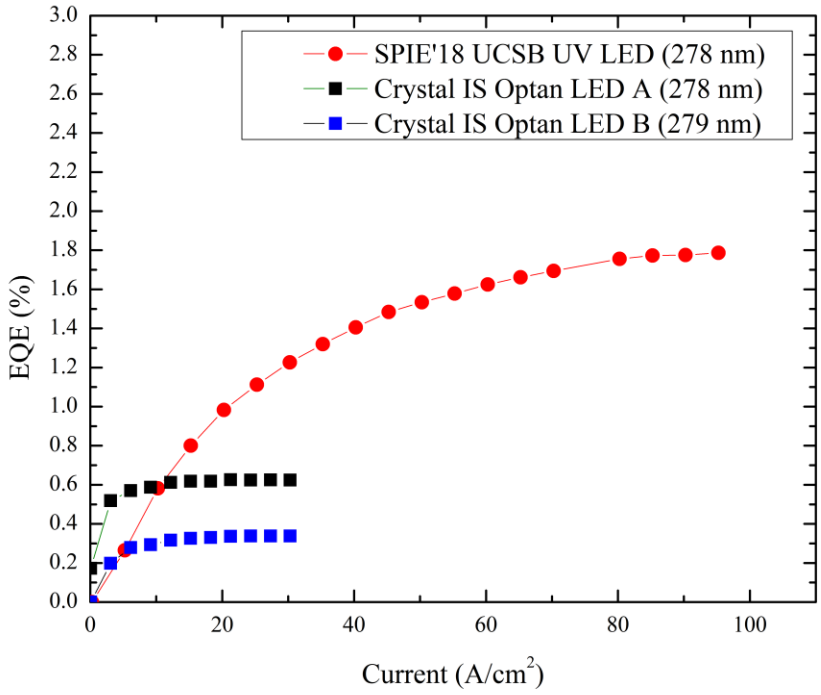

(c) External quantum efficiency (EQE) as function of current density between 278 nm TFFC LED (0.093 mm^2) and two OPTAN UV-C LEDs (~0.34 mm^2) from Crystal IS: 278 and 279 nm.

Figure 5.21. LIV, EQE and WPE for 278 nm TFFC LED with 0.1 mm^2 in p-contact area.

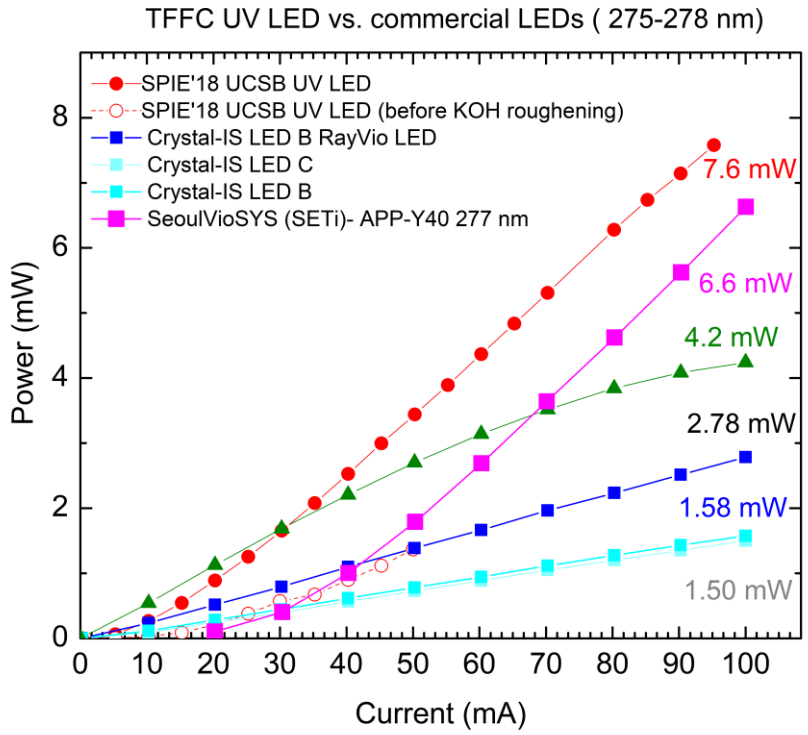

Figure 5.22. Light output (mW) as a function of current density. We compare the light output as function of current for several commercial LEDs procured at UCSB, and between 278 nm TFFC LED (0.093 mm^2).

Citations

[1] Downes O A and Blunt T P 2018 *upon protoplasm IV. On the influence of light* vol 23

[2] Krames M R, Shchekin O B, Mueller-Mach R, Mueller G O, Zhou L, Harbers G and Craford M G 2007 Status and future of high-power light-emitting diodes for solid-state lighting *IEEE/OSA J. Disp. Technol.*

[3] Hurni C A, David A, Cich M J, Aldaz R I, Ellis B, Huang K, Tyagi A, DeLille R A, Craven M D, Steranka F M and Krames M R 2015 Bulk GaN flip-chip violet light-emitting diodes with optimized efficiency for high-power operation *Appl. Phys. Lett.* **106** 031101

[4] Khanna S and Pardi D S 2012 Clostridium difficile infection: new insights into management. *Mayo Clin. Proc.* **87** 1106–17

[5] Haas J P, Menz J, Dusza S and Montecalvo M A 2014 Implementation and impact of ultraviolet environmental disinfection in an acute care setting. *Am. J. Infect. Control* **42** 586–90

[6] Anon 2013 *Ultraviolet Light Disinfection Data Sheet*

[7] Messina G, Fattorini M, Nante N, Rosadini D, Serafini A, Tani M and Cevenini G 2016 Time Effectiveness of Ultraviolet C Light (UVC) Emitted by Light Emitting Diodes (LEDs) in Reducing Stethoscope Contamination. *Int. J. Environ. Res. Public Health* **13**

[8] Pegues D A, Han J, Gilmar C, McDonnell B and Gaynes S 2017 Impact of Ultraviolet Germicidal Irradiation for No-Touch Terminal Room Disinfection on Clostridium difficile Infection Incidence Among Hematology-Oncology Patients *Infect. Control*

Hosp. Epidemiol. **38** 39–44

[9] Lucette Lagnado Hospitals Fund Potential Game-Changers in Health Tech *WSJ*

[10] Rutala W A, Gergen M F and Weber D J 2010 Room Decontamination with UV Radiation *Infect. Control Hosp. Epidemiol.* **31** 1025–9

[11] Inagaki Y and Kozawa T 2016 Chemical Reaction Pathways for MOVPE Growth of Aluminum Nitride *ECS J. Solid State Sci. Technol.* **5** P73–5

[12] Brunner D, Angerer H, Bustarret E, Freudenberg F, Höpler R, Dimitrov R, Ambacher O and Stutzmann M 1998 Optical constants of epitaxial AlGaN films and their temperature dependence *J. Appl. Phys.* **82** 5090

[13] Stutzmann M, Ambacher O, Cros A, Brandt M ., Angerer H, Dimitrov R, Reinacher N, Metzger T, Höpler R, Brunner D, Freudenberg F, Handschuh R and Deger C 1997 Properties and applications of MBE grown AlGaN *Mater. Sci. Eng. B* **50** 212–8

[14] Yun F, Reshchikov M A, He L, King T, Morkoç H, Novak S W and Wei L 2002 Energy band bowing parameter in AlxGa1−xN alloys *J. Appl. Phys.* **92** 4837–9

[15] Yoshida S, Misawa S and Gonda S 1982 Properties of $Al_x Ga_{1-x} N$ films prepared by reactive molecular beam epitaxy *J. Appl. Phys.* **53** 6844–8

[16] Ochalski T J, Gil B, Lefebvre P, Grandjean N, Leroux M, Massies J, Nakamura S and Morkoç H 1999 Photoreflectance investigations of the bowing parameter in AlGaN alloys lattice-matched to GaN *Appl. Phys. Lett.* **74** 3353

[17] Caetano C, Teles L K, Marques M, Dal Pino A and Ferreira L G 2006 Phase stability, chemical bonds, and gap bowing of $In_x Ga_{1-x} N$ alloys: Comparison between cubic and wurtzite structures *Phys. Rev. B* **74** 045215

[18] Hirayama H 2017 Chapter Three – Growth of High-Quality AlN on Sapphire and

Development of AlGaN-Based Deep-Ultraviolet Light-Emitting Diodes *Semiconductors and Semimetals* vol 96 pp 85–120

[19] Asif Khan M, Shatalov M, Maruska H P, Wang H M and Kuokstis E 2005 III–Nitride UV Devices *Jpn. J. Appl. Phys.* **44** 7191–206

[20] Hwang S, Morgan D, Kesler A, Lachab M, Zhang B, Heidari A, Nazir H, Ahmad I, Dion J, Fareed Q, Adivarahan V, Islam M and Khan A 2011 276 nm Substrate-Free Flip-Chip AlGaN Light-Emitting Diodes *Appl. Phys. Express* **4** 032102

[21] Moe C G, Masui H, Schmidt M C, Shen L, Moran B, Newman S, Vampola K, Mates T, Keller S, Speck J S, DenBaars S P, Hussel C and Emerson D 2005 Milliwatt Power Deep Ultraviolet Light Emitting Diodes Grown on Silicon Carbide *Jpn. J. Appl. Phys.* **44** L502–4

[22] Keller S and DenBaars S P 2003 Metalorganic chemical vapor deposition of group III nitrides—a discussion of critical issues *J. Cryst. Growth* **248** 479–86

[23] Chakraborty A, Moe C G, Wu Y, Mates T, Keller S, Speck J S, DenBaars S P and Mishra U K 2007 Electrical and structural characterization of Mg-doped p-type Al[sub 0.69]Ga[sub 0.31]N films on SiC substrate *J. Appl. Phys.* **101** 053717

[24] Moe C G, Schmidt M C, Masui H, Chakraborty A, Vampola K, Newman S, Moran B, Shen L, Mates T, Keller S, Denbaars S P and Emerson D 2006 Optimized doping and contact scheme for low-voltage 275-nm deep ultraviolet LEDs *J. Electron. Mater.* **35** 750–3

[25] SaifAddin B K, Zollner C J, Almogbel A, Foronda H, Wu F, Albadri A, Al Yamani A, Iza M, Nakamura S, Denbaars S P and Speck J S 2018 Developments in AlGaN and UV-C LEDs grown on SiC *Proceedings of SPIE - The International Society for*

Optical Engineering vol 10554

[26] Simon J, Protasenko V, Lian C, Xing H and Jena D 2010 Polarization-induced hole doping in wide-band-gap uniaxial semiconductor heterostructures. *Science* **327** 60–4

[27] Allerman A A, Crawford M H, Fischer A J, Bogart K H A, Lee S R, Follstaedt D M, Provencio P P and Koleske D D 2004 Growth and design of deep-UV (240–290nm) light emitting diodes using AlGaN alloys *J. Cryst. Growth* **272** 227–41

[28] Kneissl M and Rass J *III-nitride ultraviolet emitters : technology and applications*

[29] Moustakas T D and Paiella R 2017 Optoelectronic device physics and technology of nitride semiconductors from the UV to the terahertz *Rep. Prog. Phys* **80**

[30] Crawford M H 2017 Chapter One – Materials Challenges of AlGaN-Based UV Optoelectronic Devices *Semiconductors and Semimetals* vol 96 pp 3–44

[31] Muramoto Y, Kimura M and Nouda S 2014 Development and future of ultraviolet light-emitting diodes: UV-LED will replace the UV lamp *Semicond. Sci. Technol.* **29** 084004

[32] Shatalov M, Jain R, Saxena T, Dobrinsky A and Shur M 2017 Development of Deep UV LEDs and Current Problems in Material and Device Technology *Semicond. Semimetals* **96** 45–83

[33] Pernot C, Fukahori S, Inazu T, Fujita T, Kim M, Nagasawa Y, Hirano A, Ippommatsu M, Iwaya M, Kamiyama S, Akasaki I and Amano H 2011 Development of high efficiency 255-355 nm AlGaN-based light-emitting diodes *Phys. status solidi* **208** 1594–6

[34] Li D, Jiang K, Sun X and Guo C 2018 AlGaN photonics: recent advances in materials and ultraviolet devices *Adv. Opt. Photonics* **10** 43

[35] Takano T, Mino T, Sakai J, Noguchi N, Tsubaki K and Hirayama H 2017 Deep-ultraviolet light-emitting diodes with external quantum efficiency higher than 20% at 275 nm achieved by improving light-extraction efficiency *Appl. Phys. Express* **10** 031002

[36] Guo Y, Zhang Y, Yan J, Xie H, Liu L, Chen X, Hou M, Qin Z, Wang J and Li J 2017 Light extraction enhancement of AlGaN-based ultraviolet light-emitting diodes by substrate sidewall roughening *Appl. Phys. Lett.* **111** 011102

[37] Zhang Y, Krishnamoorthy S, Akyol F, Bajaj S, Allerman A A, Moseley M W, Armstrong A M and Rajan S 2017 Tunnel-injected sub-260 nm ultraviolet light emitting diodes *Appl. Phys. Lett.* **110** 201102

[38] Yun J and Hirayama H 2017 Investigation of the light-extraction efficiency in 280 nm AlGaN-based light-emitting diodes having a highly transparent p-AlGaN layer *J. Appl. Phys.* **121** 013105

[39] Ryu H-Y, Choi I-G, Choi H-S and Shim J-I 2013 Investigation of Light Extraction Efficiency in AlGaN Deep-Ultraviolet Light-Emitting Diodes *Appl. Phys. Express* **6** 062101

[40] Lachab M, Sun W, Jain R, Dobrinsky A, Gaevski M, Rumyantsev S, Shur M and Shatalov M 2017 Optical polarization control of photo-pumped stimulated emissions at 238 nm from AlGaN multiple-quantum-well laser structures on AlN substrates *Appl. Phys. Express* **10** 012702

[41] Rass J and Lobo-Ploch N 2016 Optical Polarization and Light Extraction from UV LEDs (Springer, Cham) pp 137–70

[42] Grandusky J R, Chen J, Gibb S R, Mendrick M C, Moe C G, Rodak L, Garrett G A,

Wraback M and Schowalter L J 2013 270 nm Pseudomorphic Ultraviolet Light-Emitting Diodes with Over 60 mW Continuous Wave Output Power *Appl. Phys. Express* **6** 032101

[43] Inazu T, Fukahori S, Pernot C, Kim M H, Fujita T, Nagasawa Y, Hirano A, Ippommatsu M, Iwaya M, Takeuchi T, Kamiyama S, Yamaguchi M, Honda Y, Amano H and Akasaki I 2011 Improvement of Light Extraction Efficiency for AlGaN-Based Deep Ultraviolet Light-Emitting Diodes *Jpn. J. Appl. Phys.* **50** 122101

[44] Tran B T and Hirayama H 2017 Growth and Fabrication of High External Quantum Efficiency AlGaN-Based Deep Ultraviolet Light-Emitting Diode Grown on Pattern Si Substrate *Sci. Rep.* **7** 12176

[45] Zhang Y, Allerman A A, Krishnamoorthy S, Akyol F, Moseley M W, Armstrong A M and Rajan S 2016 Enhanced light extraction in tunnel junction-enabled top emitting UV LEDs *Appl. Phys. Express* **9** 052102

[46] Muth J F, Lee J H, Shmagin I K, Kolbas R M, Jr. H C C, Keller B P, Mishra U K and DenBaars S P 1997 Absorption coefficient, energy gap, exciton binding energy, and recombination lifetime of GaN obtained from transmission measurements *Appl. Phys. Lett.* **71** 2572

[47] Kneissl M and Rass J *III-nitride ultraviolet emitters : technology and applications*

[48] Nakashima T, Takeda K, Iwaya M, Takeuchi T, Kamiyama S, Akasaki I and Amano H 2014 Improvement of light extraction efficiency of 350-nm emission UV light-emitting diodes *Phys. status solidi* **11** 836–9

[49] Reich C, Guttmann M, Feneberg M, Wernicke T, Mehnke F, Kuhn C, Rass J, Lapeyrade M, Einfeldt S, Knauer A, Kueller V, Weyers M, Goldhahn R and Kneissl

M 2015 Strongly transverse-electric-polarized emission from deep ultraviolet AlGaN quantum well light emitting diodes *Appl. Phys. Lett.*

[50] Schubert E F 2015 *Physical Foundations of Solid-State Devices* (E. Fred Schubert)

[51] Kitai A 2011 *Principles of Solar Cells, LEDs and Diodes: The role of the PN junction* (Chichester, UK: John Wiley & Sons, Ltd)

[52] Yamada K, Furusawa Y, Nagai S, Hirano A, Ippommatsu M, Aosaki K, Morishima N, Amano H and Akasaki I 2015 Development of underfilling and encapsulation for deep-ultraviolet LEDs *Appl. Phys. Express* **8** 012101

[53] Nagai S, Yamada K, Hirano A, Ippommatsu M, Ito M, Morishima N, Aosaki K, Honda Y, Amano H and Akasaki I 2016 Development of highly durable deep-ultraviolet AlGaN-based LED multichip array with hemispherical encapsulated structures using a selected resin through a detailed feasibility study *Jpn. J. Appl. Phys.* **55** 082101

[54] Peng Y, Guo X, Liang R, Cheng H and Chen M 2017 Enhanced Light Extraction from DUV-LEDs by AlN-Doped Fluoropolymer Encapsulation *IEEE Photonics Technol. Lett.* 1–1

[55] Katona T M and Matthew T 2003 Development of ultraviolet nitride-based light emitting diodes *ProQuest Diss. Theses; Ph.D.*

[56] Moe C G 2007 Growth and fabrication of deep ultraviolet light emitting diodes on silicon carbide substrates *ProQuest Diss. Theses; Ph.D.*

[57] Vampola K 2009 Improvement of III-N visible and ultraviolet light-emitting diode performance, including extraction efficiency, electrical efficiency, thermal management and efficiency maintenance at high current densities. *ProQuest Diss.*

Theses; Ph.D.

[58] Newman S A 2009 Lateral epitaxial overgrowth of aluminum nitride and near ultraviolet LEDs for white lighting applications. *ProQuest Diss. Theses; Ph.D.*

[59] Zhang W, Nikiforov A Y, Thomidis C, Woodward J, Sun H, Kao C-K, Bhattarai D, Moldawer A, Zhou L, Smith D J and Moustakas T D 2012 Molecular beam epitaxy growth of AlGaN quantum wells on 6H-SiC substrates with high internal quantum efficiency *J. Vac. Sci. Technol. B, Nanotechnol. Microelectron. Mater. Process. Meas. Phenom.* **30** 02B119

[60] Adivarahan V, Chitnis A, Zhang J P, Shatalov M, Yang J W, Simin G, Khan M A, Gaska R and Shur M S 2001 Ultraviolet light-emitting diodes at 340 nm using quaternary AlInGaN multiple quantum wells *Appl. Phys. Lett.* **79** 4240–2

[61] Almogbel A, SaifAddin B K, Zollner C, Humberto F, Iza M, Nakamura S, DenBaars S P and Speck J S 2017 Method for fabricating III-nitride layers (patent pending)

[62] Böttcher T, Einfeldt S, Figge S, Chierchia R, Heinke H, Hommel D and Speck J S 2001 The role of high-temperature island coalescence in the development of stresses in GaN films *Appl. Phys. Lett.* **78** 1976–8

[63] Banal R G, Akashi Y, Matsuda K, Hayashi Y, Funato M and Kawakami Y 2013 Crack-Free Thick AlN Films Obtained by NH_3 Nitridation of Sapphire Substrates *Jpn. J. Appl. Phys.* **52** 08JB21

[64] Foronda H M, Wu F, Zollner C, Alif M E M E, Saifaddin B, Almogbel A, Iza M, Nakamura S, DenBaars S P S P and Speck J S J S 2018 Low threading dislocation density aluminum nitride on silicon carbide through the use of reduced temperature interlayers *J. Cryst. Growth* **483** 134–9

[65] Collazo R, Xie J, Gaddy B E, Bryan Z, Kirste R, Hoffmann M, Dalmau R, Moody B, Kumagai Y, Nagashima T, Kubota Y, Kinoshita T, Koukitu A, Irving D L and Sitar Z 2012 On the origin of the 265 nm absorption band in AlN bulk crystals *Appl. Phys. Lett.* **100** 191914

[66] Ding K, Avrutin V, Özgür Ü and Morkoç H 2017 Status of Growth of Group III-Nitride Heterostructures for Deep Ultraviolet Light-Emitting Diodes *Crystals*

[67] Hwang D, Yonkee B P, SaifAddin B K, Farrell R M, Nakamura S, Speck J S and DenBaars S 2016 Photoelectrochemical liftoff of LEDs grown on freestanding c-plane GaN substrates *Opt. Express* **24** 22875

[68] Young E C, Yonkee B P, Wu F, Saifaddin B K, Cohen D A, Denbaars S P, Nakamura S and Speck J S 2015 Ultraviolet light emitting diodes by ammonia molecular beam epitaxy on metamorphic () AlGaN/GaN buffer layers *J. Cryst. Growth* **425** 389–92

[69] Benjamin Yonkee Erin Young, John Leonard and James Speck B S, DenBaars S and Nakamura S 2015 Flip Chip Blue (20-21) GaN LEDs Using Photoelectrochemical Etching for Substrate Removal *42nd International Symposium on Compound Semiconductors*

[70] SaifAddin B, Foronda H, Yonkee B, Cantore M, Oh S H, Farrell R, Margalith T, Young E C, Nakamura S, DenBaars S P and Speck J S 2015 Nanostructure Patterning of AlN Surface and Removal of SiC Substrates for High Extraction Efficiency Thin Film UV LEDs (Late News) *42nd Int. Symp. Compd. Semicond. St. Barbar. CA.*

[71] SaifAddin B K, Foronda H, Michael Iza, Nakamura S, DenBaars S P and Speck J S 2016 Epi-Transfer Technology for High EQE UV LEDs Grown on SiC (Late News) *MRS Int. Work. Nitride Semicond. (IWN 2016). Orlando, Fl.*

[72] SaifAddin B K, Foronda H, Almogbel A, Zollner C J, Iza M, Nakamura S, Denbaars S P and Speck J S 2017 First demonstration of lateral thin-film flip-chip ultraviolet light emitting diodes grown on SiC (Late News) *12th International Conference on Nitride Semiconductors (ICNS 12)* (Strasbourg, France)

[73] SaifAddin B K, Almogbel A, Zollner C J, Foronda H, Albadri A, Alyamani A, Iza M, Nakamura S, Denbaars S P and Speck J S 2018 Fabrication technology for high light-extraction ultraviolet thin-film flip-chip (UV TFFC) LEDs grown on SiC *SST (Manuscript sumbitted)* 1–21

[74] SaifAddin B, Almogbel A, Zollner C J, Albadri A, Al Yamani A, Iza M, Nakamura S, Denbaars S P and Speck J S 2018 3X Light extraction enhancement of UV-C thin-film light-emitting diodes (278 nm) via KOH roughening of AlN (Manuscript in preparation)

[75] S. M. Iftiquar Y L M J N B S K D and J Y 2012 *Photodiodes - From Fundamentals to Applications* ed I Yun (InTech)

[76] Lu B and Palacios T 2010 High Breakdown (>1500 V) AlGaN/GaN HEMTs by Substrate-Transfer Technology *IEEE Electron Device Lett.* **31** 951–3

[77] Meyer D J, Downey B P, Katzer D S, Nepal N, Wheeler V D, Hardy M T, Anderson T J and Storm D F 2016 Epitaxial Lift-Off and Transfer of III-N Materials and Devices from SiC Substrates *IEEE Trans. Semicond. Manuf.* **29** 384–9

[78] Shealy J B, Shealy J B, Patel P, Hodge M D, Vetury R and Shealy J R 2016 Single crystal aluminum nitride film bulk acoustic resonators *2016 IEEE Radio and Wireless Symposium (RWS)* (IEEE) pp 16–9

[79] Chen G, Zhao X, Wang X, Jin H, Li S, Dong S, Flewitt A J, Milne W I and Luo J K

2015 Film bulk acoustic resonators integrated on arbitrary substrates using a polymer support layer *Sci. Rep.* **5** 9510

[80] Buchine B A, Hughes W L, Degertekin F L and Wang Z L 2006 Bulk Acoustic Resonator Based on Piezoelectric ZnO Belts *Nano Lett.* **6** 1155–9

[81] Senesky D G and Pisano A P 2010 Aluminum nitride as a masking material for the plasma etching of silicon carbide structures *2010 IEEE 23rd International Conference on Micro Electro Mechanical Systems (MEMS)* (IEEE) pp 352–5

[82] Luna L E, Tadjer M J, Anderson T J, Imhoff E A, Hobart K D and Kub F J 2017 Dry Etching of High Aspect Ratio 4H-SiC Microstructures *ECS J. Solid State Sci. Technol.* **6** P207–10

[83] Dowling K M, Ransom E H and Senesky D G 2017 Profile Evolution of High Aspect Ratio Silicon Carbide Trenches by Inductive Coupled Plasma Etching *J. Microelectromechanical Syst.* **26** 135–42

[84] Choi J H, Latu-Romain L, Bano E, Dhalluin F, Chevolleau T and Baron T 2012 Fabrication of SiC nanopillars by inductively coupled SF_6/O_2 plasma etching *J. Phys. D. Appl. Phys.* **45** 235204

[85] Farrens S 2008 *Latest Metal Technologies for 3D Integration and MEMS Wafer Level Bonding (Report)*

[86] Khan F A and Adesida I 1999 High rate etching of SiC using inductively coupled plasma reactive ion etching in SF[sub 6]-based gas mixtures *Appl. Phys. Lett.* **75** 2268

[87] Cho H, Leerungnawarat P, Hays D C, Pearton S J, Chu S N G, Strong R M, Zetterling C-M, Östling M and Ren F 2000 Ultradeep, low-damage dry etching of SiC *Appl. Phys. Lett.* **76** 739

[88] Okamoto N and Ohki T 2009 SiC backside via-hole process for GaN HEMT MMICs using high etch rate ICP etching *CS MANTECH Conf. ...*

[89] Henry M D, Walavalkar S, Homyk A and Scherer A 2009 Alumina etch masks for fabrication of high-aspect-ratio silicon micropillars and nanopillars *Nanotechnology* **20** 255305

[90] Chabert P, Cunge G, Booth J-P and Perrin J 2001 Reactive ion etching of silicon carbide in SF6 gas: Detection of CF, CF2, and SiF2 etch products *Appl. Phys. Lett.* **79** 916–8

[91] Yazdi G R, Syväjärvi M and Yakimova R 2007 Formation of needle-like and columnar structures of AlN *J. Cryst. Growth* **300** 130–5

[92] Anon Reactive Ion Etching of 4H-SiC Using SF6/O2 for MEMS Application

[93] Lee Y H, Park K W, Kang S J, Yeo C I, Kim J B, Kang E K, Song Y M and Lee Y T 2015 Fabrication and analysis of thin-film GaAs solar cell on flexible thermoplastic substrate using a low-pressure cold-welding *Curr. Appl. Phys.* **15** 1312–7

[94] Kobayashi Y, Kumakura K, Akasaka T and Makimoto T 2012 Layered boron nitride as a release layer for mechanical transfer of GaN-based devices. *Nature* **484** 223–7

[95] Fiori G, Bonaccorso F, Iannaccone G, Palacios T, Neumaier D, Seabaugh A, Banerjee S K and Colombo L 2014 Electronics based on two-dimensional materials *Nat. Nanotechnol.* **9** 768–79

[96] Bai W, Yang H, Ma Y, Chen H, Shin J, Liu Y, Yang Q, Kandela I, Liu Z, Kang S-K, Wei C, Haney C R, Brikha A, Ge X, Feng X, Braun P V., Huang Y, Zhou W and Rogers J A 2018 Flexible Transient Optical Waveguides and Surface-Wave Biosensors Constructed from Monocrystalline Silicon *Adv. Mater.* **30** 1801584

[97] Nan K, Luan H, Yan Z, Ning X, Wang Y, Wang A, Wang J, Han M, Chang M, Li K, Zhang Y, Huang W, Xue Y, Huang Y, Zhang Y and Rogers J A 2017 Engineered Elastomer Substrates for Guided Assembly of Complex 3D Mesostructures by Spatially Nonuniform Compressive Buckling *Adv. Funct. Mater.* **27** 1604281

[98] Patel S, Park H, Bonato P, Chan L and Rodgers M 2012 A review of wearable sensors and systems with application in rehabilitation *J. Neuroeng. Rehabil.* **9** 21

[99] Park S Il, Brenner D S, Shin G, Morgan C D, Copits B A, Chung H U, Pullen M Y, Noh K N, Davidson S, Oh S J, Yoon J, Jang K-I, Samineni V K, Norman M, Grajales-Reyes J G, Vogt S K, Sundaram S S, Wilson K M, Ha J S, Xu R, Pan T, Kim T, Huang Y, Montana M C, Golden J P, Bruchas M R, Gereau R W and Rogers J A 2015 Soft, stretchable, fully implantable miniaturized optoelectronic systems for wireless optogenetics *Nat. Biotechnol.* **33** 1280–6

[100] Anikeeva P 2016 Optogenetics unleashed. *Nat. Biotechnol.* **34** 43–4

[101] Fujii T, Gao Y, Sharma R, Hu E L, DenBaars S P and Nakamura S 2004 Increase in the extraction efficiency of GaN-based light-emitting diodes via surface roughening *Appl. Phys. Lett.* **84** 855

[102] Holder C O, Leonard J T, Farrell R M, Cohen D A, Yonkee B, Speck J S, DenBaars S P, Nakamura S and Feezell D F 2014 Nonpolar III-nitride vertical-cavity surface emitting lasers with a polarization ratio of 100% fabricated using photoelectrochemical etching *Appl. Phys. Lett.* **105** 031111

[103] Leonard J T, Young E C, Yonkee B P, Cohen D A, Shen C, Margalith T, Ng T K, DenBaars S P, Ooi B S, Speck J S and Nakamura S 2016 Comparison of nonpolar III-nitride vertical-cavity surface-emitting lasers with tunnel junction and ITO intracavity

contacts ed J-I Chyi, H Fujioka, H Morkoç, Y Nanishi, U T Schwarz and J-I Shim (International Society for Optics and Photonics) p 97481B

[104] Lee S G, Kearns J, DenBaars S P, Forman C A, Young E C, Cohen D A, Leonard J T, Margalith T and Nakamura S 2018 Continuous-wave operation of nonpolar GaN-based vertical-cavity surface-emitting lasers *Gallium Nitride Materials and Devices XIII* vol 10532, ed J-I Chyi, H Morkoç and H Fujioka (SPIE) p 83

[105] Yonkee B P, SaifAddin B K, Leonard J T, DenBaars S P and Nakamura S 2016 Flip-chip blue LEDs grown on bulk GaN substrates utilizing photoelectrochemical etching for substrate removal *Appl. Phys. Express* **9** 56502

[106] Hwang D, Yonkee B P, Burhan SaifAddin, Farrell R M, Nakamura S, Speck J S and DenBaars S 2016 Photoelectrochemical liftoff of LEDs grown on freestanding c-plane GaN substrates *Opt. Express* **24** 22875–80

[107] Gao Y, Fujii T, Sharma R, Fujito K, Denbaars S P, Nakamura S and Hu E L 2004 Roughening Hexagonal Surface Morphology on Laser Lift-Off (LLO) N-Face GaN with Simple Photo-Enhanced Chemical Wet Etching *Jpn. J. Appl. Phys.* **43** L637–9

[108] Zhou L, Epler J E, Krames M R, Goetz W, Gherasimova M, Ren Z, Han J, Kneissl M and Johnson N M 2006 Vertical injection thin-film AlGaN⁄AlGaN multiple-quantum-well deep ultraviolet light-emitting diodes *Appl. Phys. Lett.* **89** 241113

[109] Adivarahan V, Heidari A, Zhang B, Fareed Q, Islam M, Hwang S, Balakrishnan K and Khan A 2009 Vertical Injection Thin Film Deep Ultraviolet Light Emitting Diodes with AlGaN Multiple-Quantum Wells Active Region *Appl. Phys. Express* **2** 092102

[110] Asif F, Chen H-C, Coleman A, Lachab M, Ahmad I, Zhang B, Fareed Q, Adivarahan V and Khan A 2013 Substrate Lifted-off AlGaN/AlGaN Lateral Conduction Thin-

Film Light-Emitting Diodes Operating at 285 nm *Jpn. J. Appl. Phys.* **52** 08JG14

[111] Lachab M, Asif F, Zhang B, Ahmad I, Heidari A, Fareed Q, Adivarahan V and Khan A 2013 Enhancement of light extraction efficiency in sub-300nm nitride thin-film flip-chip light-emitting diodes *Solid. State. Electron.* **89** 156–60

[112] Cho H K, Krüger O, Külberg A, Rass J, Zeimer U, Kolbe T, Knauer A, Einfeldt S, Weyers M and Kneissl M 2017 Chip design for thin-film deep ultraviolet LEDs fabricated by laser lift-off of the sapphire substrate *Semicond. Sci. Technol.* **32** 12LT01

[113] Aoshima H, Takeda K, Takehara K, Ito S, Mori M, Iwaya M, Takeuchi T, Kamiyama S, Akasaki I and Amano H 2012 Laser lift-off of AlN/sapphire for UV light-emitting diodes *Phys. status solidi* **9** 753–6

[114] Tamboli A C, Schmidt M C, Rajan S, Speck J S, Mishra U K, DenBaars S P and Hu E L 2009 Smooth Top-Down Photoelectrochemical Etching of m-Plane GaN *J. Electrochem. Soc.* **156** H47

[115] Fujii T, Gao Y, Sharma R, Hu E L, DenBaars S P and Nakamura S 2004 Increase in the extraction efficiency of GaN-based light-emitting diodes via surface roughening *Appl. Phys. Lett.* **84** 855–7

[116] Lee S, Mishkat-Ul-Masabih S, Leonard J T, Feezell D F, Cohen D A, Speck J S, Nakamura S and DenBaars S P 2017 Smooth and selective photo-electrochemical etching of heavily doped GaN:Si using a mode-locked 355 nm microchip laser *Appl. Phys. Express* **10** 011001

[117] Stonas A R, Kozodoy P, Marchand H, Fini P, DenBaars S P, Mishra U K and Hu E L 2000 Backside-illuminated photoelectrochemical etching for the fabrication of deeply

undercut GaN structures *Appl. Phys. Lett.* **77** 2610

[118] Stonas A R, Margalith T, DenBaars S P, Coldren L A and Hu E L 2001 Development of selective lateral photoelectrochemical etching of InGaN/GaN for lift-off applications *Appl. Phys. Lett.* **78** 1945

[119] Guo W, Kirste R, Bryan I, Bryan Z, Hussey L, Reddy P, Tweedie J, Collazo R and Sitar Z 2015 KOH based selective wet chemical etching of AlN, AlxGa1−xN, and GaN crystals: A way towards substrate removal in deep ultraviolet-light emitting diode *Appl. Phys. Lett.* **106** 082110

[120] Guo W, Xie J, Akouala C, Mita S, Rice A, Tweedie J, Bryan I, Collazo R and Sitar Z 2013 Comparative study of etching high crystalline quality AlN and GaN *J. Cryst. Growth* **366** 20–5

[121] Palacios T, Calle F, Varela M, Ballesteros C, Monroy E, Naranjo F B, Sánchez-García M A, Calleja E and Muñoz E 2000 Wet etching of GaN grown by molecular beam epitaxy on Si(111) *Semicond. Sci. Technol.* **15** 996–1000

[122] Lalau Keraly C, Kuritzky L, Cochet M and Weisbuch C 2013 Light Extraction Efficiency Part A. Ray Tracing for Light Extraction Efficiency (LEE) Modeling in Nitride LEDs (Springer, Dordrecht) pp 231–69

[123] David A 2013 Surface-Roughened Light-Emitting Diodes: An Accurate Model *J. Disp. Technol.* **9** 301–16

[124] Nilsson D 2014 *Doping of high-Al-content AlGaN grown by MOCVD* (Linköping University Electronic Press)

[125] Collazo R, Mita S, Xie J, Rice A, Tweedie J, Dalmau R and Sitar Z 2011 Progress on n-type doping of AlGaN alloys on AlN single crystal substrates for UV optoelectronic

applications *Phys. status solidi* **8** 2031–3

[126] Gordon L, Lyons J L, Janotti A and Van de Walle C G 2014 Hybrid functional calculations of D X centers in AlN and GaN *Phys. Rev. B* **89** 085204

[127] Fritze S, Dadgar A, Witte H, Bügler M, Rohrbeck A, Bläsing J, Hoffmann A, Krost A, Bügler M, Rohrbeck A, Bläsing J, Hoffmann A, Krost A, Bügler M, Rohrbeck A, Bläsing J, Hoffmann A and Krost A 2012 High Si and Ge n-type doping of GaN doping - Limits and impact on stress *Appl. Phys. Lett.* **100** 122104

[128] Gordon L, Varley J B, Lyons J L, Janotti A and Van de Walle C G 2015 Sulfur doping of AlN and AlGaN for improved n-type conductivity *Phys. status solidi - Rapid Res. Lett.* **9** 462–5

[129] Yonkee B P, Young E C, DenBaars S P, Nakamura S and Speck J S 2016 Silver free III-nitride flip chip light-emitting-diode with wall plug efficiency over 70% utilizing a GaN tunnel junction *Appl. Phys. Lett.* **109** 191104

[130] Buttari D, Chini A, Palacios T, Coffie R, Shen L, Xing H, Heikman S, McCarthy L, Chakraborty A, Keller S and Mishra U K 2003 Origin of etch delay time in Cl[sub 2] dry etching of AlGaN/GaN structures *Appl. Phys. Lett.* **83** 4779

[131] Adesida I, Mahajan A, Andideh E, Khan M A, Olsen D T and Kuznia J N 1993 Reactive ion etching of gallium nitride in silicon tetrachloride plasmas [a)] *Appl. Phys. Lett.* **63** 2777–9

[132] Tokuda H, Kojima T and Kuzuhara M 2012 Role of Al and Ti for ohmic contact formation in AlGaN/GaN heterostructures *Appl. Phys. Lett.* **101** 262104

[133] Srivastava S, Hwang S M, Islam M, Balakrishnan K, Adivarahan V and Khan A 2009 Ohmic Contact to High-Aluminum-Content AlGaN Epilayers *J. Electron. Mater.* **38**

2348–52

[134] Willis A J and Botha A P 1987 *5 INVESTIGATION OF RING STRUCTURES FOR METAL-SEMICONDUCTOR CONTACT RESISTANCE DETERMINATION* vol 146

[135] Lester L F, Brown J M, Ramer J C, Zhang L, Hersee S D and Zolper J C 1996 Nonalloyed Ti/Al Ohmic contacts to n-type GaN using high-temperature premetallization anneal *Cit. Appl. Phys. Lett* **69** 2737

[136] Barbara S 2017 *Novel Materials and Fabrication Techniques for Enhanced Current Spreading and Light Extraction in High Efficiency Light-emitting Diodes*

[137] Armstrong A M, Moseley M W, Allerman A A, Crawford M H and Wierer J J 2015 Growth temperature dependence of Si doping efficiency and compensating deep level defect incorporation in $Al_{0.7}Ga_{0.3}N$ *J. Appl. Phys.* **117** 185704

[138] Chichibu S F, Miyake H, Ishikawa Y, Tashiro M, Ohtomo T, Furusawa K, Hazu K, Hiramatsu K and Uedono A 2013 Impacts of Si-doping and resultant cation vacancy formation on the luminescence dynamics for the near-band-edge emission of $Al_{0.6}Ga_{0.4}N$ films grown on AlN templates by metalorganic vapor phase epitaxy *J. Appl. Phys.* **113** 213506

[139] Uedono A, Tenjinbayashi K, Tsutsui T, Shimahara Y, Miyake H, Hiramatsu K, Oshima N, Suzuki R and Ishibashi S 2012 Native cation vacancies in Si-doped AlGaN studied by monoenergetic positron beams *J. Appl. Phys.* **111** 013512

[140] Yonkee B P, Young E C, DenBaars S P, Speck J S and Nakamura S 2018 High reflectivity Ohmic contacts to n-GaN utilizing vacuum annealed aluminum *Semicond. Sci. Technol.* **33** 015015

[141] Van de Walle C G and Neugebauer J 2004 First-principles calculations for defects

and impurities: Applications to III-nitrides *J. Appl. Phys.* **95** 3851–79

[142] Van de Walle C G, Stampfl C, Neugebauer J, McCluskey M D and Johnson N M 1999 Doping of AlGaN Alloys *MRS Internet J. Nitride Semicond. Res.* **4** 890–901

[143] Kinoshita T, Obata T, Yanagi H and Inoue S 2013 High p-type conduction in high-Al content Mg-doped AlGaN *Appl. Phys. Lett.* **102** 012105

[144] SaifAddin Burhan, Iza Michael, Foronda Humberto, Almogbel Abdullah, Zollner Chris, Albadri Abdulrahman, AlYamani Ahmed, Nakamura Shuji, DenBaars Steven P. S J S 2018 First demonstration of high light-extraction thin-film flip-chip ultraviolet light emitting diodes grown on silicon carbide *Opt. Express*

[145] Haerle V, Hahn B, Kaiser S, Weimar A, Bader S, Eberhard F, Plössl A and Eisert D 2004 High brightness LEDs for general lighting applications using the new ThinGaN^{TM}-Technology *Physica Status Solidi (A) Applied Research*

[146] Kneissl M and Rass J 2016 *III-Nitride Ultraviolet Emitters* vol 227 (Cham: Springer International Publishing)

[147] Shchekin O B, Epler J E, Trottier T A, Margalith T, Steigerwald D A, Holcomb M O, Martin P S and Krames M R 2006 High performance thin-film flip-chip InGaN–GaN light-emitting diodes *Appl. Phys. Lett.* **89** 071109

[148] Foronda H M, Romanov A E, Young E C, Robertson C A, Beltz G E and Speck J S 2016 Curvature and bow of bulk GaN substrates *J. Appl. Phys.* **120** 035104

[149] Hoke W E, Torabi A, Mosca J J, Hallock R B and Kennedy T D 2005 Rapid silicon outdiffusion from SiC substrates during molecular-beam epitaxial growth of AlGaN⁄GaN⁄AlN transistor structures *J. Appl. Phys.* **98** 084510

[150] France R, Xu T, Chen P, Chandrasekaran R and Moustakas T D 2007 Vanadium-

based Ohmic contacts to n-AlGaN in the entire alloy composition *Appl. Phys. Lett.* **90** 062115

[151] Lapeyrade M, Muhin A, Einfeldt S, Zeimer U, Mogilatenko A, Weyers M and Kneissl M 2013 Electrical properties and microstructure of vanadium-based contacts on ICP plasma etched n-type AlGaN:Si and GaN:Si surfaces *Semicond. Sci. Technol.* **28** 125015

[152] Keller S, Cantu P, Moe C, Wu Y, Keller S, Mishra U K, Speck J S and DenBaars S P 2005 Metalorganic Chemical Vapor Deposition Conditions for Efficient Silicon Doping in High Al-Composition AlGaN Films *Jpn. J. Appl. Phys.* **44** 7227–33

[153] Cantu P, Wu F, Waltereit P, Keller S, Romanov A E, DenBaars S P and Speck J S 2005 Role of inclined threading dislocations in stress relaxation in mismatched layers *J. Appl. Phys.* **97** 103534

[154] Cantu P, Keller S, Mishra U K and DenBaars S P 2003 Metalorganic chemical vapor deposition of highly conductive Al0.65Ga0.35N films *Appl. Phys. Lett.* **82** 3683–5

[155] Van de Walle C G, Stampfl C and Neugebauer J 1998 Theory of doping and defects in III–V nitrides *J. Cryst. Growth* **189**–**190** 505–10

[156] Alkauskas A, McCluskey M D and Van de Walle C G 2016 Tutorial: Defects in semiconductors—Combining experiment and theory *J. Appl. Phys.* **119** 181101

[157] Mogab C J, Adams A C and Flamm D L 1978 Plasma etching of Si and SiO2—The effect of oxygen additions to CF4 plasmas *J. Appl. Phys.* **49** 3796

[158] Kuryatkov V, Borisov B, Saxena J, Nikishin S A, Temkin H, Patibandla S, Menon L and Holtz M 2005 Analysis of nonselective plasma etching of AlGaN by CF[sub 4]/Ar/Cl[sub 2] *J. Appl. Phys.* **97** 073302

[159] Mori K, Takeda K, Kusafuka T, Iwaya M, Takeuchi T, Kamiyama S, Akasaki I and Amano H 2016 Low-ohmic-contact-resistance V-based electrode for n-type AlGaN with high AlN molar fraction *Jpn. J. Appl. Phys.* **55** 05FL03

[160] Cantu P, Keller S, Wu F, Waltereit P, Romanov A E, Mishra U K, Speck J S and DenBaars S P 2003 Si doping effects on the electrical and structural properties of high Al composition AlxGa1−xN films grown by MOCVD *Phys. status solidi* **0** 2010–3

[161] Zhang J C, Zhu Y H, Egawa T, Sumiya S, Miyoshi M and Tanaka M 2008 Suppression of the subband parasitic peak by 1nm i-AlN interlayer in AlGaN deep ultraviolet light-emitting diodes *Appl. Phys. Lett.* **93** 131117

[162] Kuek J J, Pulfrey D L, Nener B D, Dell J M, Parish G and Mishra U K 2001 Effects of Band Tail Absorption on AlGaN-Based Ultraviolet Photodiodes *Phys. status solidi* **188** 311–5

[163] John S, Soukoulis C, Cohen M H and Economou E N 1986 Theory of Electron Band Tails and the Urbach Optical-Absorption Edge *Phys. Rev. Lett.* **57** 1777–80

[164] Köhler K, Gutt R, Wiegert J and Kirste L 2013 Diffusion of Mg dopant in metal-organic vapor-phase epitaxy grown GaN and $Al_x Ga_{1-x} N$ *J. Appl. Phys.* **113** 073514

[165] Guo X and Schubert E F 2001 Current crowding in GaN/InGaN light emitting diodes on insulating substrates *J. Appl. Phys.* **90** 4191–5

[166] Shatalov M, Simin G, Adivarahan V, Chitnis A, Wu S, Pachipulusu R, Mandavilli V, Simin K, Zhang J P, Yang J W and Khan M A 2002 Lateral Current Crowding in Deep UV Light Emitting Diodes over Sapphire Substrates *Jpn. J. Appl. Phys.* **41** 5083–7

[167] Li C-K and Wu Y-R 2012 Study on the Current Spreading Effect and Light

Extraction Enhancement of Vertical GaN/InGaN LEDs *IEEE Trans. Electron Devices* **59** 400–7

Appendix

A1. Process flow

The TFFC LED process could be developed further to improve its yield and robustness. Although much of the process is developed, there are many areas that could be improved further whether to increase the yield or improve bonding (Substitute low temperature Au-Au bonding with In/Au or Sn/Au). I include the process follower that I used for the first generation UV LEDs and 2nd generation UV LEDs. Moreover, an optional "haircut" lithography can be done around the thin-film LED by either: 1) etching a larger and deeper mesa around the LEDs mesa (into 80% of the AlN thickness); or, alternatively, 2) conducting a non-contact lithography after FC and substrate removal can etch away the excess area around the LED active area by KOH (which etches N-face AlN).

- Process flow for 1st generation UV LEDs

Step	Equipment	Details
Growth calibrations	MOCVD	Grown AlN, and relevant AlGaN layers calibrations
	XRD	Check AlGaN % with RSM and infer DDs in AlN with 102 and 002 scans
	Hall	Check n-AlGaN conductivity
	AFM/Hall/XRD	Check relevant layers roughness
Growth	MOCVD	Grow UV LED series. Adjust MQW emission wavelength by adjusting TMG or temperature
Anneal p-AlGaN / p-GaN	Furnace	900 ºC, Air, 3min.
Quicktest	LIV Quicktest	Measure EL check diode IV for the UV LEDs. Save all spectrum and IV data.
Remove Indium	Acid Bench	3:1 HCl:HN03 Aqua Regia, 3x 10min, mix new batch each iteration, wait 5min for boiling, 120C on hotplate
Mesa Litho	Solvent Bench	Sonicate on low: 2min Ace, 2min Iso, 3x 30s DI. 30s DI rinse. N2 dry
	PR Bench	Dehydration bake, 2min 110ºC, let cool 30sec
		Spin HMDS Program 5 (3000rpm, 30s)
		Spin **SPR220-3.0** Program 5 (3000rpm 30s)
		edge-bead removal from short edges
		Soft bake, 115ºC 90s
	Contact Aligner	Expose **"Mesa 1"**, 7.5mW/cm^2, **25s,** No Filter, Black chuck, **Hard contact**
	PR Bench	**Post exposure bake 115°C 60s**

	Develop Bench	Develop in AZ300MIF **60s**
		30 sec DI rinse flowing, N_2 dry
	Microscope	Inspect, develop more if necessary
	UV Ozone	20min (~6A/min)
Mesa Etch	RIE # 5	Load bare RIE Si carrier wafer
		Standard O2 preclean, BCL3 for 5 min (Burhan01)
		Load samples onto carrier wafer
		Run "Burhan02" to Etch SiCl4. Rate ~25 nm/min. (calibrate if needed)
		Soak sample in DI for 2min,
		Hf dip for 40 sec 3x 30s + 1min DI, N2 dry
	Solvent Bench	Strip PR in NMP 80C, 10+min, ultrasonic before submerging sample then spray with pipette, use heated bath
		3x 30s DI Dump&Rinse, N2 dry
	Microscope	Inspect, strip more if necessary
	Dektak/SEM	Measure step height 1-2 points per sample
Dielectric deposition	Solvent Bench	3min Ace, 2min Iso, 3x 30s DI Dump&Rinse, N2 dry
	ALD	Deposit **50 nm of SiO_2** using Ch3_TDMAS+250W/O*-300C
n-contact mirror Litho	Solvent Bench	3min Ace, 2min Iso, 3x 30s DI Dump&Rinse, N2 dry
	PR Bench	Dehydration bake, 2min 110C, let cool 1min
		Spin HMDS Program 5 (3000rpm, 30s)
		Spin **nLOF2020** Program 5 (3000rpm 30s)
		Edge Bead removal, Clean backside with EBR 100
		Soft bake, 110ºC 90s
	Contact Aligner	Expose "p-Contact", 7.5mW/cm^2, **10s,** With i-Line Filter, Black chuck, **Hard contact**
	PR Bench	Hardbake 110C 60s
	Develop Bench	Develop in AZ300-MIF **50s**
		2min DI rinse flowing, N2 dry
	Microscope	Inspect, develop more if necessary
	UV Ozone	20min (~6A/min)
	Dektak	Optional Inspection
n-contact mirror Dep	Acid bench	**10 sec in BOE,** 1x 30s DI Dump&Rinse **, 14 min HCL,** 3x 30s DI Dump&Rinse, N2 dry
	Ebeam 3/4	Deposit Ti/Au Ti:2A/s. Au: (2A/s to, 100A,4A/sec to 500A, 6A/sec).
		20nm/(300nm+Mesa Height)
n-contact Liftoff	Solvent Bench	Liftoff in NMP. Pre-heat at 80C, ultrasonic before submerging sample, then spray with pipette, use heated bath 10+min.
		3x 30s DI Dump&Rinse, N2 dry
	Microscope	Inspect, liftoff more if necessary
	Dektak	Optional Inspection
Anneal n-contact	RTA	850 C N2 for 30 sec. (use recipe in my folder)
	Cary 500	Measure reflectivity on DSP sap ref. samples
Redo Litho for n-contact	Solvent Bench	3min Ace, 2min Iso, 3x 30s DI Dump&Rinse, N2 dry
2nd n-contact mirror Litho	PR Bench	Dehydration bake, 2min 110C, let cool 1min
		Spin HMDS Program 5 (3000rpm, 30s)
		Spin **nLOF2020** Program 5 (3000rpm 30s)
		Edge Bead removal, **Clean backside with EBR 100**
		Softbake, **110C 90s**
		Expose "p-Contact", 7.5mW/cm^2, **10s,** With i-Line Filter, Black chuck, **Hard contact**
	PR Bench	Hardbake 110C 60s
	Develop Bench	Develop in **AZ300MIF 50s**

		2min DI rinse flowing, N2 dry
		Inspect, develop more if necessary
	UV Ozone	20min (~6A/min)
	Dektak	Optional Inspection
n-contact mirror Re-Dep	Acid bench	**10 sec in BOE,** 1x 30s DI Dump&Rinse **, 14 min HCL,** 3x 30s DI Dump&Rinse, N2 dry
	Ebeam 3	Deposit Ti/Au Ti:2A/s. Au: (2A/s to, 100A,4A/sec to 500A, 6A/sec).
		20nm/1000nm
2nd n-contact Liftoff	Solvent Bench	Liftoff in NMP, 80C, 10+min, ultrasonic for 1 min before submerging sample, then spray with pipette, use heated bath Don't ultrasonicate after that to avoid scratching the thick metal
		2min DI rinse flowing, N2 dry
	Microscope	Inspect, liftoff more if necessary
	Dektak	Optional Inspection
p-contact mirror Litho	Solvent Bench	3min Ace, 3min Iso, 3x 30s DI Dump&Rinse, N2 dry
	PR Bench	Dehydration bake, 2min 110C, let cool 1min
		Spin HMDS Program 5 (3000rpm, 30s)
		Spin **nLof 2035** Program 5 (3000rpm 30s)
		Edge Bead removal, **Clean backside with EBR 100**
		Softbake, 110C 90s
	Contact Aligner	Expose "p-Contact", 7.5mW/cm^2, **12s,** With i-Line Filter, Black chuck, **Hard contact**
	PR Bench	Hardbake 110C 60s
	Develop Bench	Develop in **AZ300MIF 55s**
		2min DI rinse flowing, N2 dry
	Microscope	Inspect, develop more if necessary
	UV Ozone	20min (~6A/min)
	Dektak	Optional Inspection
p-contact mirror Dep	Acid bench	**10 sec in BOE,** 1x 30s DI Dump&Rinse **, 14 min HCL,** 3x 30s DI Dump&Rinse, N2 dry
	Ebeam 3/4	Deposit Ni/Al/Ni/Au Ni:1.5 A/s. Al: (2A/s to 100A,3A/sec). Use low dep rate R# for Ni.
		1nm/100nm/100nm/(Dektak n-contact H-Mesa H)
p-contact Liftoff	Solvent Bench	Liftoff in NMP, 80C, 10+min, ultrasonic for 1 min before submerging sample, then spray with pipette, use heated bath Don't ultrasonicate after that to avoid scratching the thick metal
		2min DI rinse flowing, N2 dry
	Microscope	Inspect, liftoff more if necessary
	QT Lab	IV Check
Flip Chip bonding	Solvent Bench	3min Ace, 2min Iso, 4x 30s DI rinse flowing, N2 dry
	O2 Asher	O2 Plasma Clean for 200mbar/100W 30 s
	Fintech	sample area ~1.2 cm^2. Bond sample at 275C for 5 min
	Oven 200˚C	Use Carbon Fixture for bonding for 2h
Wafer thinning	Packaging lab	Use Wax at **130C** to bond sample to chuck. **Remove any extra wax with cotton swipe and Ace**
		Center wafer on ceramic chuck (for NVG). Or Center wafer on 1/2 radius steel chuck (for SouthBay) (record sample thickness with Dialer)
	NVG or Southbay	Thin SiC to about 80-100µm.
		SiC removal rate is ~ 3µm (NVG, 400/100, V Feed 3.5) and ~ 25µm (SouthBay , 6µm Allied grit, 5/6)
	Microscope	Check devices alignment
SiC ICP etching	Solvent Bench	**2min+ Ace to remove any remaining wax**, 2min Iso, 4x 30s DI rinse flowing, N2 dry
	ICP1	Run 5 min O2 clean and 115 for 2 min Load Fused Silica carrier wafer
		Run Recipe 114 for High SiC etch rate (40 µm/hr for 400 W)

		Run Recipe 115 for Low SiC etch rate (6 µm/hr for 50 W)
	Microscope/SEM	Inspect devices and for any remaining SiC. Etch more if necessary
LIV testing	QT Lab	

- Process flow for 2nd generation UV LEDs

Step	Equipment	Details
Growth calibrations	MOCVD	Grown AlN, and relevant AlGaN layers calibrations
	XRD	Check AlGaN % with RSM and infer DDs in AlN with 102 and 002 scans
	Hall	Check n-AlGaN conductivity
	AFM/Hall/XRD	Check relevant layers roughness
Growth	MOCVD	Grow UV LED series. Adjust MQW emission wavelength by adjusting TMG or temperature
Anneal p-AlGaN / p-GaN	Furnace	900 ºC, Air, 3min.
Quicktest	LIV Quicktest	Measure EL check diode IV for the UV LEDs. Save all spectrum and IV data.
Remove Indium	Acid Bench	3:1 HCl:$HN0_3$ Aqua Regia, 3x 10min, mix new batch each iteration, wait 5min for boiling, 120C on hotplate
Mesa Litho	Solvent Bench	Sonicate on low: 2min Ace, 2min Iso, 3x 30s DI. 30s DI rinse. N2 dry
	PR Bench	Dehydration bake, 2min 110ºC, let cool 30sec
		Spin HMDS Program 5 (3000rpm, 30s)
		Spin **SPR220-3.0** Program 5 (3000rpm 30s)
		edge-bead removal from short edges
		Soft bake, 115 ºC 90s
	Contact Aligner	Expose **"Mesa 1"**, 7.5mW/cm^2, **25s,** No Filter, Black chuck, **Hard contact**
	PR Bench	**Post exposure bake 115°C 60s**
	Develop Bench	Develop in AZ300MIF **60s**
		30 sec DI rinse flowing, N_2 dry
	Microscope	Inspect, develop more if necessary
	UV Ozone	20min (~6A/min)
Mesa Etch	ICP # 1	Load bare ICP Si carrier wafer
		Standard O2 preclean,
		Load samples onto carrier wafer
		Run 200 W (RF bias) BCl_3/Cl/Ar etch ~250 nm/min. (calibrate if needed)
		Soak sample in DI for 2min,
		Hf dip for 40 sec 3x 30s + 1min DI, N2 dry
	Solvent Bench	Strip PR in NMP 80C, 10+min, ultrasonic before submerging sample then spray with pipette, use heated bath
		3x 30s DI Dump&Rinse, N2 dry
	Microscope	Inspect, strip more if necessary
	Dektak/SEM	Measure step height 1-2 points per sample
Dielectric deposition	Solvent Bench	3min Ace, 2min Iso, 3x 30s DI Dump&Rinse, N2 dry
	ALD	Deposit **50 nm of SiO_2** using Ch3_TDMAS+250W/O*-300C (Also 120 C is ok)
n-contact mirror Litho	Solvent Bench	3min Ace, 2min Iso, 3x 30s DI Dump&Rinse, N2 dry
	PR Bench	Dehydration bake, 2min 110C, let cool 1min
		Spin HMDS Program 5 (3000rpm, 30s)
		Spin **nLOF2020** Program 5 (3000rpm 30s)
		Edge Bead removal, Clean backside with EBR 100
		Soft bake, 110ºC 90s

	Contact Aligner	Expose "p-Contact", 7.5mW/cm^2, **10s,** With i-Line Filter, Black chuck, **Hard contact**
	PR Bench	Hardbake 110C 60s
	Develop Bench	Develop in AZ300-MIF **50s**
		2min DI rinse flowing, N2 dry
	Microscope	Inspect, develop more if necessary
	UV Ozone	20min (~6A/min)
	Dektak	Optional Inspection
n-contact mirror Dep	Acid bench	**10 sec in BOE,** 1x 30s DI Dump&Rinse **, 14 min HCL,** 3x 30s DI Dump&Rinse, N2 dry
	Ebeam 2	Deposit V/Al/Ni/Au (10/150/100/x nm) or V/Al/V/Au (20/150/80/x nm)
		Choose x so that n-contact thickness = Mesa height
n-contact Liftoff	Solvent Bench	Liftoff in NMP. Pre-heat at 80C, ultrasonic before submerging sample, then spray with pipette, use heated bath 10+min.
		3x 30s DI Dump&Rinse, N2 dry
	Microscope	Inspect, liftoff more if necessary
	Dektak	Optional Inspection
Anneal n-contact	RTA	720 C N_2 for 30 sec for V/Al/V/Au . Ramp up in 1 min.
	Cary 500	Measure reflectivity on DSP sap ref. samples
Redo Litho for n-contact	Solvent Bench	3min Ace, 2min Iso, 3x 30s DI Dump&Rinse, N2 dry
Optional (current spreading for quick fab LEDs): Thinfilm metal Litho	PR Bench	Solvent Bench
		PR Bench
		Spin **nLOF2020** Program 5 (3000rpm 30s)
		Edge Bead removal, **Clean backside with EBR 100**
		Softbake, **110C 90s**
		Expose "p-Contact", 7.5mW/cm^2, **10s,** With i-Line Filter, Black chuck, **Hard contact**
	PR Bench	Contact Aligner
	Develop Bench	Develop Bench
		2min DI rinse flowing, N2 dry
	UV Ozone	Microscope
	Dektak	UV Ozone
		Solvent Bench
Thinfilm metal dep	Acid bench	**7 sec BOE, x 30s DI Dump& Rinse 2 min, 15 min HCL,** 4x 30s DI Dump&Rinse, N2 dry
	Ebeam 3	Deposit Ni/Au 2/3 nm
Thinfilm metal Liftoff	Solvent Bench	Liftoff in NMP, 80C, 10+min, ultrasonic for 1 min before submerging sample, then spray with pipette, use heated bath Don't ultrasonicate after that to avoid scratching the thick metal
		2min DI rinse flowing, N2 dry. Don't ultrasonicate.
	Microscope	Inspect, liftoff more if necessary
	Dektak	Optional Inspection
p-contact and n-contact Litho	Solvent Bench	3min Ace, 3min Iso, 3x 30s DI Dump&Rinse, N2 dry
	PR Bench	Dehydration bake, 2min 110C, let cool 1min
		Spin HMDS Program 5 (3000rpm, 30s)
		Spin **nLof 2035** Program 5 (3000rpm 30s)
		Edge Bead removal, **Clean backside with EBR 100**
		Softbake, 110C 90s
	Contact Aligner	Expose "p-Contact", 7.5mW/cm^2, **12s,** With i-Line Filter, Black chuck, **Hard contact**
	PR Bench	Hardbake 110C 60s

	Develop Bench	Develop in **AZ300MIF 55s**
		2min DI rinse flowing, N2 dry
	Microscope	Inspect, develop more if necessary
	UV Ozone	20min (~6A/min)
	Dektak	Optional Inspection
p-contact and n-contact Dep	Acid bench	**10 sec in BOE,** 1x 30s DI Dump&Rinse **, 14 min HCL,** 3x 30s DI Dump&Rinse, N2 dry
	Ebeam 3	Deposit Ni/Al/Ni/Au Ni:1.5 A/s. Al: (2A/s to 100A,3A/sec). Use low dep rate R# for Ni. compare to **Ni/Al/Ni/Au**
		1 nm/150nm/100/1000nm
p-contact and n-contact Liftoff	Solvent Bench	Liftoff in NMP, 80C, 10+min, ultrasonic for 1 min before submerging sample, then spray with pipette, use heated bath Don't ultrasonicate after that to aoid scratching the thick metal
		2min DI rinse flowing, N2 dry
	Microscope	Inspect, liftoff more if necessary
	QT Lab	IV Check
Flip Chip bonding	Solvent Bench	3min Ace, 2min Iso, 4x 30s DI rinse flowing, N2 dry
	O2 Asher	O2 Plasma Clean for 200mbar/100W 30 s
	Fintech	sample area ~1.2 cm^2. Bond sample at 275C for 5 min
	Oven 200˚C	Use Carbon Fixture for bonding for 2h
Wafer thinning	Packaging lab	Use Wax at **130C** to bond sample to chuck. **Remove any extra wax with cotton swipe and Ace**
		Center wafer on ceramic chuck (for NVG). Or Center wafer on 1/2 radius steel chuck (for SouthBay) Record sample thickness with Dialer
	NVG or Southbay	Thin SiC to about 80-100µm.
		SiC removal rate is ~ 3µm (NVG, 400/100, V Feed 3.5) and ~ 25µm (SouthBay , 6µm Allied grit, 5/6) Refer to SST paper [71]
	Microscope	Check devices alignment
SiC ICP etching	Solvent Bench	**2min+ Ace to remove any remaining wax**, 2min Iso, 4x 30s DI rinse flowing, N2 dry
	ICP1	Run 5 min O2 clean and 115 for 2 min Load Fused Silica carrier wafer
		Run Recipe 114 for High SiC etch rate (40 µm/hr for 400 W)
		Run Recipe 115 for Low SiC etch rate (6 µm/hr for 50 W)
	Microscope/SEM	Inspect devices and for any remaining SiC. Etch more if necessary
LIV testing	QT Lab	